DYNAMIC ANALYSIS OF PRISTINE AND DEFECTIVE SINGLE-WALLED CARBON NANOTUBES

A THESIS SUBMITTED TO
THE BOARD OF GRADUATE PROGRAMS
OF
MIDDLE EAST TECHNICAL UNIVERSITY, NORTHERN CYPRUS CAMPUS

BY

NIMA JAFARNIA

IN PARTIAL FULFILLMENT OF THE REQUIREMENTS
FOR
THE DEGREE OF MASTER OF SCIENCE
IN SUSTAINABLE ENVIRONMENT AND ENERGY SYSTEMS PROGRAM

DECEMBER 2023

Approval of the Board of Graduate Programs

Prof. Dr. Cumali Sabah

Chairperson

I certify that this thesis satisfies all the requirements as a thesis for the degree of Master of Science

Assist. Prof. Dr. Canraş Batunlu

Program Coordinator

This is to certify that we have read this thesis and that in our opinion it is fully adequate, in scope and quality, as a thesis for the degree of Master of Science.

Assoc. Prof. Dr. Volkan Esat

Supervisor

Examining Committee Members

Prof. Dr. Farhad Javidrad	METU NCC ASE	
Assoc. Prof. Dr. Volkan Esat	METU NCC MECH	
Assoc. Prof. Dr. Süleyman Aşır	NEU M. Sci. &Nano Eng.	

I hereby declare that all information in this document has been obtained and presented in accordance with academic rules and ethical conduct. I also declare that, as required by these rules and conduct, I have fully cited and referenced all material and results that are not original to this work.

Name, Last name: Nima, Jafarnia

Signature:

ABSTRACT

Dynamic Analysis of Pristine and Defective Single-Walled Carbon Nanotubes

Jafarnia, Nima
Master of Science, Sustainable Environment and Energy Systems Program
Supervisor: Assoc. Prof. Dr. Volkan Esat

December 2023, 108 pages

This study focuses on investigating the vibrational behavior of SWNTs through conducting modal analysis. The primary objective of this research is to determine the natural frequency of pristine and defective SWNTs. Therefore, a comprehensive computational analysis using finite element modeling is performed on both pristine and defective SWNTs under cantilever and bridge boundary conditions with various diameters, lengths, and chirality. The results indicate that the natural frequency of all types of SWNTs decreases as the length increases. Moreover, since the impact of length is more prominent than diameter, the diameter's impact can be neglected by the increase of length. Another part of this article focuses on the impacts of vacancy defects and Stone-Wales defects. It is observed that the double vacancy defects have the most degrading effects on the natural frequency of the SWNTs. This research's aim is to contribute to the development of nanoscale technologies and the improvement of the field of materials science.

Keywords: Carbon nanotubes, Natural frequency, Vibration, Stone-Wales defects, Vacancy defects

ÖZ

Bozulmamış ve Arızalı Tek Duvarlı Karbon Nanotüplerin Dinamik Analizi

Jafarnia, Nima
Yüksek Lisans, Sürdürülebilir Çevre ve Enerji Sistemleri Programı
Tez Yöneticisi: Doç. Dr. Volkan Esat

Aralık 2023, 108 sayfa

Bu çalışma, Tek Duvarlı Karbon Nanotüpler'in (TDKNT) modal analiz yoluyla titreşim davranışını araştırmaya odaklanmaktadır. Bu araştırmanın temel amacı, bozulmamış ve kusurlu TDKNT'lerin doğal frekanslarını belirlemektir. Bu nedenle, çeşitli çap, uzunluk ve kiraliteye sahip bozulmamış ve kusurlu TDKNT'ler ankastre mesnet – boşta uç ve köprü (ankastre mesnet – ankastre mesnet) sınır koşulları altında sonlu elemanlar yöntemi kullanılarak kapsamlı bir şekilde incelenmiştir. Sonuçlar, uzunluk arttıkça tüm TDKNT türlerinin doğal frekansının azaldığını göstermektedir. Ayrıca, çap ile doğal frekans arasında tutarlı bir ilişki görülemediğinden, çap büyüdükçe doğal frekansın artabildiği veya azalabildiği gözlemlenmiştir. Bu makalenin bir diğer amacı da atom boşluğu ve Stone-Wales kusurlarının etkilerini incelemektir. Çift boşluk kusurlarının TDKNT'lerin doğal frekansı üzerinde en fazla bozucu etkiye sahip olduğu görülmektedir. Bu araştırma, nano ölçekli teknolojilerin gelişmesine ve malzeme biliminin ilerlemesine katkıda bulunmayı hedeflemektedir.

Anahtar Kelimeler: Karbon nanotüpler, Doğal frekans, Titreşim, Stone-Wales kusurları, Boşluk kusurları

To my beloved family

ACKNOWLEDGMENTS

Embarking on this academic journey has been an enriching and transformative experience. I would like to express my heartfelt appreciation to my esteemed supervisor, Dr. Volkan Esat, for his unwavering guidance, insightful feedback, and unwavering support. His mentorship has been instrumental in shaping my academic growth and fostering my passion for research.

I would also like to extend my deepest gratitude to my mother and my sister. Their love, encouragement, and belief in my abilities have been the driving force behind my success. They have always been a source of strength and comfort, providing me with the support I needed to navigate the ups and downs of this journey.

Finally, I thank my family, friends, and everyone else who contributed to my academic pursuits. Your support, motivation, and belief in my potential have been a constant source of inspiration. I am truly humbled by your contributions and cherish the memories and lessons learned throughout this experience.

TABLE OF CONTENTS

LIST OF TABLES

TABLES

LIST OF FIGURES

FIGURES

LIST OF SYMBOLS

θ	Chiral angle (degrees)
$\emptyset$	Torsional angle (radians)
v	Poisson's ratio
2α	Rotation angle change (radians)
ΔL	Axial displacement change (nm)
Δr	Bond stretching variation (nm)
Δd	Diameter change (nm)
$\Delta\tau$	Increment of the twisting angle (radians)
$\Delta\phi$	Bond angle due to twisting
$\Delta\theta$	In-plane increment (radians)
A	Area of the cross-section (nm^2)
a	Length of the unit vector (nm)
C	CNT's Circumference (nm)
C_h	Chiral vector
d	Diameter (nm)
E	Young's modulus (TPa or Gpa)
F	Force (N)
G	Shear modulus (TPa or Gpa)
I	Moment of Inertia (nm^4)
J	Polar moment of inertia (nm^4)
k	Force constant (N/m)
k_θ	Bending resistance's force constant
k_τ	Torsional resistance's force constant
k_r	Bond stretching resistance's force constant
L	Length (nm)
M	Pure bending moment (N.m)
m	Chiral vector's index
n	Chiral vector's index

r	Distance between two interacting atoms (nm)
T	Applied torsion (N.m)
t	Thickness (nm)
U	Steric potential energy
U_r	Bond stretching energy
U_θ	Bond angle bending energy
U_φ	Dihedral angle torsion energy
U_{vdW}	Van der Waals energy
U_w	Out-of-plane torsion energy
$U_{electrostatic}$	Electrostatic potential energy

CHAPTER 1

INTRODUCTION

1.1 Significance of Carbon Nanotubes

Different researchers have increasingly investigated nanomaterials and nanotechnology in the past decades. The reason behind this increased focus on nanotechnology lies in the fact that it can lead various areas of research to nanoscopic level [2]. In 1991, Iijima discovered that cylindrically shaped carbon structures could be made by utilizing an arc-discharge evaporation technique [1]. Following his work, several researchers developed new synthesis techniques that made the production of these cylinders more plausible [2]. These cylinders were named carbon nanotubes. Carbon nanotubes (CNTs) have remarkable mechanical and electrical properties. These properties differentiate them from commonly used materials such as stainless steel and graphite fibers [3]. Owing to their exceptional characteristics, CNTs are energy efficient and can be used in different sectors. Since energy consumption and greenhouse gas emissions have been rapidly increasing over the past century, resulting in temperature rise on Earth, potential solutions are deemed necessary [2]. Therefore, carbon nanotubes can be one of the solutions to this critical issue that we as humans are facing right now.

Due to carbon nanotubes' exceptional properties, they are used in multiple industries such as agriculture, tools manufacturing, etc. Some different applications of carbon nanotubes in different industries are shown in Figure 1.1.

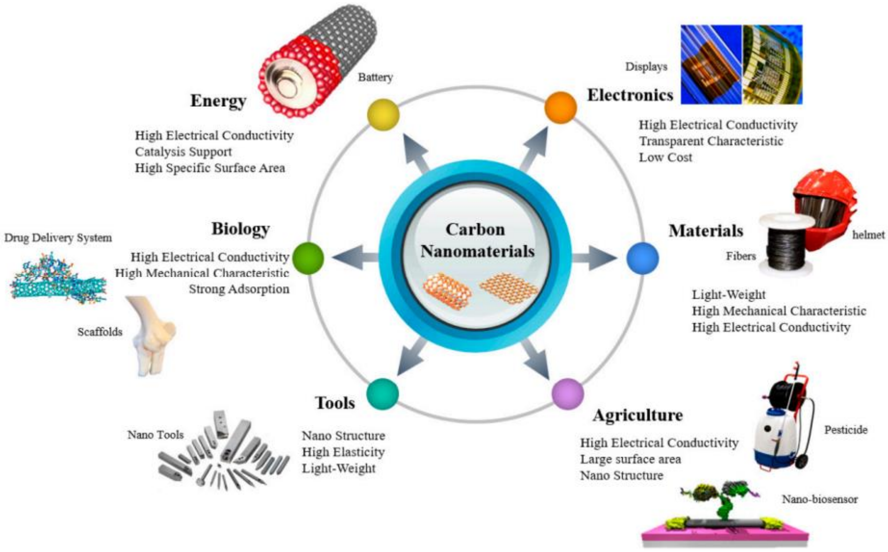

Figure 1.1: Different applications of carbon nanotubes in different sectors [8]

1.2 Geometry of Carbon Nanotubes

In simple terms, carbon nanotubes are just rolled-up graphene sheets. Thus, if we roll up a graphene sheet into a hollow cylinder-shaped configuration, its diameter differs between 1 to 50 nm, and its length is more than 10 μm CNTs are created.

The chiral vector C_h and the chiral angle θ are the primary parameters that are required to define the geometry of CNTs. Two-unit vectors named a_1 and a_2 and two integers named m and n are used to define the chiral vector of a CNT [5]. The following is the equation of the chiral vector [5]:

$$C_h = na_1 + ma_2 \tag{1.1}$$

As depicted in Figure 1.2, the fundamental structure of the CNTs is defined according to the chiral vector or which angle the graphene sheet has been rolled into a cylindrical-shaped structure.

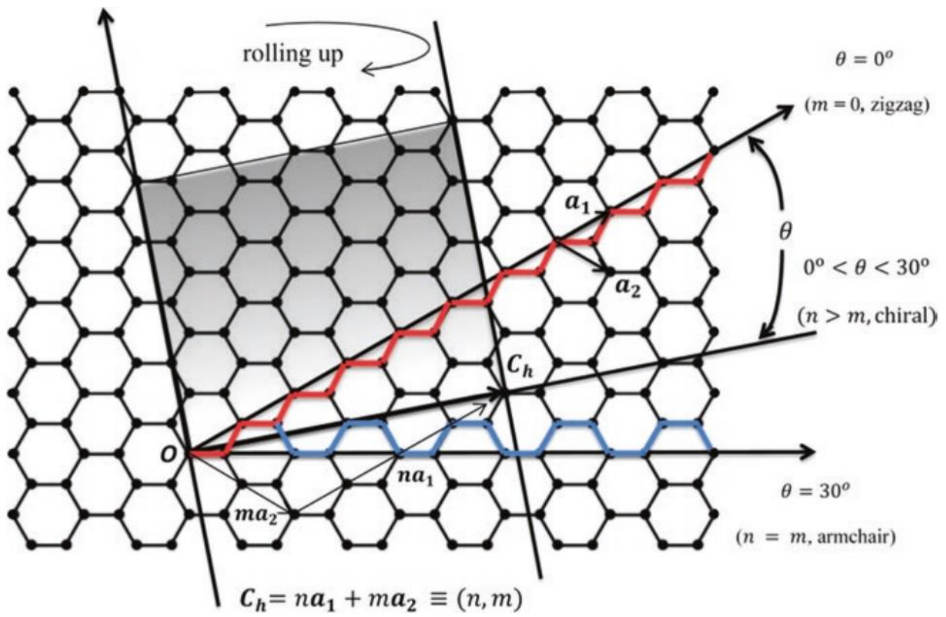

Figure 1.2: Illustration of a graphene sheet and geometrical characteristics for a CNT [6].

The following equation is used to calculate the diameter of a CNT [6]:

$$d_{CNT} = \frac{a_0\sqrt{m^2 + mn + n^2}}{\pi} \tag{1.2}$$

In Equation 1.2 (1.2), $a_0 = \sqrt{3}b$, where b = 0.142 nm which is the length of the length of the C-C bond in the nanotube [5].

The following formula is used for calculating the circumference of a CNT [5]:

$$L = |C_h| = a\sqrt{n^2 + m^2 + nm} \tag{1.3}$$

The chiral angle can also be evaluated using the following equation [5]:

$$\sin\theta = \frac{\sqrt{3}m}{2\sqrt{n^2 + m^2 + nm}} \tag{1.4}$$

$$\cos\theta = \frac{2n + m}{2\sqrt{n^2 + m^2 + nm}} \tag{1.5}$$

$$\tan\theta = \frac{\sqrt{3}m}{2n + m} \tag{1.6}$$

The carbon nanotubes are categorized into three different configurations based on the chiral vector values (m, n) or their chiral angle (θ) [6]:

1. Armchair: If m = n or its chiral angle (θ) is equal to 30 degrees, then the carbon nanotube is named armchair.
2. Zigzag: If m = 0 or its chiral angle (θ) is equal to 0 degrees, then the carbon nanotube is named zigzag.
3. Chiral: If $m \neq n \neq 0$ or its chiral angle (θ) is between 0 to 30 degrees, then the carbon nanotube is named chiral.

The rolling-up process and the side view for all three types of CNTs (armchair, zigzag, and chiral) are depicted in Figure 1.3 and Figure 1.4, respectively.

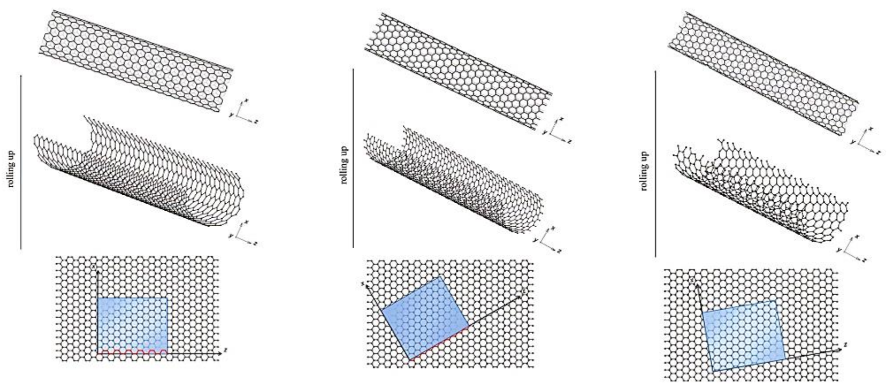

(1) (2) (3)

Figure 1.3: (1) Process of rolling a graphene sheet to an armchair CNT (2) Process of rolling a graphene sheet to a zigzag CNT, (3) Process of rolling a graphene sheet to a chiral CNT [6].

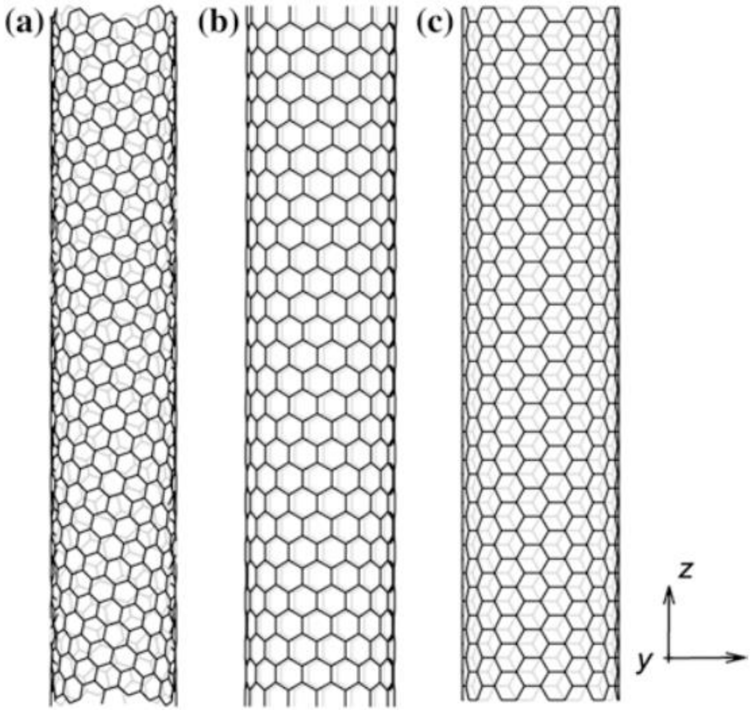

Figure 1.4: Side view of (a) Chiral (b) Zigzag (c) Armchair carbon nanotubes [6].

1.3 Types of Carbon Nanotubes

The number of graphene layers is the criteria used to classify the carbon nanotubes. Carbon nanotubes consisting of a single graphene layer are called single-walled carbon nanotubes (SWNTs). SWNTs diameter is between 0.4 to 2 nm [10]. The other class of carbon nanotubes is multi-walled carbon nanotubes (MWNTs). MWNTs are formed of two or more coaxial cylinders; each is a cylindrical-shaped graphene sheet (SWNT). The outer diameter of MWNT varies from 2 to 100 nm, and their inner is between 1 to 3 nm [10]. In MWNTs, the SWNTs are connected to each other by the van der Walls forces between the carbon atoms of different walls of the nanotube [6]. In order to calculate this force, the Lennard-Jones parameters are required [6]. A schematic illustration of single-walled and multi-walled carbon nanotubes is depicted in Figure 1.5.

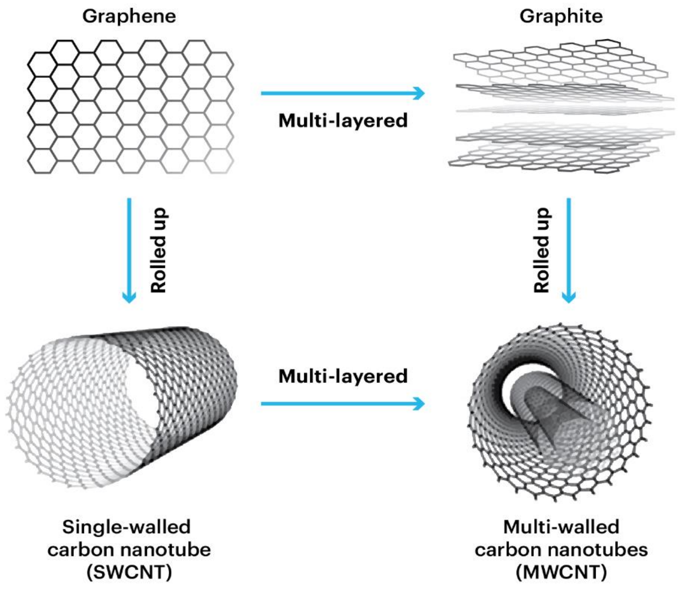

Figure 1.5: Schematic illustration of single-walled and multi-walled carbon nanotubes [9].

1.4 Defects in Carbon Nanotubes

While carbon nanotubes have exceptional mechanical and electrical properties, these properties can be significantly affected by defects in their structures [7]. These defects can be caused by external effects or throughout their synthesis process [7]. Some of the common defects in carbon nanotubes are vacancy defects, Stone-Wales defects, atomic substitutions, and chirality defects [6]. Vacancy defects appear once the nanotube lattice lacks carbon atoms in its structure [6]. As a result of these missing atoms from the structure of the nanotube, its mechanical properties and thermal conductivity get weakened [7]. Vacancies in carbon nanotubes may occur because of exposure to radiation or extremely high temperatures [7].

Another type of defect that can cause changes in the mechanical and electrical properties of a CNT is the Stone-Wales defect [6]. Stone-Wales defects happen as a result of the rotation of two carbon atoms inside the nanotube lattice, which causes the nearby bonds to restructure and form two heptagons and two pentagons instead of four hexagons [7]. Thermal or radiation stress is the leading cause of this defect [7]. Vacancy, di-vacancy, and Stone-Wales defects are shown in Figure 1.6.

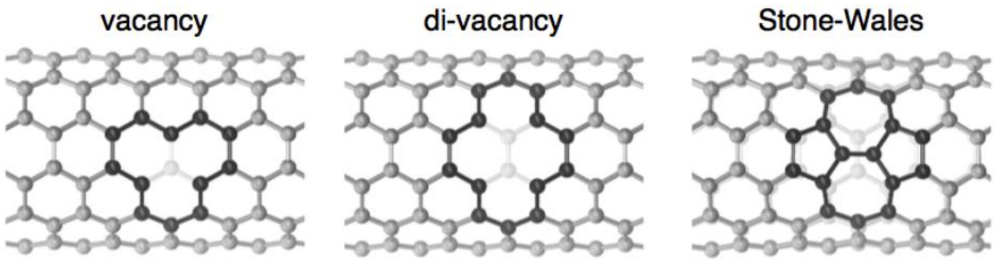

Figure 1.6: Illustration of vacancy, di-vacancy, and Stone-Wales defects [7]

Atomic defects and chirality defects are the other types of defects that can affect the properties of a CNT. Atomic defects happen when carbon atoms are substituted by other atoms, such as nitrogen or boron [12]. Furthermore, when the carbon nanotube deviates from its ideal chirality configuration, chirality defects appear [6]. As previously stated, depending on how the carbon atoms are arranged, each carbon nanotube has a specific ideal chirality configuration; when a CNT deviates from this configuration, chirality defects occur.

Carbon nanotube defects do not always have a negative impact on the material's properties. In some specific cases, these defects can be purposefully introduced into the nanotube to modify its properties and allow it to be used for a particular application. Optimization of carbon nanotubes for various applications necessitates a thorough understanding of these defects and how to incorporate them into a nanotube [6].

1.5 Mechanical Properties of Carbon Nanotubes

Carbon atoms are known to be able to sustain immense tensile stresses due to their covalent bonds (Figure 1.7) [8]. CNTs are also made of carbon atoms, which results in them having remarkable strength. For instance, the comparison between the tensile strength of steel and CNT indicates that CNTs are approximately 100 times stronger than steel [6,11]. A comparison between the ultimate tensile strength of some engineering materials with CNT is illustrated in Figure 1.9. Stiffness is also another property that is known to be high in CNTs. Their Young's modulus is approximately 1-5 TPa which is significantly higher than any other common engineering material. To give an example, CNT's Young's modulus is almost 4 times higher than steel [6,11]. In addition to their exceptional stiffness, CNTs are resilient even under severe deformation, frequently regaining their original form without permanent damage. The main reason behind this resilience is also the covalent bonds between the carbon atoms [11]. The comparison between Young's modulus of some engineering materials with CNT is shown in Figure 1.8. In addition to the exceptional mechanical properties, CNTs also have low density (around $1.3\,\frac{g}{cm^3}$) that makes them ideal for industries that require light-weight materials such as aerospace [11]. It is important to note that the mechanical properties of CNTs can differ due to changes in multiple parameters such as chirality, diameter, length, and presence of defects [6].

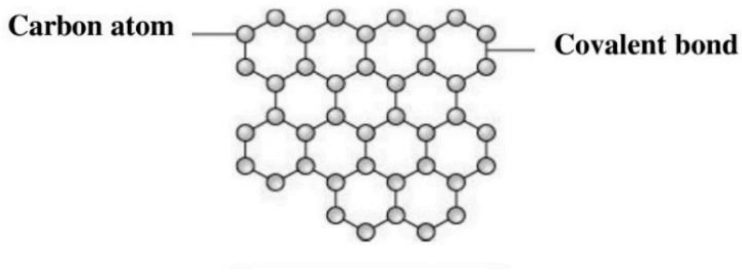

Figure 1.7: Conceptual design of a graphene sheet [8].

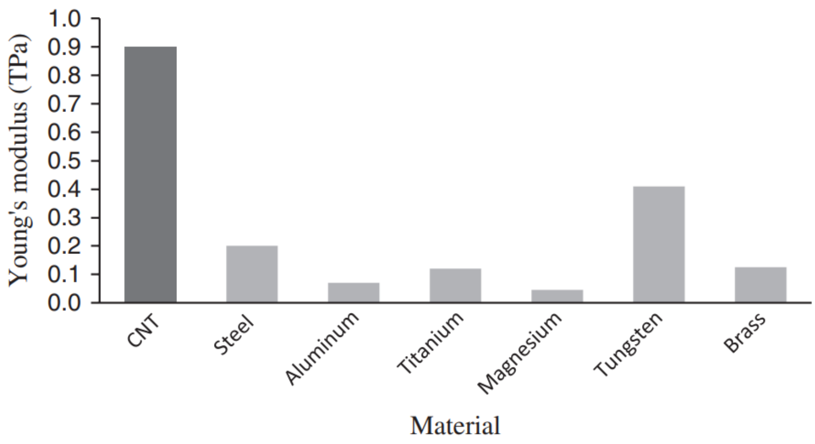

Figure 1.8: Comparison between Young's modulus of some engineering materials with CNT [6].

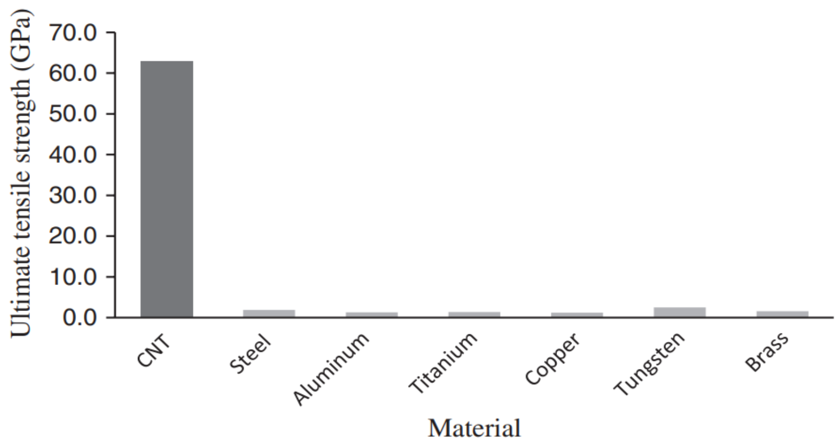

Figure 1.9: Comparison between the ultimate tensile strength of some engineering materials with CNT [6].

1.6 Sustainability Aspects of Carbon Nanotubes

Energy and the environment have been the primary topic of discussion regarding climate change [13]. Research indicates that environmental contamination and deterioration are mainly caused by greenhouse gas emissions from the consumption of fossil fuels, and this issue must be addressed in order to mitigate the detrimental effects of these emissions on the Earth [13]. Nanomaterials have been considered as one of the plausible solutions to this challenge, and their unique properties and potential for utilization in a variety of sectors have attracted significant scientific attention [13]. The following are the applications of CNTs that benefits the environment and save energy [13]:

- Application of carbon nanotubes with solar energy: Solar energy has been widely known as one of the most promising renewable energy sources around the world due to its abundance and widespread dispersion [13]. Carbon nanotubes have been utilized to increase the efficiency of solar cells through a variety of different methods [14,15]. One of these methods is implementing carbon nanotubes as counter electrodes, which has shown improvements in the transportation, performance, and photocurrent production of solar cells [14,15].
- Carbon nanotubes as greenhouse gas absorbents: The air quality of the Earth has been degraded due to air pollutants. Previously, unreliable traditional gas sensors have been used to improve air quality. Carbon nanotubes have shown great potential as gas-sensing materials due to their high capacity to absorb substances [16,17]. Materials that are integrated with carbon nanotubes have overcome the difficulties which are associated with pristine carbon nanotubes and are being utilized in different sectors to improve air quality [16,17].

- Carbon nanotube applications in wastewater treatment: Pathogens have always been challenging to extract from water due to their evasive nature. SWNTs possess' a high absorption capacity which can be implemented to extract pathogens from water. Thus, treatment-based applications incorporated with SWNTs have shown promising results [18,19].
- Carbon nanotube application in agriculture: Research indicated an immense potential for CNTs regarding plant and seed development [20,21,22]. The seeds treated with carbon nanotubes have shown increased water absorption and faster growth rate than regular seeds [21]. The exact mechanism behind this faster-paced growth is currently unknown. Moreover, researchers have found that CNTs integrated with cadmium can impair wheat development, while pristine CNTs increase the defensive capabilities of wheat seedlings [23]. An application of carbon nanotubes in agriculture is indicated in Figure 1.10.

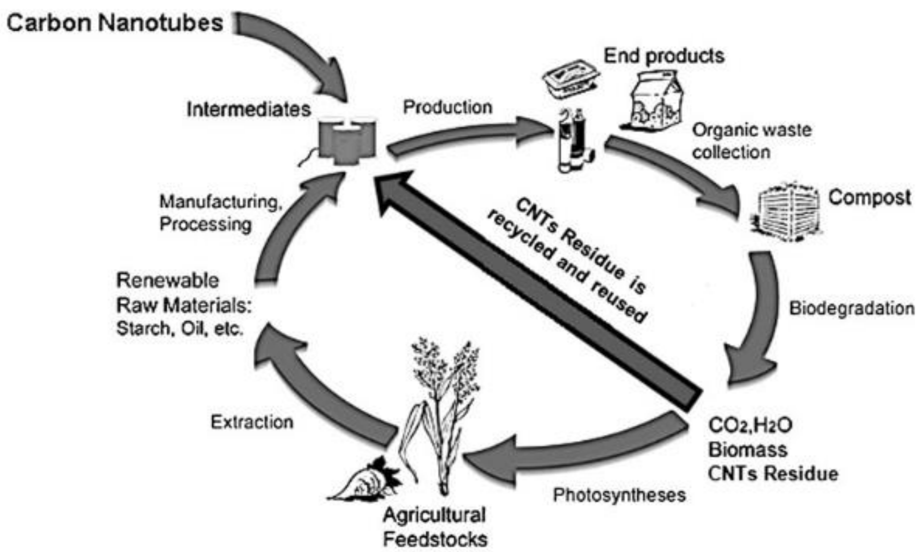

Figure 1.10: Implementation of carbon nanotubes in agriculture [13].

1.7 Aims and Objectives of the Thesis

The primary focus of this research is on the modal analysis of pristine and defective single-walled carbon nanotubes (SWNTs). Conducting modal analysis on SWNTs would lead to determining the natural frequencies and mode shapes of this material which is one of the major objectives of conducting this type of analysis. Determination of natural frequencies of different types of SWNTs (armchair, zigzag, and chiral) would help develop our knowledge further on the mode shapes of this material. Analyzing the mode shapes of SWNTs can further our understanding of the structure, symmetry, and stability of SWNTs. This more profound understanding of SWNT can be used in the optimization of SWNT-based equipment. It is also important to note that modal analysis of defective SWNTs also enables the enhanced evaluation of mechanical properties of this material, such as Young's modulus, Poisson's ratio, and bending stiffness. These properties are crucial for any implementation of SWNTs in different sectors. Therefore, a thorough assessment of them would lead to designing optimized nanoscale devices incorporated with SWNTs.

In conclusion, the main goal behind this research is to understand better how defects on SWNTs can affect the reliability, durability, and failure mechanism of materials that are being incorporated with SWNTs. Comprehension of the effect of defects would lead to researchers being able to lessen the negative impact of these defects while utilizing them to design desirable features such as mechanical flexibility or specialized optical responses.

CHAPTER 2

LITERATURE REVIEW

2.1 Review of Existing Literature on SWNTs

The vibrational properties of carbon nanotubes have been a fascinating field of research for researchers over the past two decades. This field has been thoroughly investigated and analyzed by numerous researchers, and they have established a solid foundation for the further development of research in this area. This section of the thesis is dedicated to discussing previous research in this area in addition to research on the synthesis of carbon nanotubes. A complete evaluation of existing research in this area would advance our knowledge and assist us in identifying potential gaps in the literature so that they could be addressed.

2.1.1 Synthesis Methods of Carbon Nanotubes

Since 1991, when the Japanese researcher, Iijima, has synthesized CNTs, synthesis methods of carbon nanotubes have been developing. Since then, the synthesis of this material has been done by seven different methods. These methods are the electric arc discharge method, laser ablation method, thermal synthesis process, chemical vapor deposition (CVD), vapor-phase growth, flame synthesis method, and plasma-enhanced chemical vapor deposition (PECVD) [2]. Many researchers have utilized the aforementioned seven methods. The pertinent research will be discussed in the following sections.

2.1.1.1 Electric arc discharge method

Arc discharge evaporation was the method that was initially used by Iijima (1991). He utilized this specific method to synthesize CNTs. In comparison to alternative methods, defects appear at a lower rate using arc discharge evaporation. A carbon-based electrode at approximately 1700 ℃ is exposed to an arc discharge so that at the negative end of the electrode, CNTs would be generated [1]. Several different metals, such as nickel and iron, along with graphite, are used in this process. The inclusion of catalysts to create CNTs is also optional using this method [24]. Still, the synthesis of MWNTs seems more plausible without catalysts than SWNTs [24]. Moreover, because this process uses a metallic catalyst, the properties of the nanotubes created are poor even though the number of CNTs synthesized is generally high [24]. Thus, the implementation of purification seems obligatory after creating CNTs through this process [24]. CNTs synthesized by Iijima are illustrated in Figure 2.1.

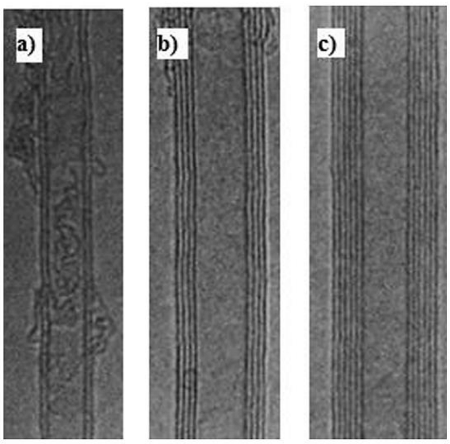

Figure 2.1: Indication of CNTs synthesized by Iijima [1]. These CNTs consist of multiple concentric shells [1]. In Figure (b), there is a closer look at CNTs depicted in Figure (a). Furthermore, Figure (c) provides an even more magnified view of CNTs shown in Figure (b).

2.1.1.2 Laser ablation method

Thess et al. (1996), using small quantities of Nickel and Cobalt at a high temperature (1200 ℃), implemented the laser ablation method to synthesize carbon nanotubes. In this method, the laser is used to vaporize the graphite required for making carbon nanotubes in a chamber, resulting in forming thin tubes with great diameters. Moreover, Since consistent pressure is needed for this method, helium, and argon are utilized. While this approach produces CNTs with excellent quality and purity and is cost-effective, the production is CNTs is much less compared to arc-discharge methods. CNTs created by this method are depicted in Figure 2.2.

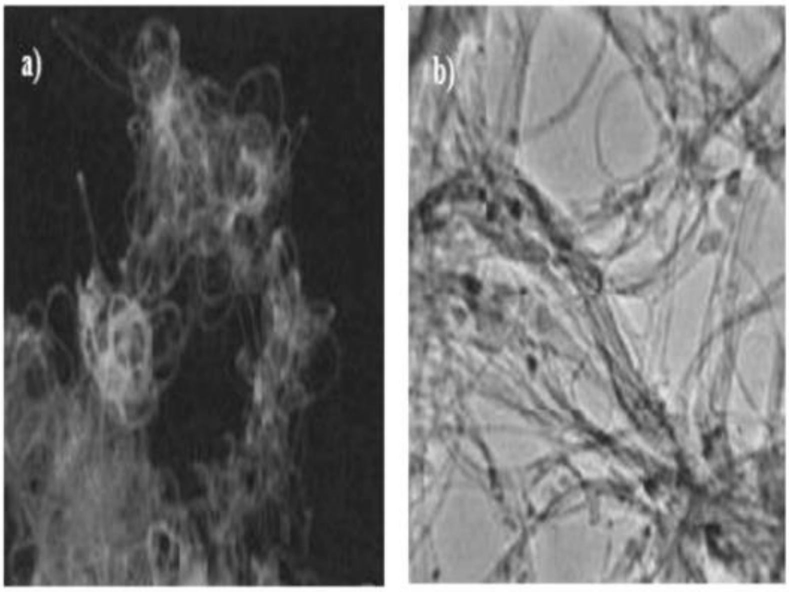

Figure 2.2: Illustration of CNTs synthesized using laser ablation method [25].

2.1.1.3 Thermal synthesis process

The aforementioned CNT production methods (arc-discharge and laser ablation) are synthesis methods that are plasma-based [2]. Thus, the temperature needs to be meticulously monitored for these techniques [2]. Additionally, there are other methods, such as plasma-enhanced chemical vapor deposition (CVD). These synthesis techniques utilize carbon feedstock as the main component, along with catalysts such as iron and nickel to synthesize CNTs [2]. Moreover, it is possible to incorporate extra active feedstock to ease the synthesis process. The thermal synthesis process is one of the methods that would facilitate the chemical vapor deposition process [2].

2.1.1.4 Chemical vapor deposition (CVD)

The currently employed synthesis methods for CNTs have two major setbacks. These setbacks are the necessity for purification of the synthesized CNTs, and the high temperature required to conduct these procedures. In 1996, chemical vapor deposition (CVD) was initially used to create CNTs [26,27]. The benefits of this method were that the growth conditions surrounding the production of CNTs could be controlled precisely, and the number of CNTs produced was substantial as well. CVD requires atmospheric pressure and utilizes two different configurations, which are horizontal and vertical [28]. In this method, the base material is heated in an oven while adding gases that contain carbon, such as methane, to the system. The nature of the experiment requires these gases to be gradually added to the chamber. Moreover, other gases, such as argon and hydrogen, are used as catalysts [28].

2.1.1.5 Vapor-phase growth [29]

Vapor phase growth is an advanced variation of the chemical vapor deposition (CVD) method where the substrate is not utilized. The lack of substrate will make the process of synthesizing CNTs more sophisticated. This method makes use of a metal as a catalyst along with two furnaces that are operating at low temperatures in the chamber. The first furnace is responsible for creating the catalytic particles. After that, they reach the second furnace, and the diffusion of carbon atoms leads to CNTs being produced. Some cases use argon as the catalyst. CNTs created by the vapor-phase growth method are depicted in Figure 2.3.

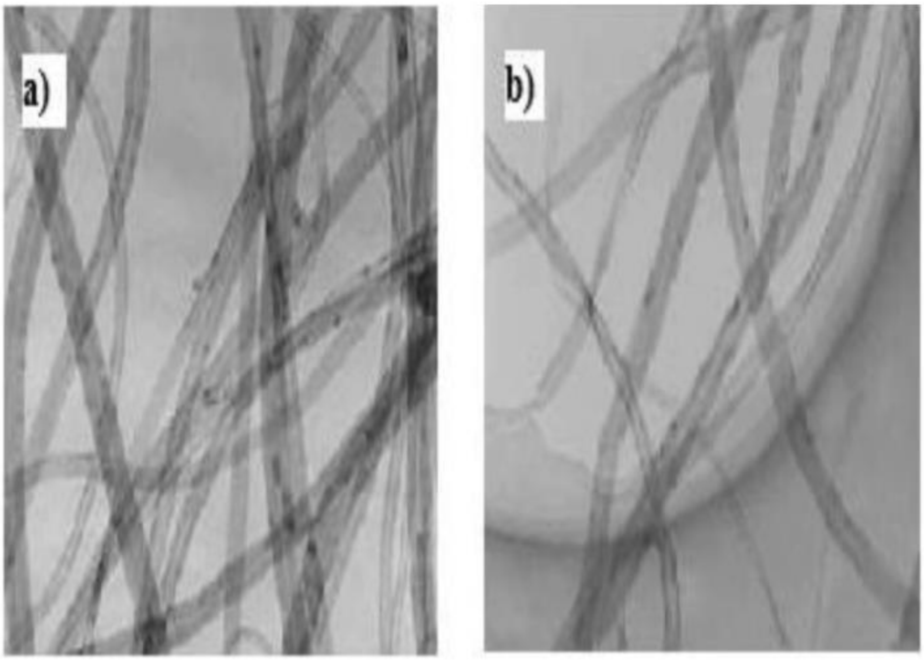

Figure 2.3: CNTs synthesized using vapor-phase growth method [29]

2.1.1.6 Flame synthesis method

An alternative method that is being used to synthesize CNTs is flame synthesis [30]. This process uses flame as a substrate to provide the environment required to produce different types of carbon nanotubes. Oxidizer integrated with varying gases of fuel like methane and acetylene is used to form the gaseous mixture needed for synthesizing CNTs. For ease of operation, the utilization of a catalyst is mandatory [30]. In contrast to other methods, flame synthesis reaches the required process in an authothermal process. In order to attain an appropriate environment for the synthesis, a vaporized catalyst might be necessary to add to the flame [30].

2.1.1.7 Plasma enhanced chemical vapor deposition (PECVD) [31]

Plasma enhanced chemical vapor deposition (PECVD) is an advanced method stemming from the chemical vapor deposition (CVD) method. PEVCD is more efficient than CVD in terms of temperature and regulating the development of CNTs. In general, PEVCD requires less temperature and produces more pure CNTs because of the plasmatic energy it uses to split the gas molecules that form the CNTs. PEVCD is the most efficient method to produce SWNT, which makes this method extremely crucial compared to previous ones. CNTs generated using plasma enhanced chemical vapor deposition method are depicted in Figure 2.4.

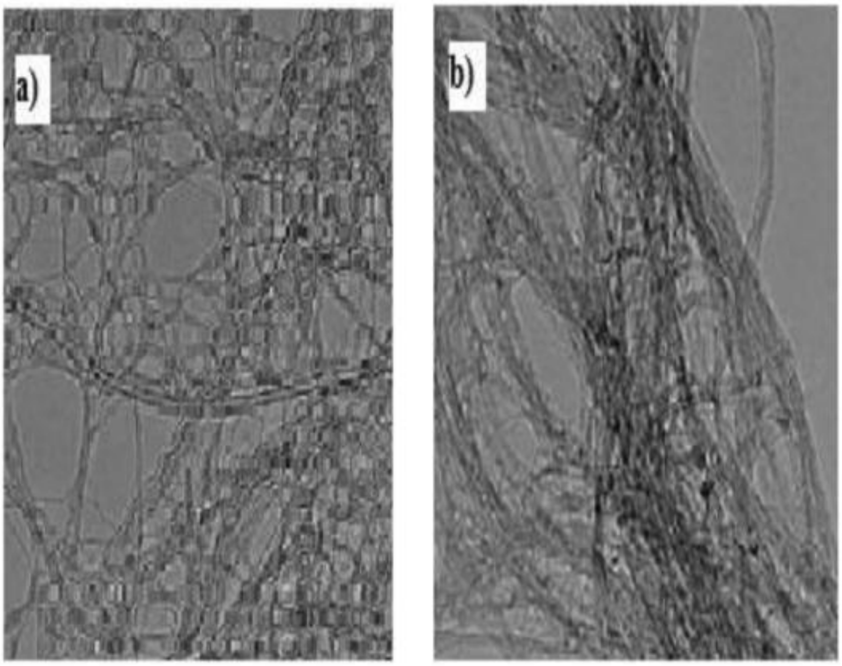

Figure 2.4: CNTs synthesized using plasma enhanced chemical vapor deposition method (PECVD) [31].

2.1.2 Vibration Analysis of Pristine SWNTs

Vibration analysis of pristine SWNTs has been done previously by multiple researchers using multiple methods, and this section is dedicated to the discussion of these methods.

Sakhaee-Pour et al. (2009) analyzed SWNTs' vibration using beam elements. Their work determined the natural frequency of bridge and cantilever SWNTs with different chirality, lengths, and diameters using finite element modeling. Using the same approach, Mir et al. (2008) conducted finite element modeling to determine the natural frequency of zigzag and armchair SWNTs. Arghavan and Singh (2011) studied the free and forced vibration of cantilever and bridge SWNTs by utilizing a mathematical model. Using this model, they reported different natural frequencies and mode shapes for several zigzag and armchair SWNTs. The first eight mode shapes of a (6,0) zigzag cantilever SWNT studied by Arghavan and Singh (2011) are illustrated in Figure 2.5. Chowdhury et al. (2010) used molecular mechanics approach to conduct vibrational analysis on zigzag and armchair SWNTs for different aspect ratios. Their results indicate that the increase in the aspect ratio of the nanotube will result in a decrease in its natural frequency. The vibration of SWNTs filled with water is studied by modeling the van der Waals (vdW) interaction between the water and the SWNT [54].

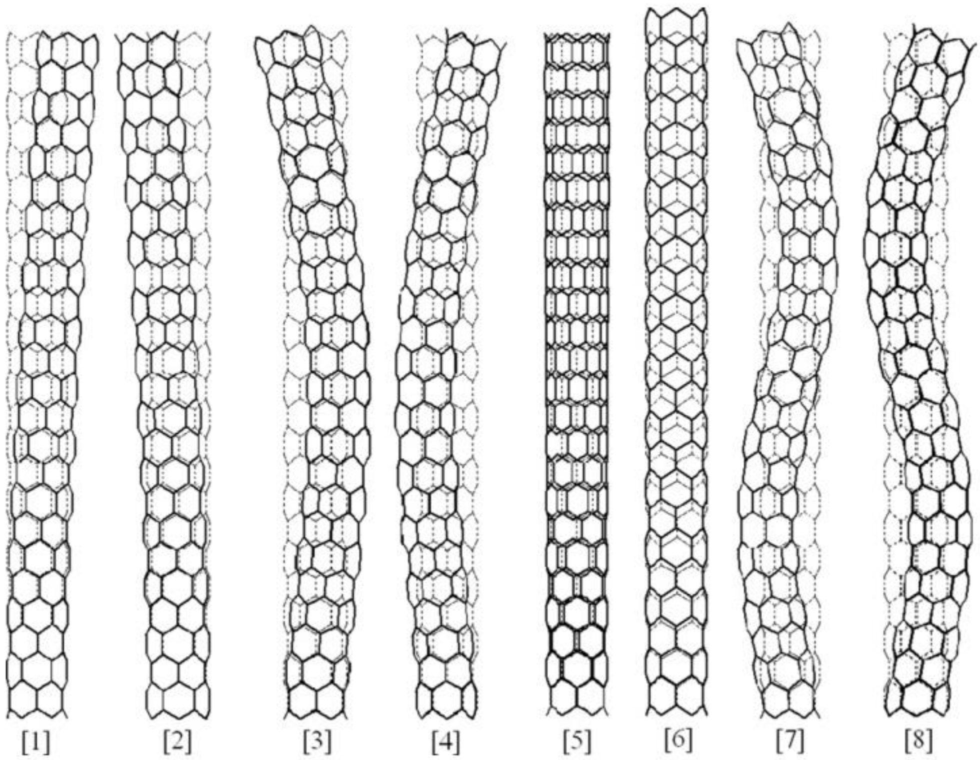

Figure 2.5: Mode shapes of the first eight natural frequencies of a (6,0) zigzag SWNT with cantilever boundary condition (Arghavan and Singh, 2011).

Bocko and Lengvarsky (2014) investigated the vibration of SWNT for four different boundary conditions using a continuum approach which is on the basis of the nonlocal theory of the beam. Fatahi-Vajari and Imam (2016) developed a fourth-order partial differential equation to investigate the natural frequency of SWNTs based on a novel approach called doublet mechanics which only incorporates the scale parameters and chirality effects. Using the same method, they also investigated the axial vibration of SWNTs [57]. Bensattalah et al. (2016) analyzed chirality and thermal effects on SWNTs by utilizing the nonlocal elasticity theory and the Euler–Bernoulli and Timoshenko beam theories to conduct free vibration analysis. Their results showed that the chirality of SWNTs affects the frequency ratio of SWNTs by a large percentage. Lee and Lee (2012) performed modal analysis on SWNTs and nanocones with varying disclination angles by conducting finite element modeling with the Ansys software (Figure 2.6).

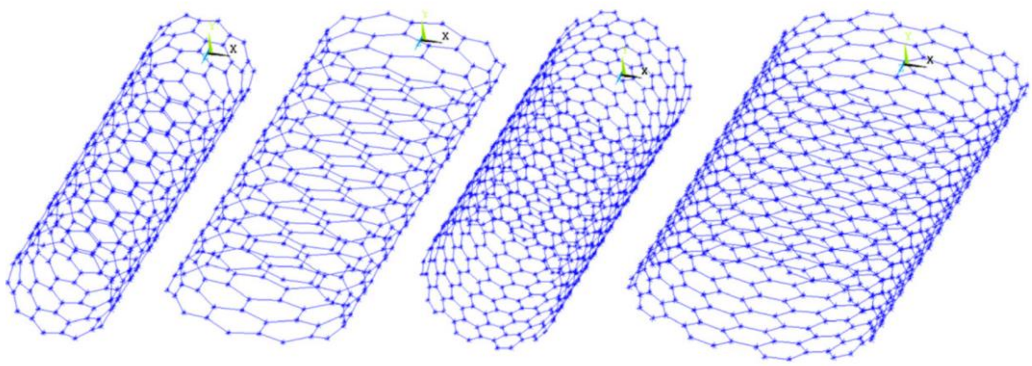

Figure 2.6: Finite element modeling of SWNTs with circle and ellipse sections (Lee and lee, 2012)

The first four mode shapes of the SWNTs with multiple lengths using the molecular dynamics method and Fourier analysis were investigated by Pine et al. (2014). Using the same method, Chang and Huang (2013) examined the vibrational behavior of SWNTs with different chirality. They studied the effects of various lengths and diameters on the vibrational behavior of SWNTs (Figure 2.7). Mungra and Webb (2015) incorporated a continuum mechanics approach to be able to model the vibrational behavior of SWNTs. By incorporating this method, they studied various SWNTs with different aspect ratios [61]. Moreover, their results showed that SWNTs have the potential to be implemented in different sensors in various industries [61]. By considering multiple tube wall thicknesses, lengths, and different boundary conditions of SWNTs, Ansari et al. (2012) studied the vibrational behavior of the SWNTs using a semi-analytical finite element method.

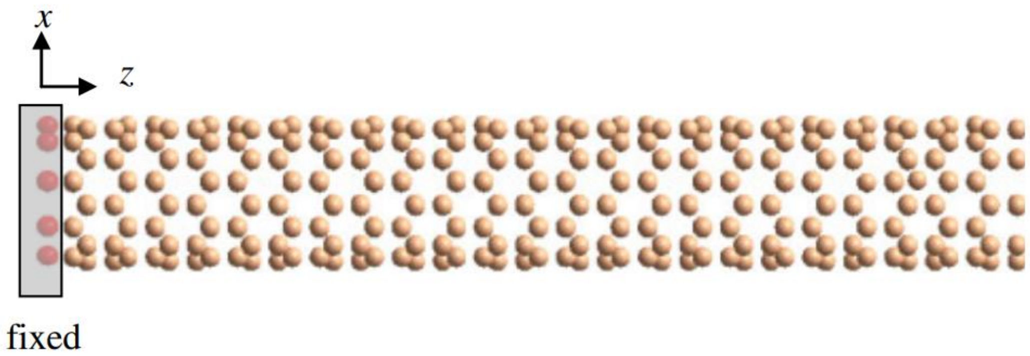

Figure 2.7: Atomistic simulation of a (9,0) cantilever zigzag SNWT (Chang and Huang, 2013).

2.1.3 Vibration Analysis of Defective SWNTs

Different researchers have studied the effects of defects on the structure of SWNTs. These defects can change the characteristics of SWNTs, and since synthesizing SWNTs usually results in their structures, it is evident that the impact of these defects is required to be studied. This section is dedicated to the methods previous researchers implemented while studying the vibrational behavior of defective SWNTs.

Talla et al. (2010) studied the changes in the resonant frequency of defective SWNTs that are affected by structural defects, especially Stone-Wales ones. They used resonance Raman spectroscopy to determine the natural frequencies of defective SWNTs [63]. Muc et al. (2013) conducted an axial vibration analysis of the defective SWNTs by using the Euler beam model, an orthotropic model, and 3D finite element modeling. Joshi et al. (2011) utilized the continuum mechanics method to perform dynamic analysis on cantilever SWNTs affected by pinhole defects with different chirality (Figure 2.8). Their results indicate that the natural frequency of the lengthier nanotube gets more affected by the defects, and the diameter of the nanotube is not as impactful as its length on the SWNT's natural frequency [65].

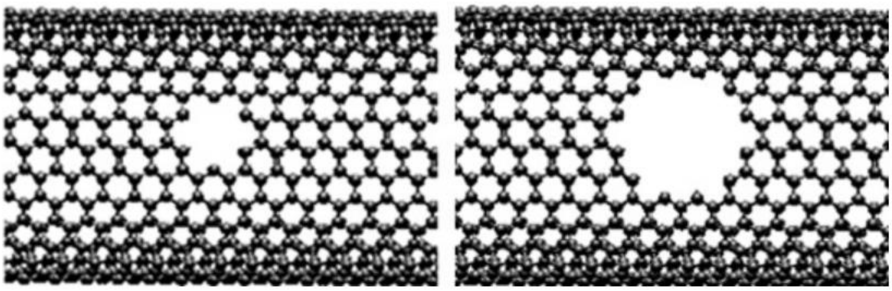

Figure 2.8: SWNTs with pinhole defect (Joshi et al., 2011).

Thorough conducting vibration analysis on SWNTs, Goel et al. (2020), using molecular dynamics simulations, studied a variety of parameters of defective SWNTs like aspect ratio, chirality, and the number of vacancy defects on the resonant frequency of cantilever SWNTs. Their results showed that the number of defects and how they are positioned on the SWNTs drastically affect the resonant frequency of the nanotube (Figure 2.9). Moreover, using a similar method, they analyzed the effects of hexa-vacancy defects on bridged SWNTs that indicated as the length of the nanotube increases, the effect of chirality on the resonant frequency of the nanotube decreases [67].

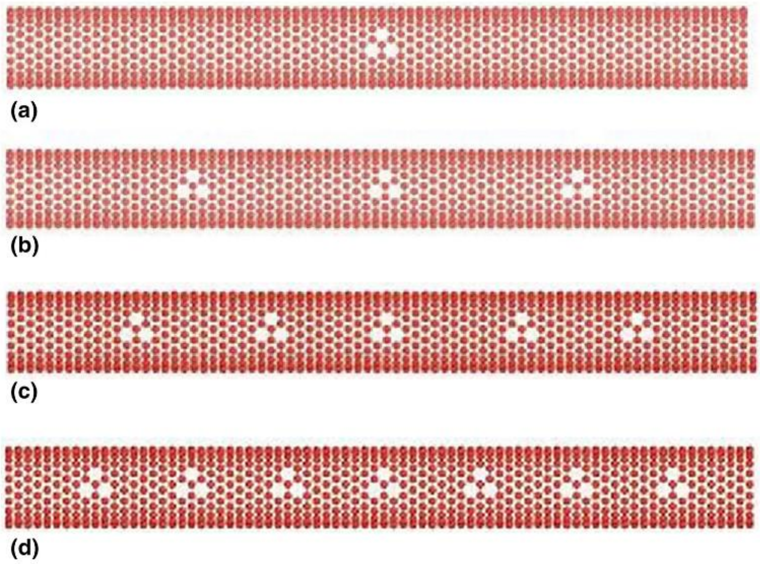

Figure 2.9: Molecular dynamics simulation with different number of defects on the nanotube. (a) one, (b) three, (c) five, and (d) seven defects (Goel et al., 2020).

Ghavamian et al. (2013) investigated the effect of randomly distributed defects on carbon nanotubes using finite element modeling. They studied the impact of Si-doping, carbon vacancy, and perturbation defects on SWNTs (Figure 2.10) [68]. The results showed that stability and the fundamental frequency of the nanotubes get reduced by introducing defects to the SWNTs structure [68]. Bedi et al. (2022) studied the effects of defects on the structure of defective and pristine SWNTs and graphene sheets by simulating the nanotubes using molecular dynamics. This study was conducted on cantilever SWNTs, and graphene sheets to determine the effects of aspect ratio and chirality while taking into account the number of defects on the fundamental frequency of SWNTs and graphene sheets [69]. The results of this study indicate that vacancy defects have a more significant impact than Stone-Wales defects on the natural frequency of Single-Walled Carbon Nanotubes (SWNTs) [69].

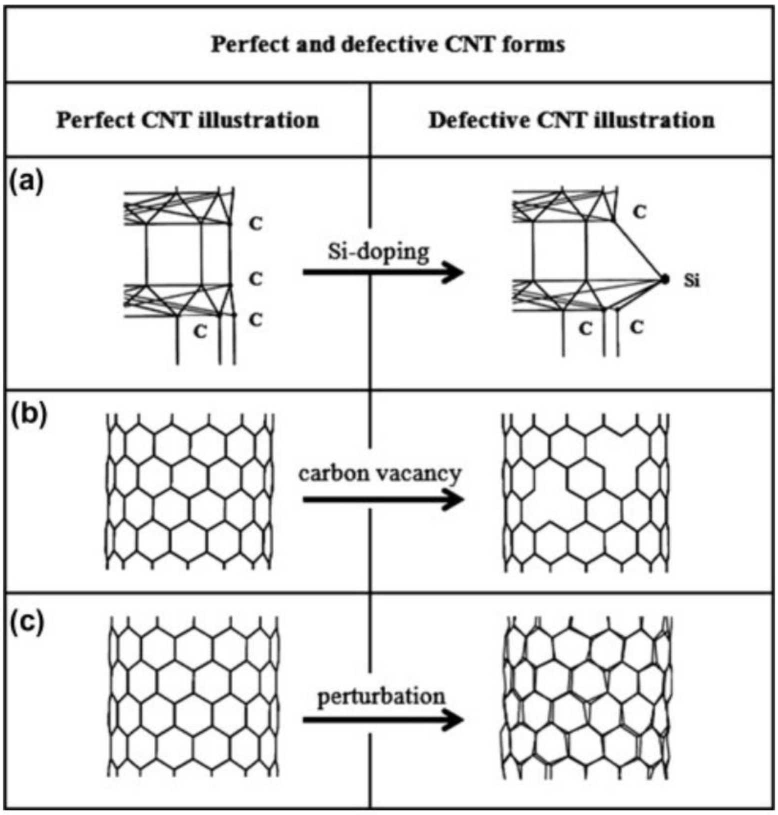

Figure 2.10: An illustration of Si-doping, carbon vacancy, and perturbation defects on SWNTs (Ghavamin et al., 2013).

Georgantzinos et al. (2014) employed a structural mechanics method to simulate the SWNTs with vacancy defects by using spring elements. The results of this study indicate that as the size of the vacancy defect increases, it has a greater impact on the fundamental frequency of the SWNT [70]. Chen et al. (2011) utilized 3D finite element models on the basis of continuum mechanics approach to study the effects of Stone-Wales and vacancy defects on SWNTs. They concluded that three of the crucial parameters which affect the vibrational properties of the SWNTs aside from the number of defects are length, diameter, and the defects' position [71]. Hudson et al. (2018) used order reduction methods to perform modal analysis on defective SWNTs. Furthermore, Parvane et al. (2011), and Shariati et al. (2014), studied the vibrational characteristics of pristine and defective SWNTs by employing the structural mechanics method.

2.2 Unaddressed Areas in Existing Research

Generally, the theories used for studying SWNTs are either molecular dynamics or structural mechanics. Several researchers have used these methods to study different characteristics of SWNTs. In the existing literature, molecular dynamics is more common than structural mechanics to simulate the SWNTs to study their vibrational behavior. Primarily, researchers utilizing molecular dynamics have studied the vibrational behavior of zigzag and armchair pristine SWTNs under different boundary conditions, lengths, and diameters. Therefore, the literature regarding defective SWNTs is quite scarce using this method.

Additionally, researchers who studied the SWNTs using the structural mechanics approach have studied the vibrational behavior of pristine armchair and zigzag SWNTs, and due to the difficulties of simulating chiral SWNTs in finite element modeling software, it has seldomly been investigated. Also, the vibrational behavior of defective SWNTs by utilizing the structural mechanics method has been analyzed only by a few researchers, and it is mostly regarding vacancy defects rather than Stone-Wales defects. Thus, this study aims to study the vibrational characteristics of pristine and defective armchair, zigzag, and chiral SWNTs to fulfill the gaps in the literature.

CHAPTER 3

THEORY AND METHODOLOGY

3.1 Equivalent-Continuum Modelling of SWNTs

3.1.1 Finite Element Modeling of Pristine SWNTs

The modeling of the SWNTs has been done by considering them as a frame structure while considering the bonds between the atoms as beam elements and the atoms of carbon as joints. The finite element modeling of the hexagonal lattice of the SWNT is indicated in Figure 3.1. The software used for this study is Marc Mentat 2020, which is used for conducting linear and nonlinear finite element modeling.

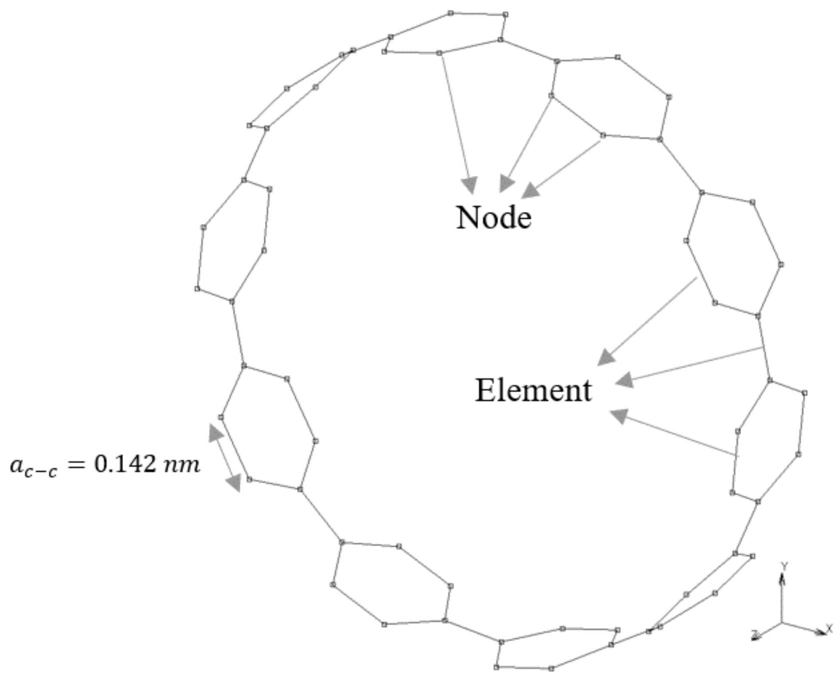

Figure 3.1: Finite element modeling concept of the repeating structure of a SWNT

The basis behind predicting the behavior of carbon-carbon (C-C) bonds is through understanding and implementing the concept of energy equilibrium state. In order to utilize this state, aside from the force constant of the molecular mechanics, the torsional, axis, and bending stiffness are also needed from structural mechanics [34-37]. The atomic interaction between the carbon atoms is indicated in Figure 3.2.

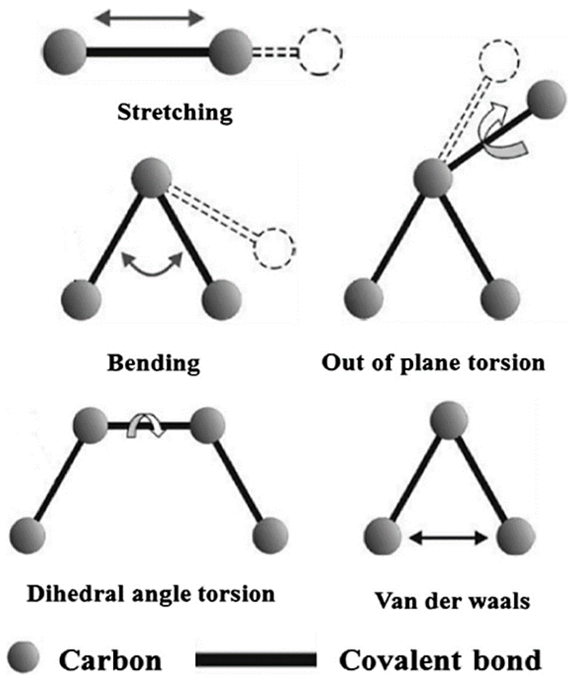

Figure 3.2: Interatomic interaction in molecular mechanics [32]

Equation 3.1 shows the steric potential energy. This equation indicates that the steric potential energy is the summation of bond stretching (U_r), bond angle bending (U_θ), dihedral angle torsion (U_φ), van der Waals (U_{vdW}), out-of-plane torsion (U_w), and electrostatic potential energy ($U_{electrostatic}$) [34-37].

$$U_{total} = \sum U_r + \sum U_\theta + \sum U_\phi + \sum U_w + \sum U_{vdW} + \sum U_{electrostatic} \tag{3.1}$$

Since bond stretching and bong angle bending are vital to the simulation, they were converted into a harmonic function indicated in Equation 3.2.

$$U(t) = \frac{1}{2}kx^2(t) = \frac{1}{2}kA^2\cos^2(\omega t - \varphi) \tag{3.2}$$

Other Equations necessary to calculate the total energy based on molecular mechanics theory are Equations 3.3, 3.4, and 3.5 which are the equations that are used to calculate bond stretching, bond angle bending, dihedral angle torsion, and out-of-plane torsion. In these equations $k_r, k_\theta, and\ k_\tau$ are the forced constant corresponding to each interatomic reaction related to the equation. Moreover, $\Delta r, \Delta\theta, and\ \Delta\phi$ are the changes in bond length, bond angle due to bending, and bond angle due to twisting, correspondingly [32].

$$U_r = \frac{1}{2}k_r(r - r_0)^2 = \frac{1}{2}k_r(\Delta r)^2 \tag{3.3}$$

$$U_\theta = \frac{1}{2}k_\theta(\theta - \theta_0)^2 = \frac{1}{2}k_\theta(\Delta\theta)^2 \tag{3.4}$$

$$U_\tau = U_\phi + U_w = \frac{1}{2}k_\tau(\Delta\phi)^2 \tag{3.5}$$

Using the Equations 3.6, 3.7, and 3.8, the axial elastic strain energy (U_N), bending elastic strain energy (U_M), and torsional elastic strain energy (U_T) of a beam can be calculated (Figure 3.3). In these equations, L is the distance between two carbon atoms ($a_{c-c} = 0.142\ nm$), and A, J and I are the geometrical characteristics of the beam corresponding to area of cross section, polar moment of inertia, and area moment of inertia which are given in Equation 3.9. Furthermore, $\Delta L, 2\alpha, \Delta\beta, E,$

$and\ G$ used in these equations are the displacement in axial direction, variation in rotation angle, twist angle, Young's moduli, and shear moduli, respectively [32].

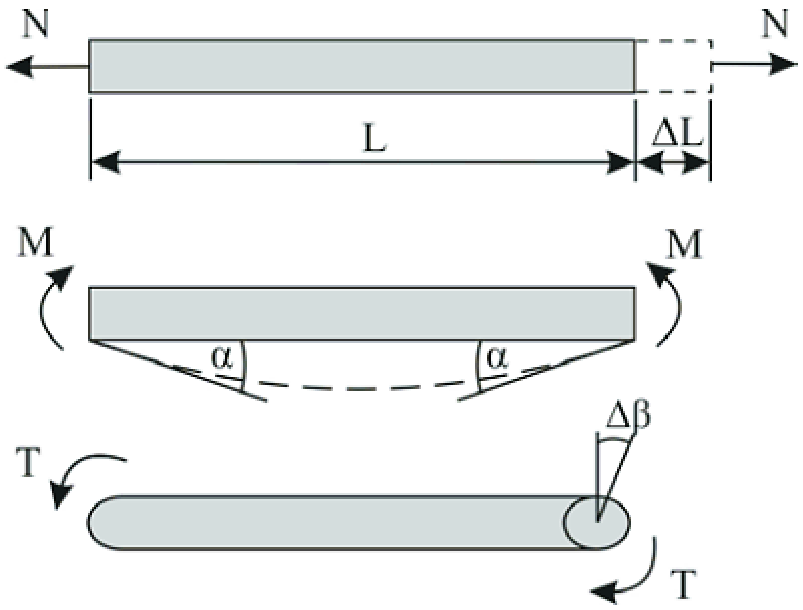

Figure 3.3: Depiction of a consistent beam subjected to solely tensile forces, a bending moment, and a torsion moment [33].

$$U_N = \frac{1}{2}\int_0^L \frac{F^2}{EA} dL = \frac{1}{2}\frac{F^2 L}{EA} = \frac{1}{2}\frac{EA}{L}(\Delta L)^2 \quad where \quad \frac{EA}{L} = k_r \tag{3.6}$$

$$U_M = \frac{1}{2}\int_0^L \frac{M^2}{EI} dL = \frac{2EI}{L}\alpha^2 = \frac{1}{2}\frac{EI}{L}(2\alpha)^2 \quad where \quad \frac{EI}{L} = k_\theta \tag{3.7}$$

$$U_T = \frac{1}{2}\int_0^L \frac{T^2}{GJ} dL = \frac{1}{2}\frac{T^2 L}{GJ} = \frac{1}{2}\frac{GJ}{L}(\Delta\beta)^2 \quad where \quad \frac{GJ}{L} = k_\tau \tag{3.8}$$

$$A = \frac{\pi}{4}\, d^2, \ \ I = \frac{\pi}{64}\, d^4, \ \ J = \frac{\pi}{32} d^4 \tag{3.9}$$

As mentioned before, in order to be able to model the SWNTs as frame structure, both the theories of molecular dynamics and structural mechanics should be considered. Thus, from the previous equations, three force constants are determined. These force constants are k_r, k_θ, k_τ [32]. These constants are the basis of the modeling of SWNTs as frame structures. In order to predict the linear behavior of SWNTs, these constants need to be determined. Therefore, several researchers have studied how these constants can be calculated. One of the first and most prominent studies that have been done on these constants was conducted by Li and Chou (2003), which was later verified by applying them to graphite. The values for these constants are given in Equation 3.10 [38].

$$k_r = 652\frac{nN}{nm},\ k_\theta = 0.867\ nN.\frac{nm}{rad^2}\ , k_\tau = 0.278\ nN.\frac{nm}{rad^2} \tag{3.10}$$

Li and Chou (2003) neglected the effect of out-of-plane torsion in their analysis. This assumption did not take into account the bending resistance of SWNT. Thus, other researchers, such as Tserpes and Papanikos (2005), using the approach implemented by Li and Chou (2003), got the values for *E* and *G* as 5.49 TPa and 871 GPa, respectively. These values of *E* and *G* give the value of Poisson's ratio as 2.15, which can be only feasible if the material is anisotropic. That indicates the values for $U_T\ and\ U_M$ are flawed [41]. In order to overcome these flaws, Scarpa and Adhikari (2008) incorporated a different method to calculate Young and shear modulus that are given in Equations 3.11 and 3.12.

$$E = \frac{4k_r L}{\pi d^2} \tag{3.11}$$

$$G = \frac{32 k_\theta L}{\pi d^4} \tag{3.12}$$

Using the equation $G = E/2(1 + v)$, Scarpa and Adhikari (2008) determined the values for the cross-sectional parameters of the beam. These cross-sectional characteristics of the circular beam element utilized in C-C bond finite element modeling are given in Table 3.1. The simulation of the bonds between the carbon atoms was conducted using a 3D beam element named Type 98. The beam nodes consist of six degrees of freedom, with three related to rotational movement around the x, y, and z axes, and the remaining three associated with translational movement along the x, y, and z axes. The aforementioned beam and values are used by Zuberi and Esat (2016) and also in this study. The benefit of incorporating this element is that it indicates both linear and nonlinear elastic material behavior in addition to its transverse shear effect [43].

Table 3.1: Cross-sectional characteristics of the circular beam element utilized in C-C bond finite element modeling.

Bond Length (L)	Bond Diameter (d)	Young's Modulus (E)	Shear Modulus (G)	Poisson's ratio (v)
0.142 nm	0.0844 nm	16.71 TPa	8.08 TPa	0.034

The simulation of SWNTs was done in Marc Mentat software. An illustration of finite element model of an armchair (12, 12) SWNT is indicated in Figure 3.4.

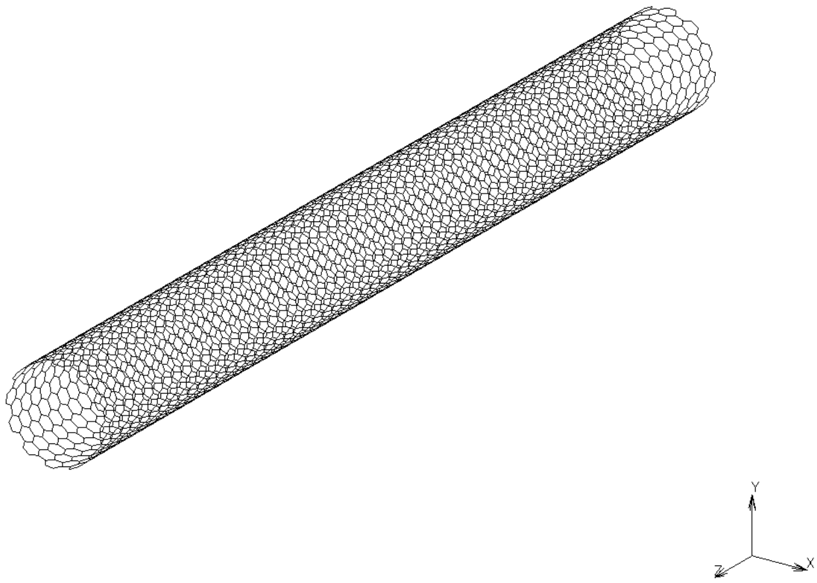

Figure 3.4: Finite element model of an armchair (12,12) SWNT.

This study's main aim is to determine the natural frequencies and mode shapes of different pristine and defective SWNTs. So, calculating the natural frequencies of the SWNTs is not possible without its geometry, mass, and boundary conditions [44]. In addition, the density of the beams is also necessary [44]. The geometry of the SWNTs is already defined, and the boundary conditions will be discussed later in this chapter. Still, the mass and density have not been discussed yet. Thus, it is assumed that the mass of each carbon atom, which is modeled as nodes with extremely small diameters without any rotational degrees of freedom, is $1.9943 * 10^{-29}$ tonne [44]. Furthermore, the density of the beams is considered as $2.3 * 10^{-27}\ tonne/nm^3$ [44]. The geometry of the mass element implemented in this study is depicted in Figure 3.5.

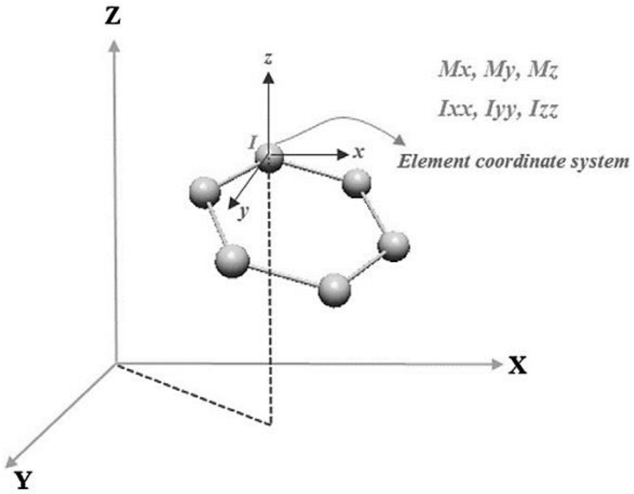

Figure 3.5: Geometry of the mass element used for SWNT simulation [44].

3.1.2 Finite Element Modeling of Defective SWNTs

The simulation of the frame structure of the defective SWNTs is similar to pristine SWNTs, which is discussed in the previous section. The difference between these two types of SWNTs is defects that are introduced to the structure of the SWNT analyzed. Two types of defects are introduced to the structure of SWNTs for this study. These defects are named vacancy and Stone-Wales defects. The process of implementing them into an SWNT structure is depicted in Figure 3.6. Moreover, this study aims to depict how introducing these defections would impact the natural frequency of different types of CNTs in cantilever and bridge boundary conditions. Thus, up to six defects are implemented in the structure. The location of these defects is illustrated in Figure 3.7.

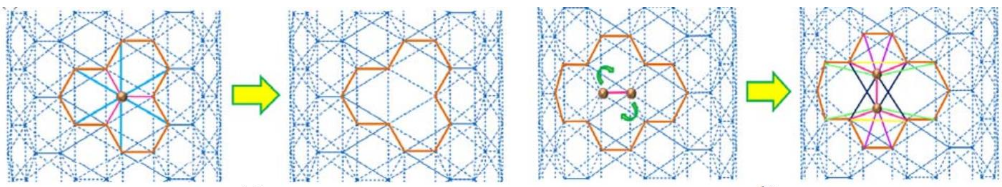

Figure 3.6: Process of introducing (a) vacancy defect (b) Stone-Wales defect into the SWNTs structure [45].

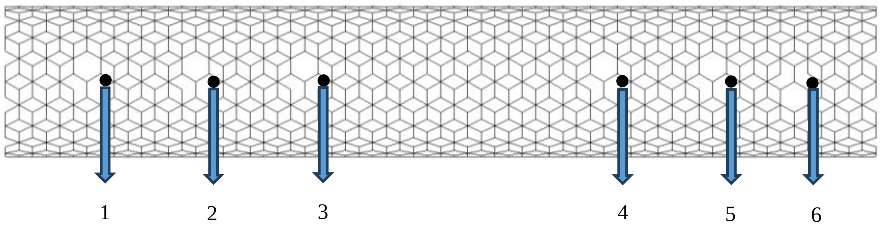

Figure 3.7: Selected location of the defects introduced to the SWNT structure.

3.1.3 Characteristics and Boundary Conditions of SWNTs

This study aims to determine various natural frequencies and mode shapes of armchair, zigzag, and chiral pristine and defective SWNTs. In order to do that, armchair, zigzag, and chiral SWNTs are analyzed in different lengths and diameters using Marc Mentat finite element modeling software. The SWNTs diameters, chirality, and lengths investigated in this study are indicated in Table 3.2, Table 3.3, Table 3.4, Table 3.5,

Table 3.6, and Table 3.7. The diameter and lengths studied from different types of carbon nanotubes were chosen approximately close to one another so that the results of them can be compared. Furthermore, two boundary conditions for the modal analysis of SWNTs are studied. These boundary conditions are cantilever and bridge, that are indicated in Figure 3.8, and Figure 3.9, respectively.

Table 3.2: Characteristics of armchair SWNT models.

Armchair SWNTs	Diameter (nm)	Chirality (deg)
(3,3)	0.4068	30
(5,5)	0.678	30

(10,10)	1.356	30
(12,12)	1.6272	3

Table 3.3: Lengths utilized for finite element modeling of armchair SWNTs.

Length (nm)	0.9838	1.9676	3.9352	7.8704	15.7408

Table 3.4: Characteristics of zigzag SWNT models.

Zigzag SWNTs	Diameter (nm)	Chirality (deg)
(5,0)	0.391444	0
(10,0)	0.782887	0
(15,0)	1.174331	0
(20,0)	1.565774	0

Table 3.5: Lengths utilized for finite element modeling of zigzag SWNTs.

Length (nm)	1.136	1.988	4.118	7.952	15.62

Table 3.6: Characteristics of chiral SWNT models.

Chiral SWNTs	Diameter (nm)	Chirality (deg)
(4,2)	0.414265	19.1
(8,4)	0.82853	19.1
(12,6)	1.242795	19.1

(16,8)	1.65706	19.1

Table 3.7: Lengths utilized for finite element modeling of chiral SWNTs.

Length (nm)	1.12788	2.25576	4.51152	7.89516	15.79032

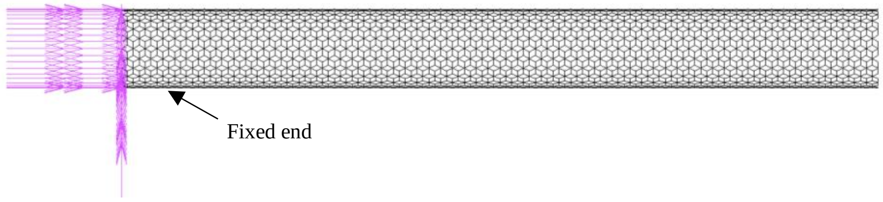

Figure 3.8: Illustration of Cantilever Boundary Condition for a SWNT

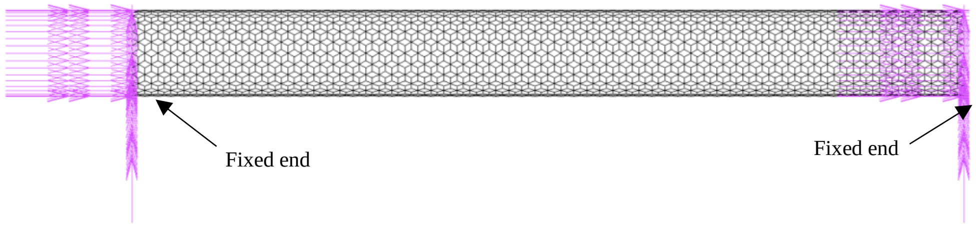

Figure 3.9: Illustration of the Bridge Boundary Condition for a SWNT

3.2 Model Validation

Using the finite element modeling discussed in the previous sections, the frame structure of different types of SWNTs is modeled in Marc Mentat 2020 software by using beam element type 98 to connect the C-C bonds. Furthermore, after modeling the geometry, the boundary conditions and carbon atom masses are specified in the software so that the modal analysis of different types of SWNTs can be conducted. By conducting the modal analysis, the natural frequency and the mode shapes of these SWNTs can be extracted from the software.

As the main purpose of this study is to determine the natural frequency of SWNTs with different lengths and diameters, an armchair SWNT was modeled with a length of 7.383 nm and a diameter of 0.814 nm. Our results were compared with the results obtained by Sakhaee-Pour et al. (2009). The results are depicted in Figure 3.10. While Sakhaee-Pour et al. (2009) employed an experimental equation to simulate SWNTs, our study took a different approach. Still, the results obtained from our study exhibit strong agreement with this study, thus validating our model for further investigation. The model utilized by Sakhaee-Pour et al. (2009) was later used by other researchers in later years, which indicates the validity of this model [47,48].

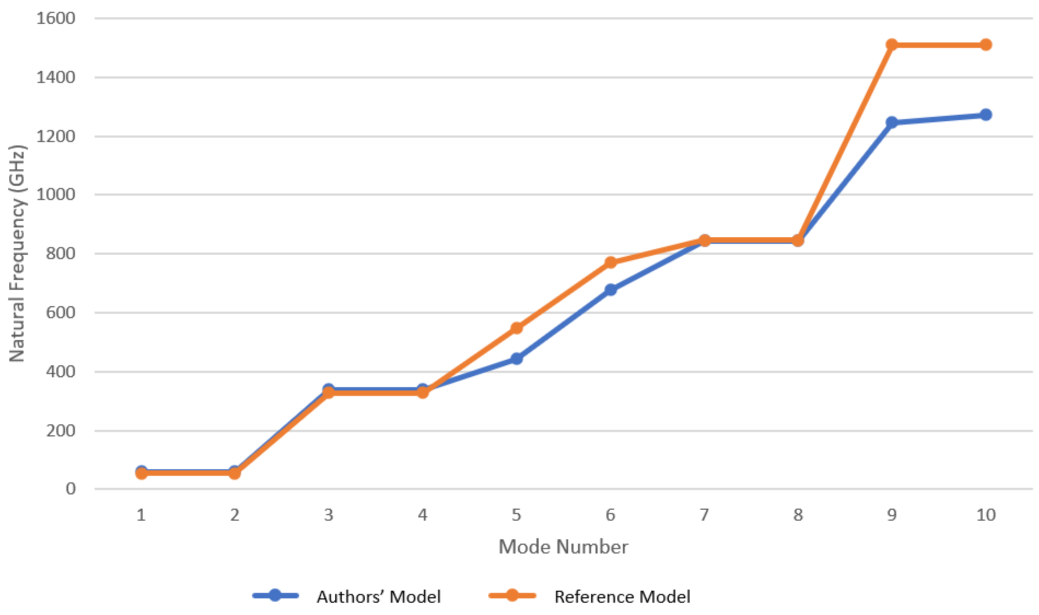

Figure 3.10: Comparison between author's model and Sakhaee-Pour et al. (2009) for an armchair SWNT with a length of 7.383 nm and diameter of 0.814 nm.

In Figure 3.10 variations in specific mode numbers may have been caused by differences in mechanical properties or modeling approaches applied to the studied single-walled carbon nanotubes (SWNTs).

CHAPTER 4

RESULTS AND DISCUSSION

4.1 Modal Analysis of Pristine Carbon Nanotubes

Understanding the dynamic behavior of materials is possible by conducting modal analysis on them [44]. SWNTs are no exception, and to understand their dynamic characteristics, modal analysis is required to be conducted. Thus, this section is dedicated to analyzing the modal behavior of pristine SWNTs with cantilever and bridge boundary conditions. The natural frequency and mode shapes of SWNTs with different diameter, length, and chirality can be determined by conducting modal analysis. Understanding the dynamic behavior of SWNTs helps scientists and engineers to predict the instability and failures associated with this material [44]. Moreover, it can be used to design and optimize SWNT-based structures by predicting the natural frequencies that can be used for different applications, such as nanoscale sensors. In summary, comprehending the vibrational characteristics of SWNTs with different boundary conditions leads to a better understanding of their mechanical properties and supports the development of innovative nanoscale applications [44].

4.1.1 Cantilever Boundary Condition

Modal analysis of pristine armchair, zigzag, and chiral SWNTs has been conducted under cantilever boundary condition (Figure 3.8). Four different SWNTs have been chosen for different configurations of the nanotube. The following SWNTs are being analyzed in this study:

- Armchair (n=m): (3,3), (5,5), (10,10), and (12,12)
- Zigzag (n,0): (5,0), (10,0), (15,0), and (20,0)

- Chiral (n≠m): (4,2), (8,4), (12,6), and (16,8)

The reason behind the selection of these SWNTs for each configuration is that their diameter is similar (Table 3.2, Table 3.4, and

Table 3.6). Therefore, their results are comparable. These nanotubes are being studied in 5 different lengths so that the effect of length on the natural frequency of SWNTs can be comprehensively examined and understood (Table 3.3, Table 3.5, and Table 3.7). Due to the nature of the SWNTs modeling, the lengths for armchair, zigzag, and chiral cannot be the same, but the modeling was done in a way that the five lengths studied are for all these three configurations are close.

The outcomes of the modal analysis of the pristine armchair SWNTs are depicted in Table 4.1, Table 4.2, Figure 4.1, and Figure 4.2. Additionally, the modal analysis results for pristine zigzag SWNTs are demonstrated in Table 4.3, Table 4.4, Figure 4.3, and Figure 4.4. Similarly, the modal analysis results of pristine chiral SWNTs are shown in Table 4.5, Table 4.6, Figure 4.5, and Figure 4.6. Furthermore, the mode shapes of a cantilever armchair (10,10) SWNT are depicted in Figure 4.7.

Table 4.1: Natural frequencies (GHz) of a cantilever armchair (a) (3,3), and (b) (5,5) SWNT

(a)	Length (nm)	0.9838	1.9676	3.9352	7.8704	15.7408
Mode Number	1	1073	336	92	24	6
	2	1073	336	92	24	6
	3	2665	1345	509	143	37
	4	3766	1526	509	143	37
	5	3766	1526	676	339	103
	6	4326	2300	1168	380	103
	7	4326	3326	1235	380	170
	8	4431	3326	1235	588	197
	9	5425	4036	2028	697	197
	10	5538	4266	2084	697	295
	11	5538	4266	2084	1016	317
	12	7681	4868	2994	1070	317
	13	7681	4869	2994	1070	460
	14	7925	5159	3380	1480	460
	15	7925	5159	3482	1480	509
(b)	Length (nm)	0.9838	1.9676	3.9352	7.8704	15.7408
Mode Number	1	1461	513	149	39	10
	2	1461	513	149	39	10
	3	1822	1438	723	228	61
	4	1822	1657	743	228	61
	5	2844	1657	743	363	166
	6	3591	1960	1167	579	166
	7	3591	1960	1643	579	182
	8	4143	2101	1643	588	295
	9	4143	2101	1684	1015	312
	10	4204	2298	1684	1015	312
	11	4472	3180	1732	1088	492
	12	4491	3180	1732	1498	492
	13	4491	3941	1962	1498	545
	14	5456	3941	1962	1643	697
	15	5456	4234	2170	1643	697

Table 4.2: Natural frequencies (GHz) of a cantilever armchair (a) (10,10), and (b) (12,12) SWNT

(a)	Length (nm)	0.9838	1.9676	3.9352	7.8704	15.7408
Mode Number	1	1108	553	266	76	20
	2	1108	553	266	76	20
	3	1402	773	426	374	116
	4	1402	773	426	384	116
	5	1731	1191	685	384	188
	6	1731	1191	685	411	295
	7	2314	1484	747	411	296
	8	2314	1495	1022	451	296
	9	2682	1495	1022	451	410
	10	2932	1689	1160	587	410
	11	3077	1689	1160	592	416
	12	3078	2188	1166	592	416
	13	3091	2188	1266	837	434
	14	3091	2213	1266	837	434
	15	3141	2213	1274	876	476
(b)	Length (nm)	0.9838	1.9676	3.9352	7.8704	15.7408
Mode Number	1	1106	495	302	89	24
	2	1106	495	302	89	24
	3	1138	825	312	287	135
	4	1138	825	312	287	135
	5	1704	857	652	347	188
	6	1705	857	652	347	284
	7	1705	1441	749	376	284
	8	1705	1441	809	425	292
	9	2344	1488	809	425	292
	10	2554	1498	937	543	295
	11	2554	1498	937	543	321
	12	2783	1558	1067	587	321
	13	2783	1558	1067	803	336
	14	2843	1973	1165	828	336
	15	2843	1973	1263	834	386

Table 4.3: Natural frequencies (GHz) of a cantilever zigzag (a) (5,0), and (b) (10,0) SWNT

(a)	Length (nm)	1.136	1.988	4.118	7.952	15.62
Mode Number	1	777	285	71	19	5
	2	777	285	71	19	5
	3	2440	1438	423	120	32
	4	3385	1515	423	120	32
	5	3385	1515	709	329	88
	6	3593	2112	1040	329	88
	7	5217	3540	1114	370	171
	8	5217	3540	1114	543	171
	9	5942	4229	2021	628	189
	10	5942	5148	2021	628	278
	11	6817	5148	2115	1008	281
	12	6817	5379	3061	1008	281
	13	6920	5379	3061	1109	415
	14	7892	5633	3112	1454	415
	15	7892	5633	3491	1454	568

(b)	Length (nm)	1.136	1.988	4.118	7.952	15.62
Mode Number	1	1267	547	150	43	11
	2	1267	547	150	43	11
	3	1455	1297	712	248	69
	4	1455	1297	762	248	69
	5	2450	1445	762	372	187
	6	3110	1838	1091	570	187
	7	3110	1838	1253	632	190
	8	3657	2063	1253	632	291
	9	3657	2063	1340	1112	353
	10	3740	2214	1340	1112	353
	11	3740	3132	1605	1114	556
	12	3755	3132	1605	1245	556
	13	4707	3563	1735	1245	570
	14	4707	3563	1735	1262	789
	15	5690	3891	2100	1262	789

Table 4.4: Natural frequencies (GHz) of a cantilever zigzag (a) (15,0), and (b) (20,0) SWNT

(a)	Length (nm)	1.136	1.988	4.118	7.952	15.62
Mode Number	1	976	654	217	64	17
	2	976	654	217	64	17
	3	1451	704	563	343	102
	4	1451	704	563	343	102
	5	1733	1446	712	372	190
	6	1733	1520	742	551	268
	7	2452	1520	742	551	268
	8	2818	1606	925	575	294
	9	2818	1606	925	581	484
	10	3073	2045	1101	581	484
	11	3073	2045	1240	681	549
	12	3129	2173	1240	681	549
	13	3129	2173	1565	812	554
	14	3661	2230	1565	812	554
	15	3661	2872	1650	882	568
(b)	Length (nm)	1.136	1.988	4.118	7.952	15.62
Mode Number	1	928	499	270	84	23
	2	928	499	270	84	23
	3	1117	795	333	312	132
	4	1117	795	333	312	132
	5	1512	938	627	364	190
	6	1512	938	627	364	295
	7	1841	1446	713	372	309
	8	1841	1493	884	410	309
	9	2452	1493	884	410	316
	10	2578	1503	994	546	316
	11	2578	1503	994	546	332
	12	2667	1724	1004	577	332
	13	2667	1724	1004	833	342
	14	2858	2130	1104	833	342
	15	2858	2130	1237	874	403

Table 4.5: Natural frequencies (GHz) of a cantilever chiral (a) (4,2), and (b) (8,4) SWNT

(a)	Length (nm)	1.12788	2.25576	4.51152	7.89516	15.79032
Mode Number	1	876	259	69	23	6
	2	894	265	70	23	6
	3	2390	1212	397	140	36
	4	2936	1280	405	142	36
	5	3041	1297	608	348	100
	6	3390	1995	1004	375	101
	7	3585	2781	1008	380	174
	8	3888	2913	1020	579	193
	9	4186	2929	1751	695	194
	10	4704	3486	1772	703	290
	11	5125	3700	1823	1044	313
	12	5372	3742	2575	1079	314
	13	5394	4570	2597	1089	456
	14	2858	2130	1104	833	342
	15	2858	2130	1237	874	403
(b)	Length (nm)	1.12788	2.25576	4.51152	7.89516	15.79032
Mode Number	1	1298	475	138	47	12
	2	1320	475	138	47	12
	3	1341	1113	645	268	73
	4	1341	1130	684	268	73
	5	2535	1284	684	370	185
	6	2931	1550	1017	584	197
	7	2998	1570	1095	667	197
	8	2998	1782	1107	667	293
	9	3098	1782	1174	1095	367
	10	3615	2009	1180	1105	367
	11	3698	2570	1405	1108	555
	12	3698	2632	1414	1121	572
	13	3919	2984	1545	1123	572
	14	4166	2984	1818	1146	802
	15	4166	3301	1831	1146	802

Table 4.6: Natural frequencies (GHz) of a cantilever chiral (a) (12,6), and (b) (16,8) SWNT

(a)	Length (nm)	1.12788	2.25576	4.51152	7.89516	15.79032
Mode Number	1	956	566	196	70	18
	2	956	566	196	70	18
	3	1395	613	496	363	107
	4	1476	613	496	363	107
	5	1479	1290	653	374	187
	6	1479	1290	654	483	277
	7	2258	1299	654	483	277
	8	2314	1378	836	518	293
	9	2314	1406	836	518	488
	10	2553	1717	1019	585	488
	11	2553	1760	1091	636	493
	12	2581	1913	1091	636	493
	13	2645	1913	1366	842	494
	14	2703	2010	1384	842	494
	15	2703	2417	1445	856	508
(b)	Length (nm)	1.12788	2.25576	4.51152	7.89516	15.79032
Mode Number	1	952	426	244	90	24
	2	952	426	244	90	24
	3	1027	699	293	277	136
	4	1027	699	293	277	136
	5	1529	789	557	339	188
	6	1529	789	557	339	274
	7	1565	1256	656	376	274
	8	1640	1256	779	428	282
	9	2313	1278	779	428	282
	10	2313	1278	873	541	294
	11	2354	1309	873	541	312
	12	2492	1394	913	585	312
	13	2492	1470	913	775	339
	14	2575	1754	1019	775	339
	15	2610	1802	1101	800	380

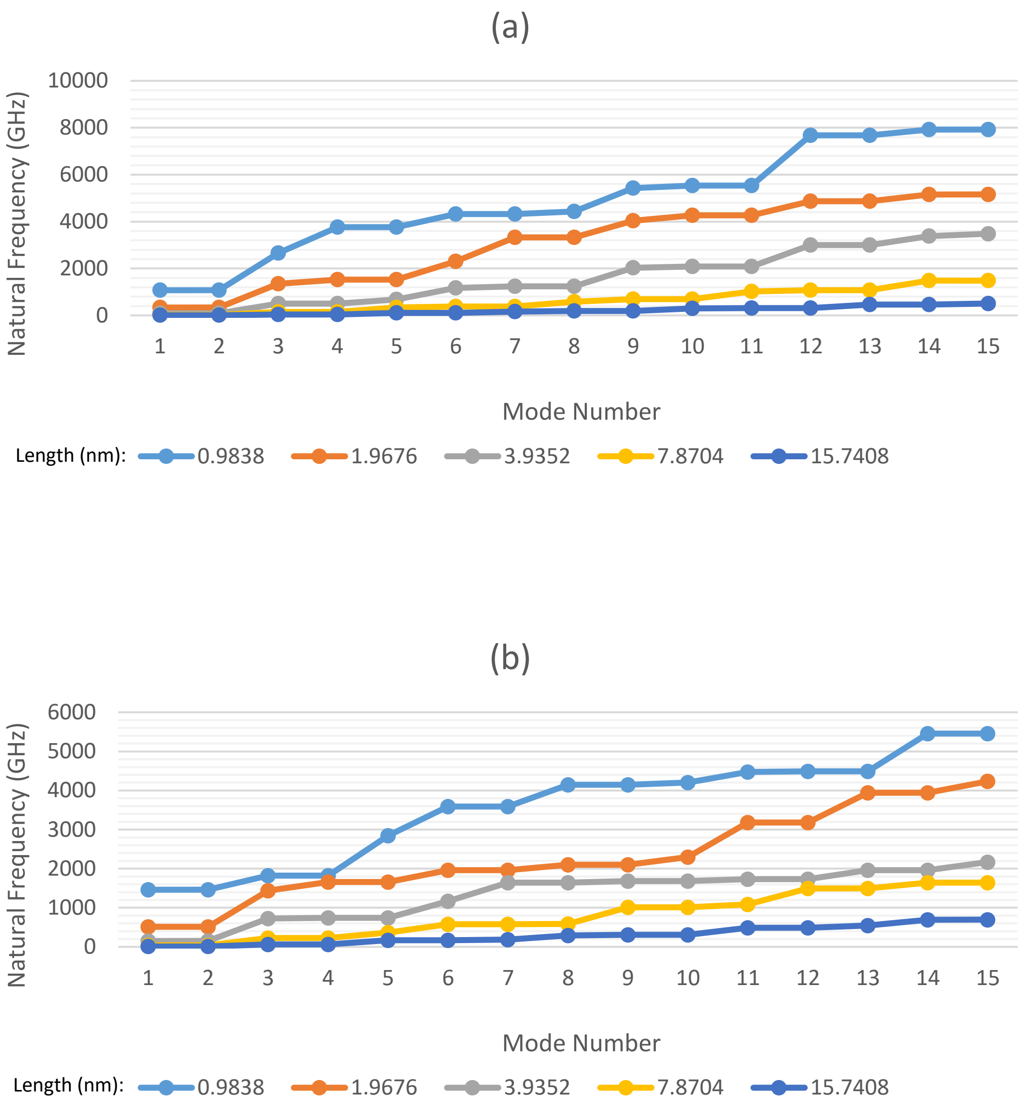

Figure 4.1: Natural frequency of a cantilever armchair (a) (3,3), and (b) (5,5) SWNT

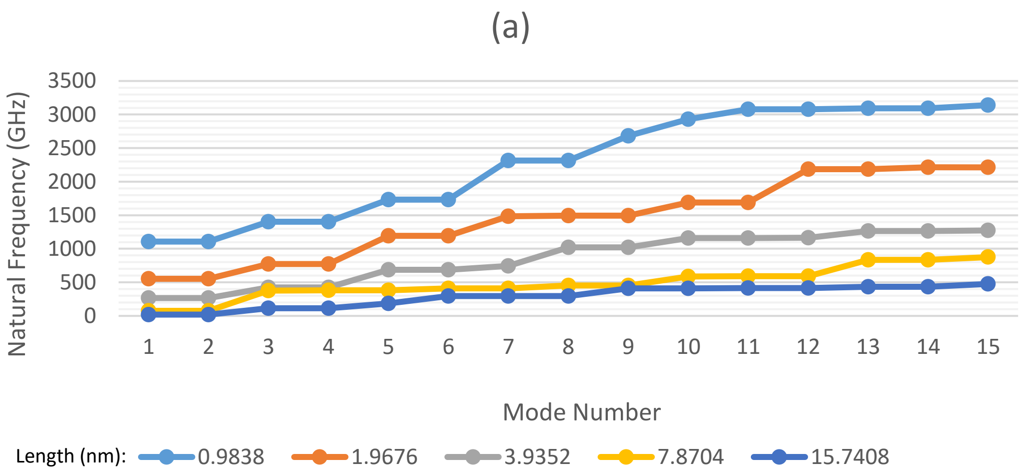

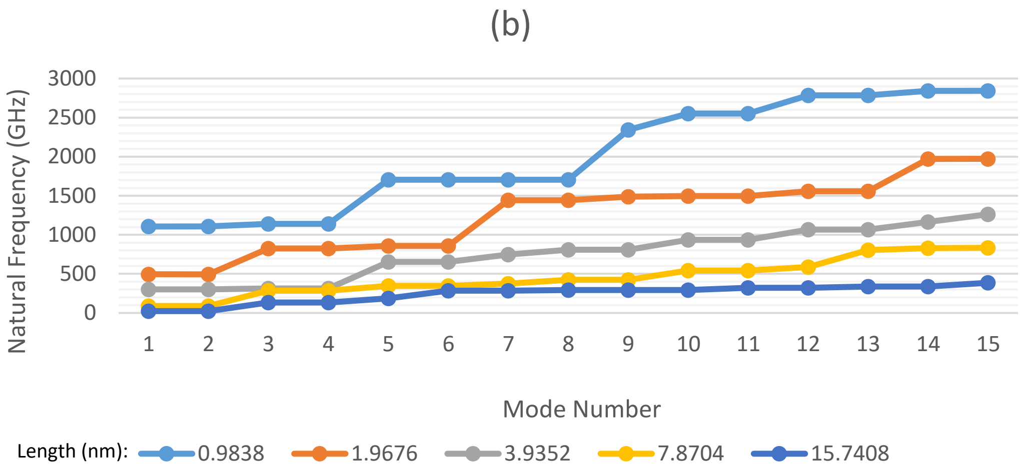

Figure 4.2: Natural frequency of a cantilever armchair (a) (10,10), and (b) (12,12) SWNT

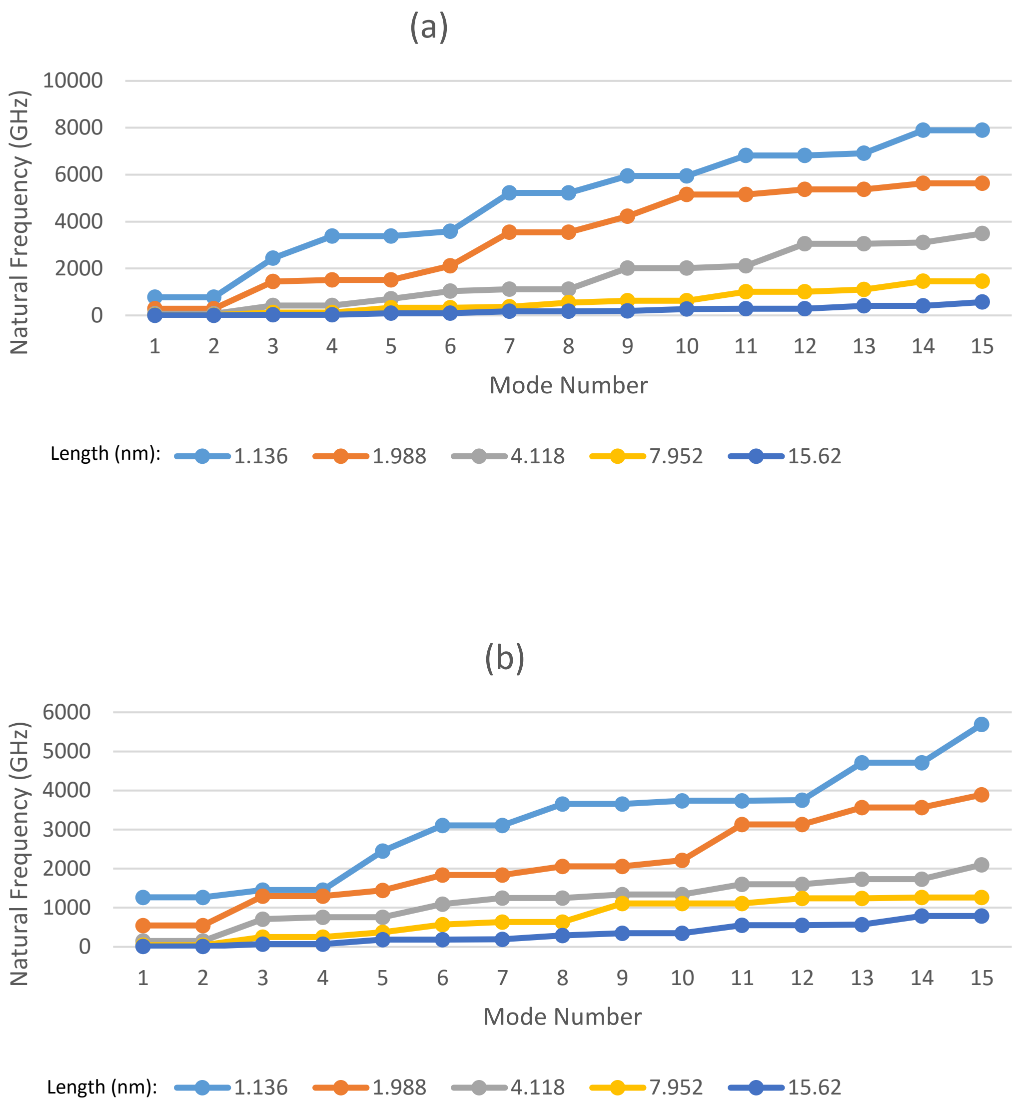

Figure 4.3: Natural frequency of a cantilever zigzag (a) (5,0), and (b) (10,0) SWNT

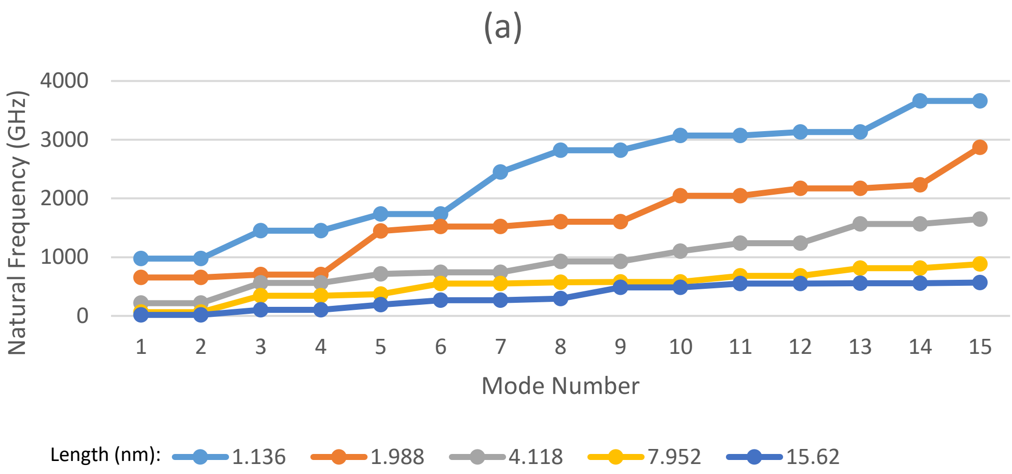

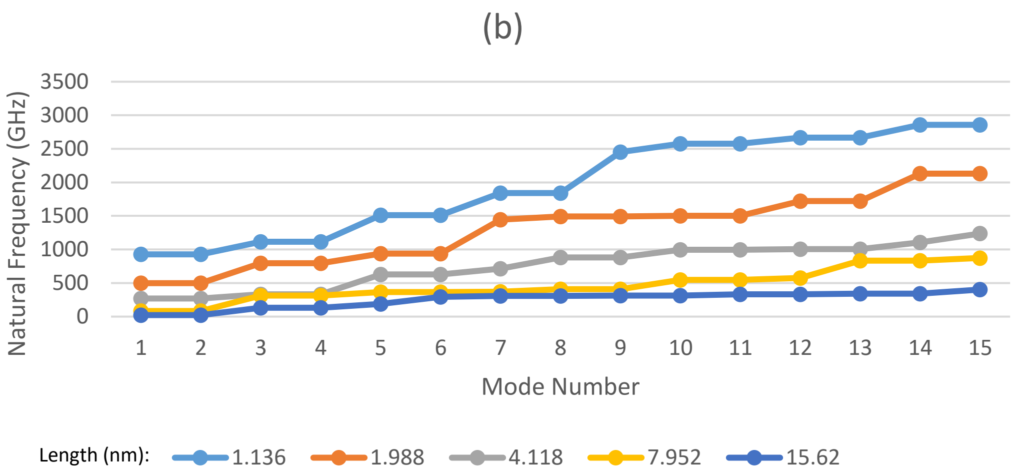

Figure 4.4: Natural frequency of a cantilever zigzag (a) (15,0), and (b) (20,0) SWNT

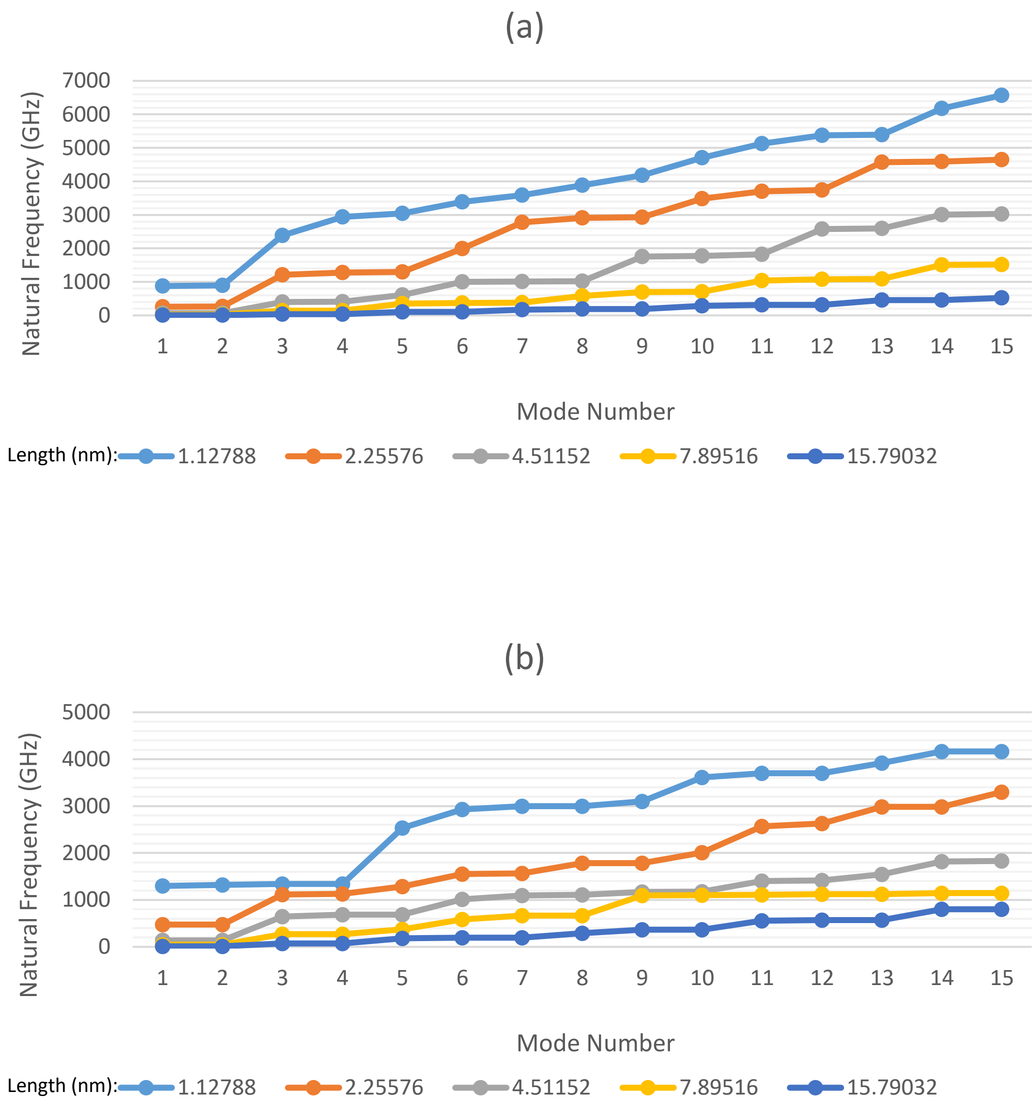

Figure 4.5: Natural frequency of a cantilever chiral (a) (4,2), and (b) (8,4) SWNT

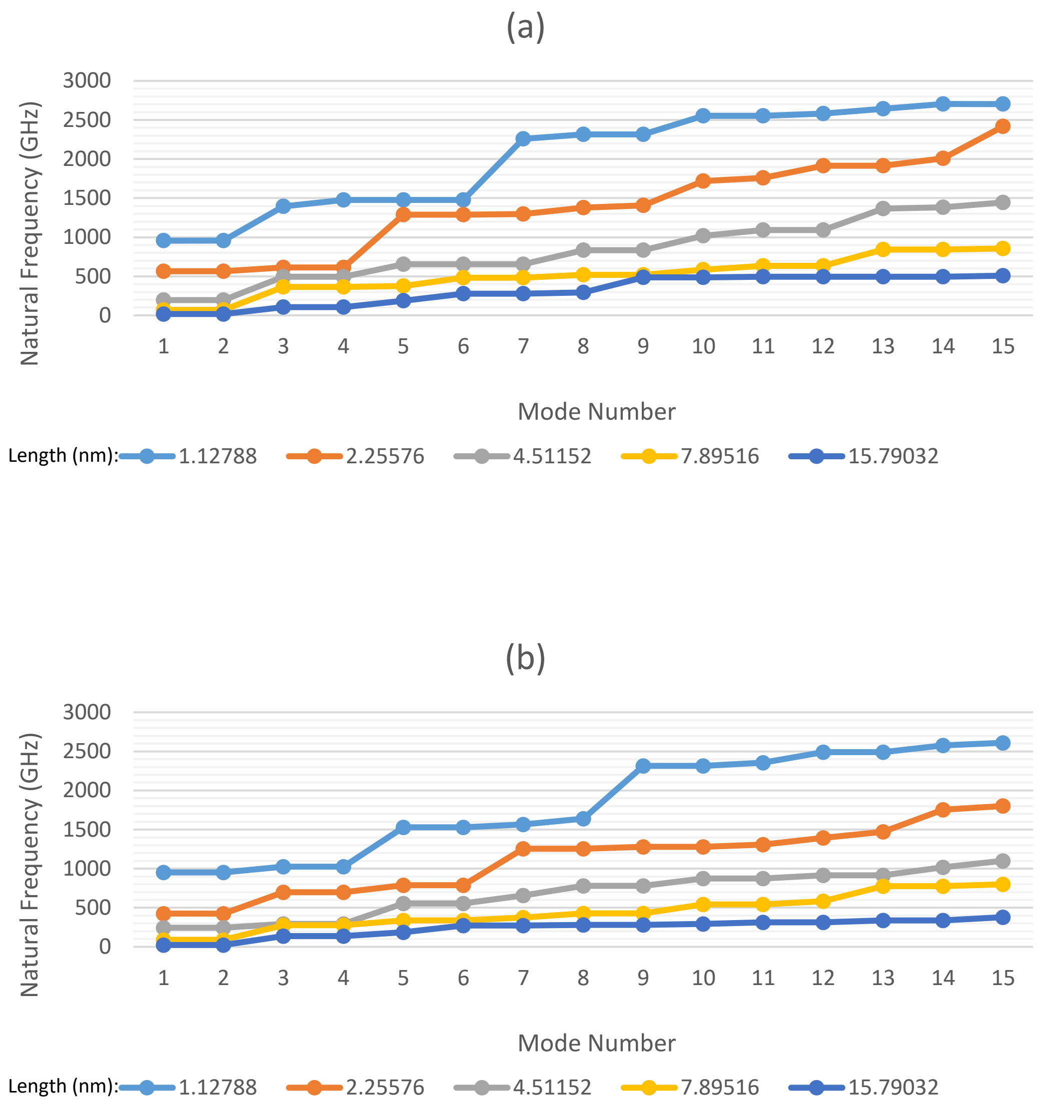

Figure 4.6: Natural frequency of a cantilever chiral (a) (12,6), and (b) (16,8) SWNT

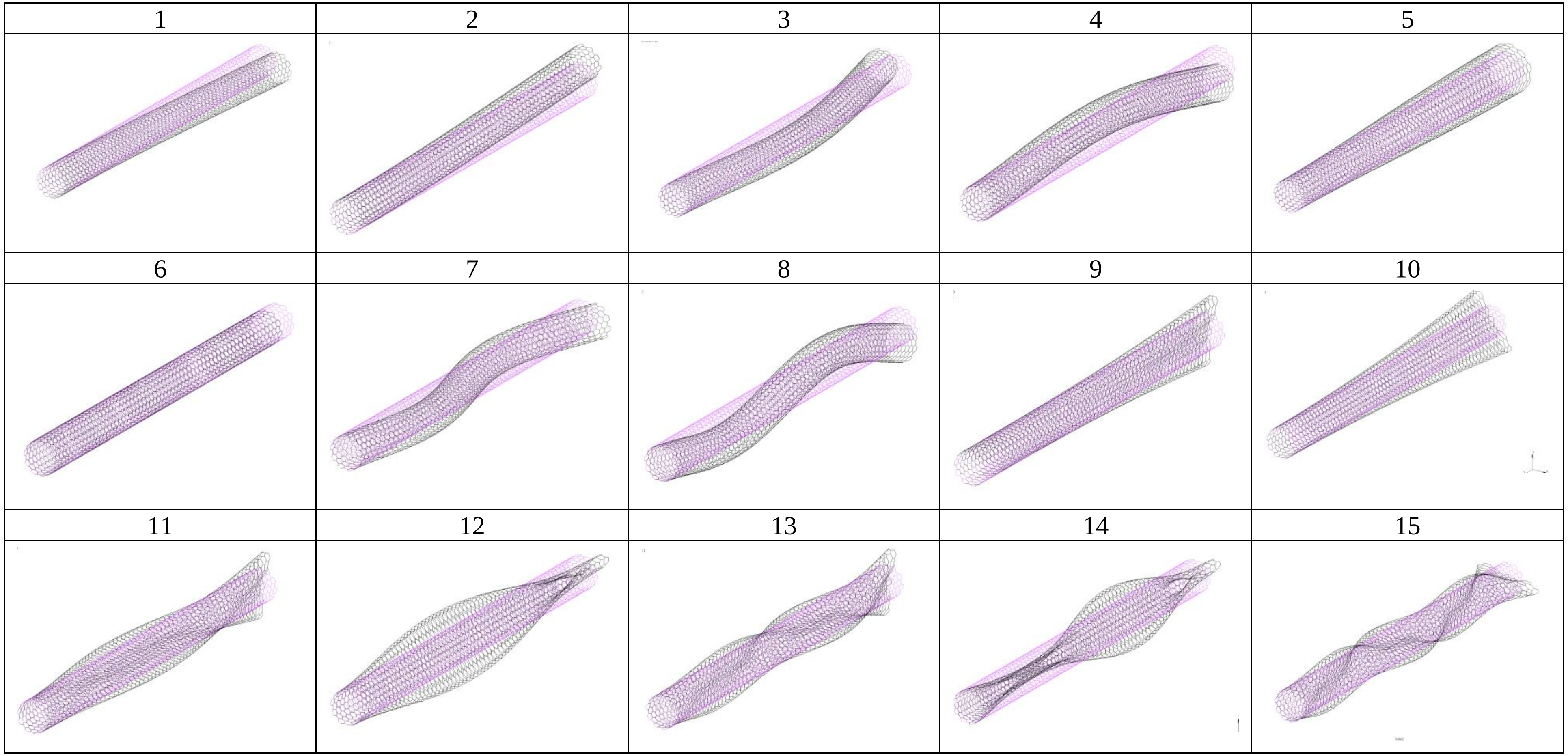

Figure 4.7: Mode shapes of a cantilever armchair (10,10) SWNT

In vibrational analysis, the first two mode shapes usually hold the most significance [49]. Nevertheless, as this study aims to analyze SWNTs comprehensively, the first 15 mode shapes have been investigated. Between all the SWNTs, the effect of length is the most prominent. So, when the length increases, the natural frequency of the nanotube will decrease. Moreover, the diameter does not have the same effect on the nanotube. Depending on the size of the diameter and the SWNT's chirality, the nanotube's natural frequency can increase and decrease. Still, the increase in diameter will result in the initial mode shapes increasing less than the ones with smaller diameters. Additionally, the natural frequencies for shorter SWNTs are extremely high, indicating that nanotubes with these lengths are unrealistic. Thus the lengthier nanotubes show a more realistic representation of the SWNTs that can be utilized in different industries. Also, regarding the chirality of SWNTs, the effect of chirality could change the natural frequency up to 20% if we have shorter SWNTs. Still, when the nanotube is longer, this effect could decrease to around 2%, sometimes even 0%. So, it can be concluded that even though chirality is one of the prominent characteristics of the SWNTs, its effect on natural frequency could be negligible if we have long SWNTs.

4.1.2 Bridge Boundary Condition

The modal analysis of three different configurations of SWNTs (armchair, zigzag, and chiral) under the bridge boundary condition (Figure 3.9) was done just like in the previous section. The only difference between this section and the previous one is the change in the boundary condition. The following are the SWNTs studied under the bridge boundary condition:

- Armchair (n=m): (3,3), (5,5), (10,10), and (12,12)
- Zigzag (n,0): (5,0), (10,0), (15,0), and (20,0)
- Chiral (n≠m): (4,2), (8,4), (12,6), and (16,8)

The results of the modal analysis of the pristine armchair SWNTs are depicted in Table 4.7, Table 4.8, Figure 4.8, and Figure 4.9. Also, the modal analysis results for pristine zigzag SWNTs are demonstrated in Table 4.9, Table 4.10, Figure 4.10, and Figure 4.11. In the same vein, the results of the modal analysis of pristine chiral SWNTs are shown in Table 4.11, Table 4.12, Figure 4.12, and Figure 4.13. The mode shapes of a bridge armchair (10,10) are demonstrated in Figure 4.14. Comparing this figure with Figure 4.7 shows that the change of boundary condition in SWNTs can also significantly affect their mode shapes.

Table 4.7: Natural frequencies (GHz) of a bridge armchair (a) (3,3), and (b) (5,5) SWNT

(a)	Length (nm)	0.9838	1.9676	3.9352	7.8704	15.7408
Mode Number	1	3722	1474	505	145	38
	2	3722	1474	505	145	38
	3	5741	2825	1184	375	103
	4	5741	3131	1184	375	103
	5	5884	3132	1385	684	196
	6	7480	4703	2006	684	196
	7	7481	4904	2006	686	315
	8	8747	4904	2366	1048	315
	9	8747	5089	2770	1048	341
	10	9108	5089	2905	1184	456
	11	11181	5454	2905	1371	456
	12	11181	5454	3852	1450	592
	13	11637	5651	3852	1450	615
	14	12264	6471	4156	1878	615
	15	12813	6471	4693	1878	682
(b)	Length (nm)	0.9838	1.9676	3.9352	7.8704	15.7408
Mode Number	1	3505	1859	720	228	62
	2	3505	1859	720	228	62
	3	4271	2040	1480	560	165
	4	4271	2040	1570	560	165
	5	5744	3014	1570	734	309
	6	5744	3056	1723	979	309
	7	6257	3056	1723	979	365
	8	7018	3750	1932	1184	484
	9	7018	3750	1932	1446	484
	10	8279	4553	2327	1446	592
	11	8279	4553	2327	1467	685
	12	8462	4688	2365	1675	685
	13	8609	4925	2560	1675	731
	14	8609	4925	2560	1707	904
	15	8713	5508	2878	1707	904

Table 4.8: Natural frequencies (GHz) of a bridge armchair (a) (10,10), and (b) (12,12) SWNT

(a)	Length (nm)	0.9838	1.9676	3.9352	7.8704	15.7408
Mode Number	1	2979	1369	651	370	116
	2	2979	1369	651	370	116
	3	3081	1574	950	444	286
	4	3081	1574	950	444	286
	5	3573	2054	1183	574	377
	6	3573	2054	1183	574	415
	7	3823	2496	1235	757	415
	8	3823	2496	1235	806	431
	9	4627	2571	1473	806	431
	10	4674	2571	1473	808	471
	11	4775	2692	1527	808	471
	12	5986	2692	1848	1100	503
	13	6057	3107	1848	1100	503
	14	6057	3258	1872	1176	541
	15	6155	3258	1872	1176	541

(b)	Length (nm)	0.9838	1.9676	3.9352	7.8704	15.7408
Mode Number	1	2777	1319	610	339	133
	2	2777	1319	610	339	133
	3	2957	1358	901	404	290
	4	2957	1358	901	404	290
	5	3053	1854	982	519	317
	6	3053	1854	982	519	317
	7	3509	2028	1187	760	321
	8	3509	2028	1187	795	321
	9	3743	2374	1196	795	378
	10	3743	2374	1196	821	379
	11	3960	2617	1532	821	379
	12	4719	2617	1605	856	478
	13	4812	2694	1605	856	478
	14	5580	2694	1657	875	552
	15	5639	2749	1657	875	552

Table 4.9: Natural frequencies (GHz) of a bridge zigzag (a) (5,0), and (b) (10,0) SWNT

(a)	Length (nm)	1.136	1.988	4.118	7.952	15.62
Mode Number	1	3408	1551	437	123	32
	2	3408	1551	437	123	32
	3	5030	2941	1116	332	89
	4	5801	3458	1116	332	89
	5	5801	3458	1435	632	172
	6	6668	4337	2010	632	172
	7	6668	5266	2010	746	282
	8	7493	5266	2108	1010	282
	9	8077	5534	2849	1010	380
	10	8077	5534	3030	1094	417
	11	9263	5710	3030	1454	417
	12	9624	5798	4103	1454	558
	13	9624	5798	4103	1488	574
	14	11297	6876	4202	1949	574
	15	11297	6876	4223	1949	754
(b)	Length (nm)	1.136	1.988	4.118	7.952	15.62
Mode Number	1	2913	1748	743	249	70
	2	2913	1748	743	249	70
	3	3495	1947	1306	614	186
	4	3495	1947	1306	614	186
	5	4403	2952	1442	749	349
	6	4403	2975	1558	1074	349
	7	5040	2975	1558	1074	382
	8	5499	3722	1618	1148	549
	9	5500	3722	1618	1253	549
	10	6148	3735	2042	1253	585
	11	6148	3735	2042	1291	763
	12	6703	4457	2209	1291	776
	13	6703	4457	2599	1375	776
	14	7383	4473	2599	1375	1025
	15	7383	4473	2691	1495	1025

Table 4.10: Natural frequencies (GHz) of a bridge zigzag (a) (15,0), and (b) (20,0) SWNT

(a)	Length (nm)	1.136	1.988	4.118	7.952	15.62
Mode Number	1	2561	1406	711	335	103
	2	2561	1406	711	335	103
	3	2790	1903	871	570	262
	4	2790	1903	871	570	262
	5	3309	1990	1174	664	382
	6	3309	1990	1174	664	471
	7	3870	2666	1443	750	471
	8	3870	2666	1606	762	551
	9	4908	2851	1606	762	551
	10	4908	2851	1751	858	563
	11	5041	2954	1751	858	563
	12	5141	3213	1792	1132	591
	13	5141	3213	1792	1132	591
	14	5270	3542	1801	1158	591
	15	5434	3542	1801	1260	643

(b)	Length (nm)	1.136	1.988	4.118	7.952	15.62
Mode Number	1	2316	1344	592	355	131
	2	2316	1344	592	355	131
	3	2399	1370	925	392	313
	4	2399	1370	925	392	313
	5	2743	1955	951	525	318
	6	2743	1955	951	525	318
	7	3053	1970	1141	750	337
	8	3053	1970	1141	797	337
	9	3581	2378	1220	797	382
	10	3581	2378	1220	840	396
	11	4048	2506	1443	840	396
	12	4559	2506	1655	885	492
	13	4559	2801	1655	885	492
	14	4590	2801	1722	935	552
	15	4590	2941	1722	935	552

Table 4.11: Natural frequencies (GHz) of a bridge chiral (a) (4,2), and (b) (8,4) SWNT

(a)	Length (nm)	1.12788	2.25576	4.51152	7.89516	15.79032
Mode Number	1	3262	1257	404	143	37
	2	3431	1294	409	144	37
	3	5162	2525	983	374	101
	4	5350	2736	999	377	101
	5	5370	2815	1242	689	193
	6	6715	4079	1707	696	194
	7	6961	4463	1737	705	312
	8	7346	4562	2043	1066	314
	9	7680	4686	2481	1077	351
	10	8059	4688	2512	1166	454
	11	9942	5007	2556	1409	456
	12	10176	5116	3365	1487	583
	13	10386	5122	3417	1503	616
	14	10793	5894	3712	1938	620
	15	11512	5930	4061	1960	701
(b)	Length (nm)	1.12788	2.25576	4.51152	7.89516	15.79032
Mode Number	1	2859	1497	665	267	74
	2	2940	1511	665	267	74
	3	3724	1695	1164	641	195
	4	3724	1695	1165	641	195
	5	4098	2470	1318	748	361
	6	4098	2504	1378	1101	361
	7	5486	2675	1383	1101	372
	8	5744	3309	1441	1119	561
	9	5901	3309	1441	1119	561
	10	6506	3344	1774	1163	588
	11	6506	3344	1786	1164	745
	12	6711	3786	2060	1177	785
	13	6727	3828	2304	1261	785
	14	6727	3858	2322	1263	1027
	15	6739	3858	2330	1423	1109

Table 4.12: Natural frequencies (GHz) of a bridge chiral (a) (12,6), and (b) (16,8) SWNT

(a)	Length (nm)	1.12788	2.25576	4.51152	7.89516	15.79032
Mode Number	1	2685	1205	632	352	107
	2	2685	1205	632	352	107
	3	2708	1654	788	515	269
	4	2766	1663	788	515	269
	5	3520	1791	1034	624	377
	6	3520	1792	1034	624	478
	7	3620	2333	1334	757	478
	8	3620	2333	1431	785	492
	9	4939	2402	1431	785	492
	10	5087	2425	1586	834	506
	11	5087	2706	1587	834	506
	12	5294	2843	1587	1115	537
	13	5294	2843	1590	1115	537
	14	5296	3295	1598	1179	589
	15	5437	3295	1598	1287	595
(b)	Length (nm)	1.12788	2.25576	4.51152	7.89516	15.79032
Mode Number	1	2370	1178	528	331	135
	2	2370	1178	528	331	135
	3	2545	1179	846	408	280
	4	2545	1179	846	408	280
	5	2640	1720	846	518	308
	6	2692	1727	846	518	308
	7	3170	1786	1019	760	324
	8	3170	1786	1019	792	324
	9	3361	2042	1075	792	373
	10	3361	2042	1075	800	373
	11	3810	2260	1339	800	378
	12	4352	2260	1449	848	475
	13	4352	2373	1449	848	475
	14	4864	2393	1534	862	557
	15	4874	2599	1534	862	557

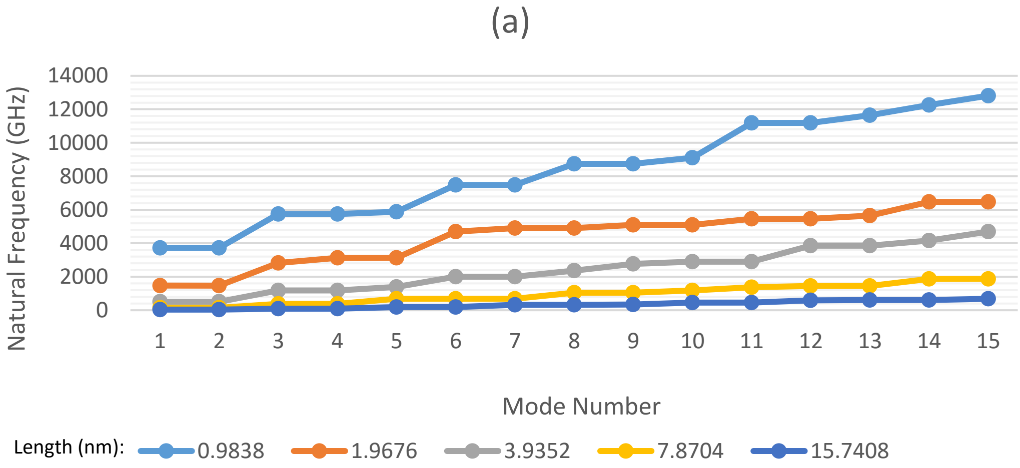

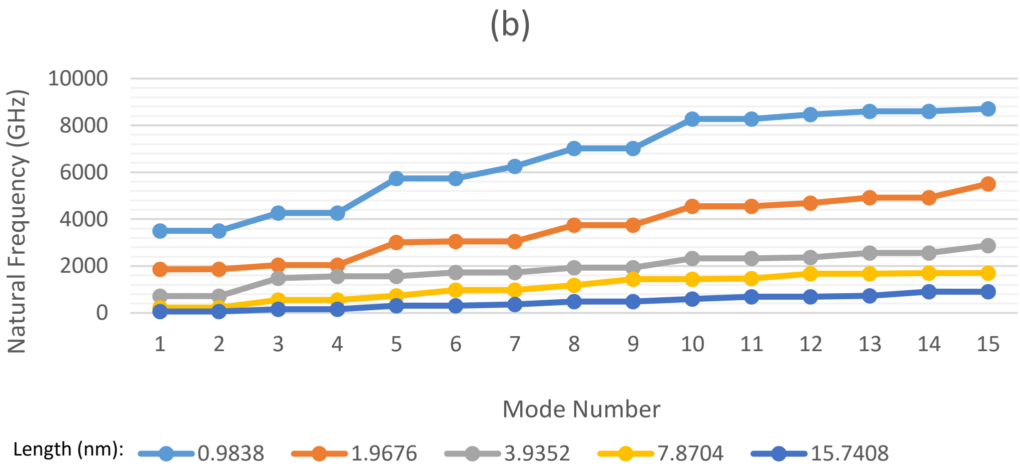

Figure 4.8: Natural frequencies (GHz) of a bridge armchair (a) (3,3), and (b) (5,5) SWNT

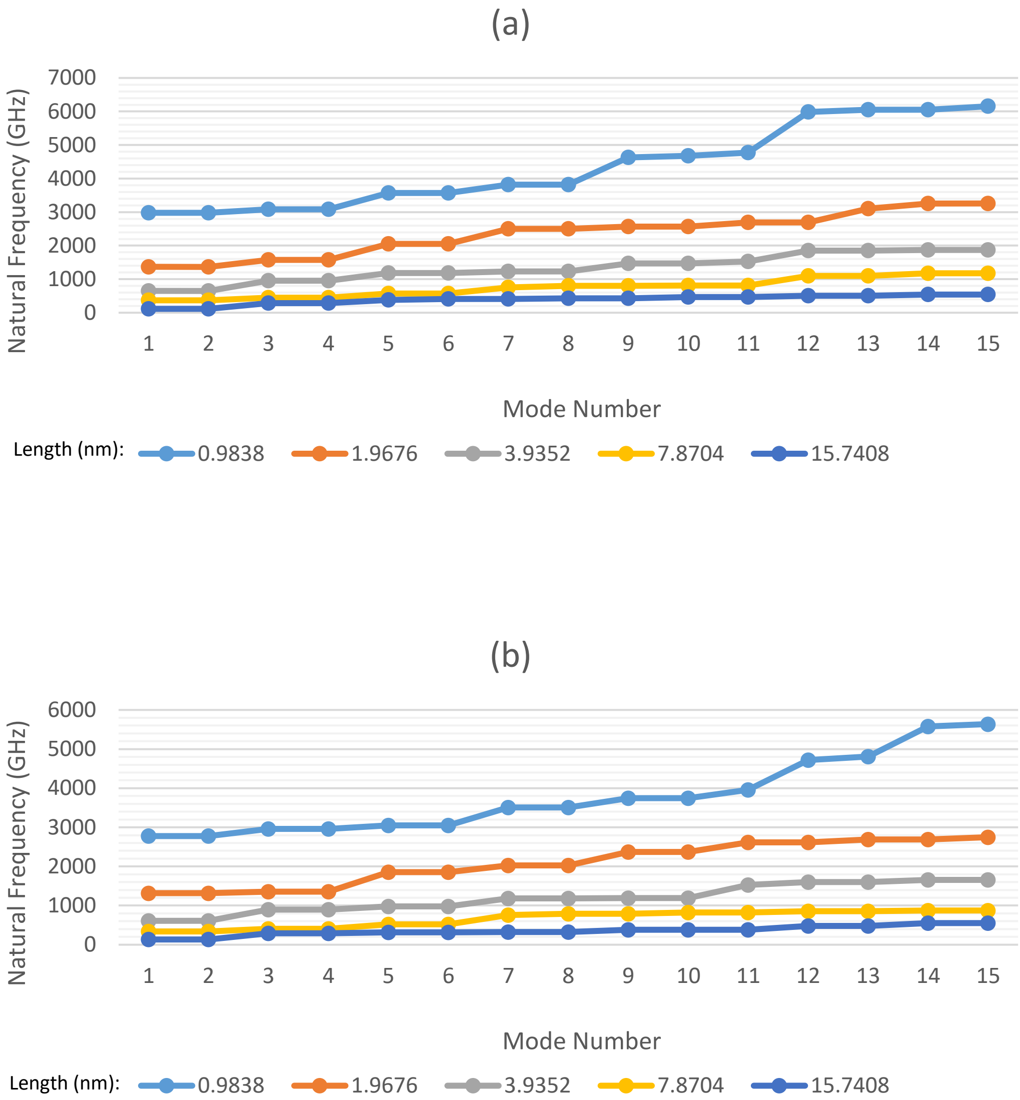

Figure 4.9: Natural frequencies (GHz) of a bridge armchair (a) (10,10), and (b) (12,12) SWNT

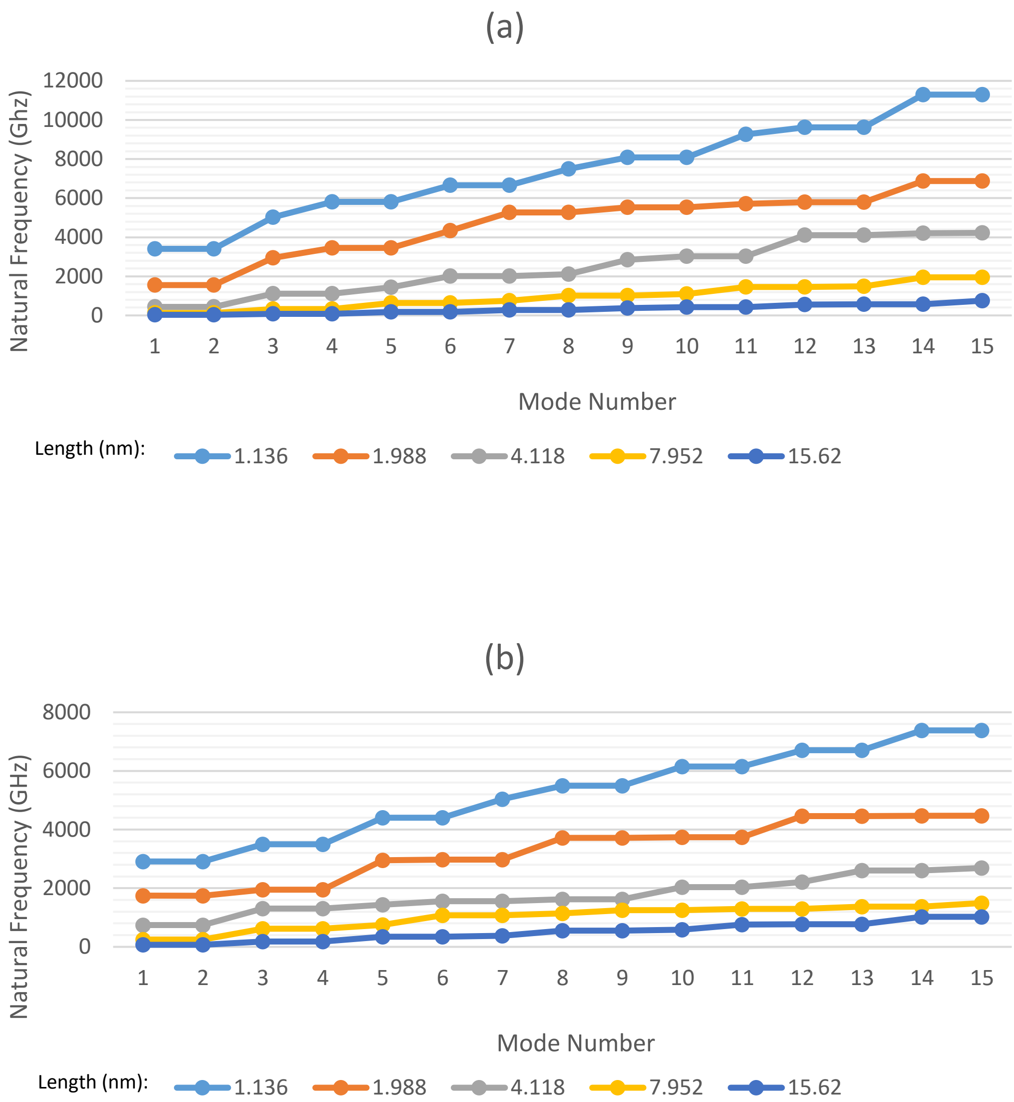

Figure 4.10: Natural frequencies (GHz) of a bridge zigzag (a) (5,0), and (b) (10,0) SWNT

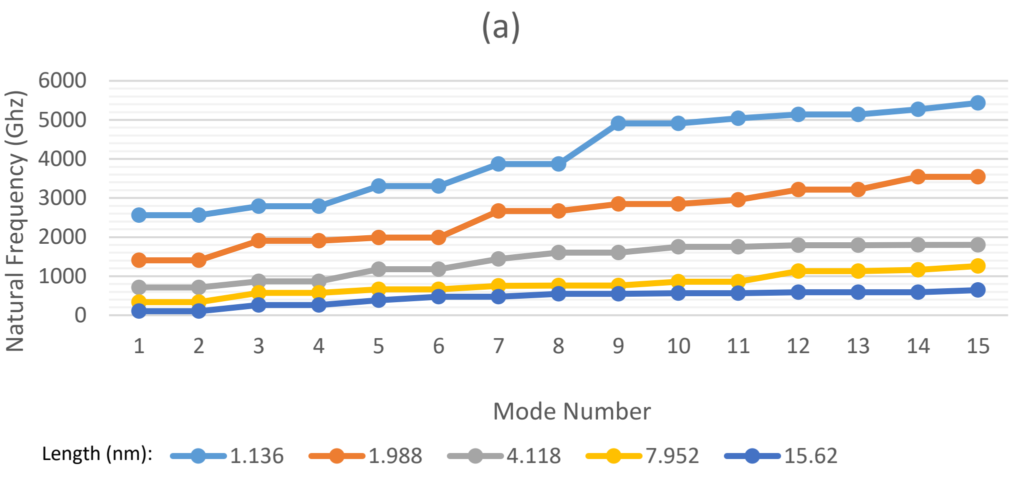

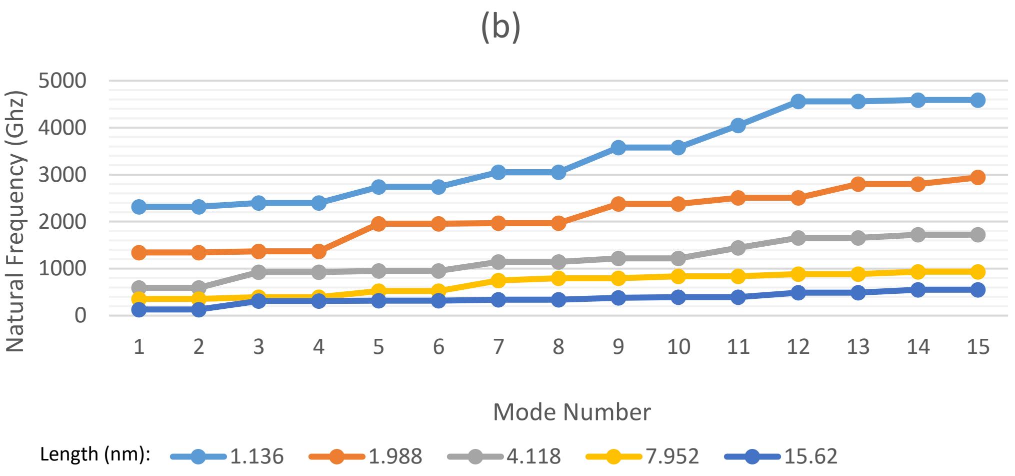

Figure 4.11: Natural frequencies (GHz) of a bridge zigzag (a) (15,0), and (b) (20,0) SWNT

(a)

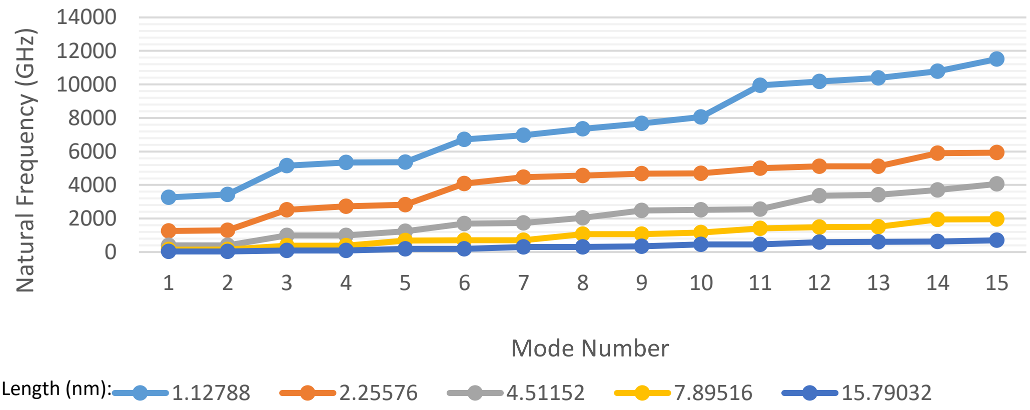

(b)

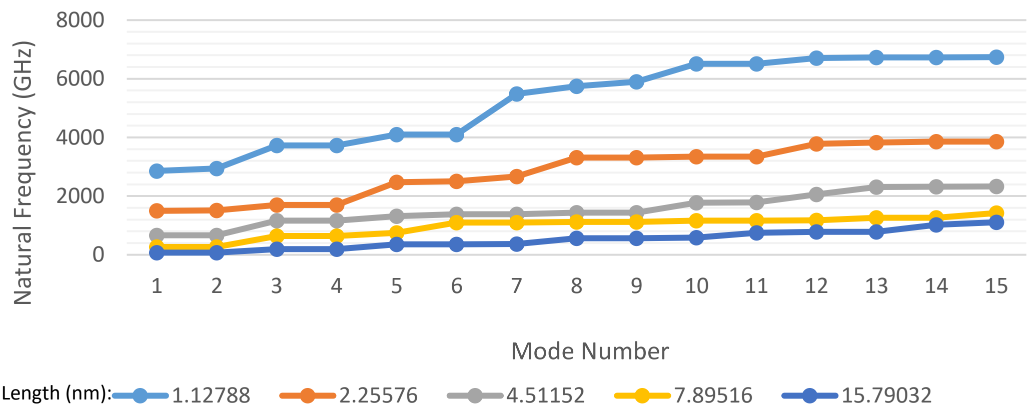

Figure 4.12: Natural frequencies (GHz) of a bridge chiral (a) (4,2), and (b) (8,4) SWNT

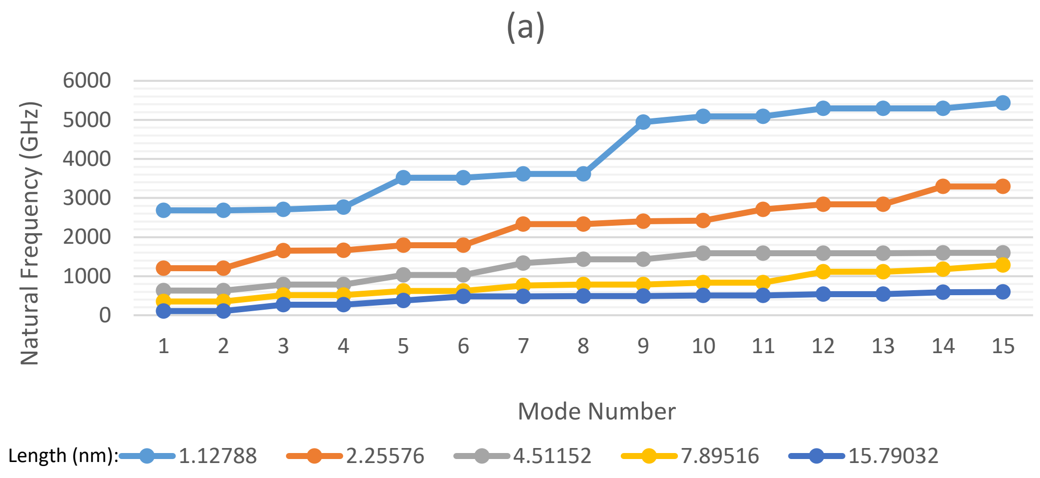

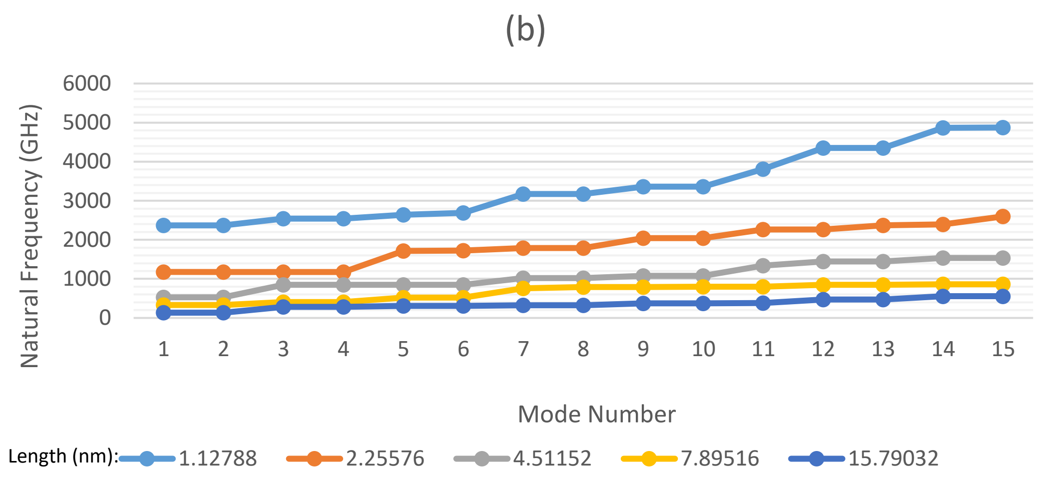

Figure 4.13: Natural frequencies (GHz) of a bridge chiral (a) (12,6), and (b) (16,8) SWNT

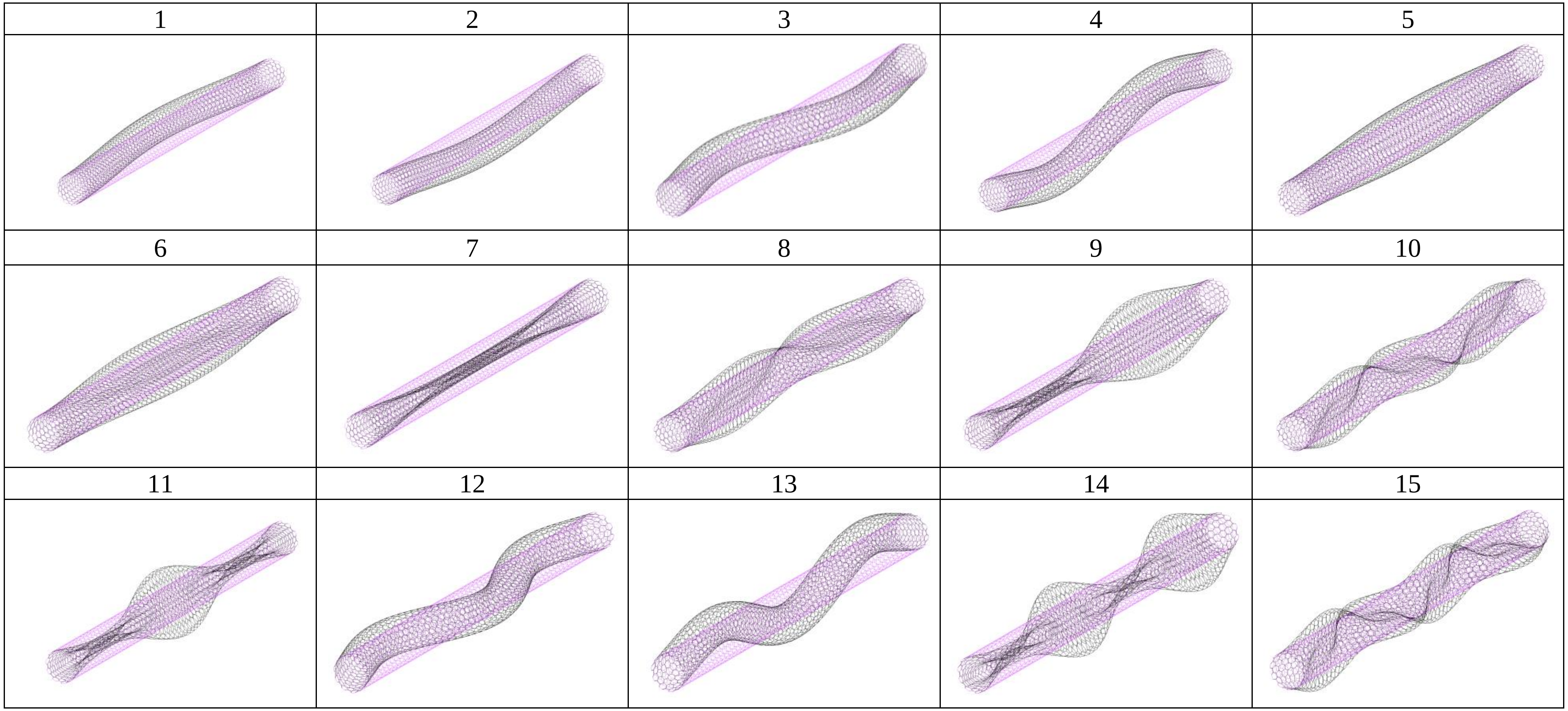

Figure 4.14: Mode shapes of a bridge armchair (10,10) SWNT

Since similar SWNTs were studied under different boundary conditions, their results can be compared. Due to constrained movement because of the nature of the bridge boundary condition, the SWNTs under this boundary condition have higher natural frequency compared (up to 300%) to the corresponding SWNTs with cantilever boundary conditions. It is important to note that increasing the length of the nanotubes will not lessen the impact of the constraint movement of the bridge boundary condition, so the natural frequency of longer SWNTs is still drastically affected by the change in the boundary condition. Similar to the cantilever boundary condition, the increase in length decreases the natural frequency. Moreover, the increase in diameter can increase or decrease the natural frequency depending on the chirality or the length of the SWNT. Nevertheless, the impact of length is much more evident than the impact of diameter. Furthermore, unlike the cantilever boundary condition, the effect of chirality is also quite significant due to the constraint movement of the SWNTs. Therefore, the change in the chirality of the SWNTs can also make quite a bit of difference in the natural frequency, even for the lengthier SWNTs.

4.2 Modal Analysis of Defective Carbon Nanotubes

The previous sections discussed the importance of conducting modal analysis on pristine SWNTs. However, pristine SWNTs are not a realistic representation of the SWNTs that can be implemented in various industries. Because SWNTs during the synthesis cannot be synthesized perfectly, thus, their structure is exposed to some defections. These SWNTs are called defective carbon nanotubes. The defections on carbon nanotubes will affect their natural frequency because their structure will be changed. So, this section is dedicated to discussing the effects of different defections on the structure of SWNTs. Similar to pristine SWNTs, the modal analysis is conducted on defective SWNTs for both cantilever and bridge boundary conditions. Moreover, this section aims to discuss the effects of the number of vacancy defects and Stone-Wales defects on SWNTs with various lengths, diameters, and chirality.

4.2.1 Cantilever Boundary Condition

The vacancy and Stone-Wales Defect are two common defects to which SWNTs can be exposed during their purification process [50-52]. And their effects can change the structures of pristine SWNTs. This can make the implementation of this material in nanocomposites and nanomaterials challenging. Thus, it is crucial to see how the number of defects introduced to the structure can affect the natural frequency of SWNTs. The number of defects introduced to the structure would be 1, 2, 4, and 6, and their positions are depicted in Figure 3.7. The type of defects studied are single vacancy, double vacancy, and Stone-Wales. These defects are illustrated in Figure 1.6. The defects are first analyzed independently, then a combination of them is introduced to the SWNT to see how it affects the natural frequency of this material. The SWNTs studied are the following:

- Armchair (n=m): (5,5), and (10,10)
- Zigzag (n,0): (10,0), and (15,0)
- Chiral (n≠m): (8,4), and (12,6)

The diameters of the different SWNTs selected for this study are quite close to one another (Table 3.2, Table 3.4, and

Table 3.6), so their results can be compared. Also, the effect of the defects on these nanotubes has been studied for a specific length for each nanotube. The length selected for the armchair configuration is 7.8704 nm, for the zigzag configuration is 7.952 nm, and for the chiral configuration is 7.89516 nm. Furthermore, the similar lengths of the SWNTs allow for meaningful comparisons of their outcomes.

The results of the modal analysis of defective cantilever armchair SWNT are depicted in Table 4.13, Table 4.14, and Table 4.15. Similarly, the modal analysis results of defective cantilever zigzag SWNT are shown in Table 4.16, Table 4.17, and Table 4.18. Furthermore, the results of the modal analysis of defective cantilever chiral SWNT are presented in Table 4.19, Table 4.20, and Table 4.21.

In order to see the effects of the vacancy and Stone-Wales defects together, a new model is created. In this model, three double vacancy defects and three Stone-Wales defects are introduced to the SWNT, and then the modal analysis is conducted. This model is a representation of a real SWNT that can be synthesized in a lab. This model is studied for (10,10), (15,0), and (12,6) SWNTs. The results of the modal analysis of this model for all three SWNTs are depicted in Table 4.22. The mode shapes of a cantilever armchair (10,10) with three double vacancy defects and three Stone-Wales defects are shown in Figure 4.15.

Table 4.13: Natural frequencies (GHz) of a cantilever armchair (a) (5,5), and (b) (10,10) SWNT with single vacancy defect

(a)	Number of defects	0	1	2	4	6
Mode Number	1	39	37	37	37	36
	2	39	39	39	39	39
	3	228	225	224	223	217
	4	228	226	225	224	223
	5	363	354	347	346	339
	6	579	570	568	558	543
	7	579	576	570	568	567
	8	588	582	577	574	569
	9	1015	993	995	976	962
	10	1015	1014	1004	987	978
	11	1088	1072	1066	1044	1012
	12	1498	1481	1458	1434	1419
	13	1498	1493	1491	1459	1433
	14	1643	1643	1643	1614	1612
	15	1643	1643	1643	1614	1612

(b)	Number of defects	0	1	2	4	6
Mode Number	1	76	75	75	73	73
	2	76	75	75	75	75
	3	374	372	371	362	358
	4	384	380	379	376	373
	5	384	380	380	378	375
	6	411	405	404	404	403
	7	411	408	408	408	403
	8	451	447	447	446	443
	9	451	447	447	447	446
	10	587	583	582	576	573
	11	592	587	585	581	576
	12	592	587	586	584	583
	13	837	828	822	818	815
	14	837	828	828	823	818
	15	876	866	863	854	851

Table 4.14: Natural frequencies (GHz) of a cantilever armchair (a) (5,5), and (b) (10,10) SWNT with double vacancy defect

(a)	Number of defects	0	1	2	4	6
Mode Number	1	39	39	39	33	32
	2	39	39	40	39	39
	3	228	228	223	217	199
	4	228	228	227	223	222
	5	363	363	363	341	332
	6	579	573	537	519	488
	7	579	576	574	551	543
	8	588	589	590	566	562
	9	1015	987	943	925	907
	10	1015	1002	1003	982	951
	11	1088	1083	1050	1030	990
	12	1498	1424	1410	1373	1276
	13	1498	1479	1457	1420	1414
	14	1643	1628	1626	1626	1612
	15	1643	1636	1634	1634	1625
(b)	Number of defects	0	1	2	4	6
Mode Number	1	76	76	76	71	70
	2	76	76	76	76	76
	3	374	375	375	362	358
	4	384	383	382	377	368
	5	384	384	383	379	378
	6	411	410	409	409	408
	7	411	411	411	411	411
	8	451	451	451	449	447
	9	451	451	451	450	450
	10	587	588	584	571	566
	11	592	591	590	581	571
	12	592	592	590	588	587
	13	837	831	814	810	804
	14	837	834	833	825	817
	15	876	872	861	852	837

Table 4.15: Natural frequencies (GHz) of a cantilever armchair (a) (5,5), and (b) (10,10) SWNT with Stone-Wales defect

(a)	Number of defects	0	1	2	4	6
Mode Number	1	39	38	37	37	36
	2	39	38	37	37	37
	3	228	225	224	223	219
	4	228	225	225	224	223
	5	363	358	353	350	345
	6	579	572	563	557	538
	7	579	576	575	567	551
	8	588	580	577	572	559
	9	1015	1009	997	967	935
	10	1015	1013	1005	973	949
	11	1088	1074	1064	1052	1039
	12	1498	1489	1419	1367	1355
	13	1498	1496	1473	1420	1414
	14	1643	1500	1491	1471	1460
	15	1643	1586	1573	1572	1545
(b)	Number of defects	0	1	2	4	6
Mode Number	1	76	75	74	73	73
	2	76	75	74	74	73
	3	374	372	369	366	363
	4	384	381	380	375	373
	5	384	382	382	379	377
	6	411	406	399	395	391
	7	411	409	407	406	404
	8	451	448	448	445	442
	9	451	450	449	448	447
	10	587	584	579	574	562
	11	592	590	590	582	571
	12	592	592	591	589	584
	13	837	835	829	807	788
	14	837	837	835	829	823
	15	876	873	871	860	846

Table 4.16: Natural frequencies (GHz) of a cantilever zigzag (a) (10,0), and (b) (15,0) SWNT with single vacancy defect

(a)	Number of defects	0	1	2	4	6
	1	43	41	40	40	39
	2	43	42	42	43	43
	3	248	244	244	243	240
	4	248	246	245	244	243
	5	372	365	360	360	354
	6	570	563	557	558	553
	7	632	624	621	617	598
Mode Number	8	632	630	627	619	619
	9	1112	1076	1075	1056	1051
	10	1112	1112	1101	1077	1068
	11	1114	1113	1111	1109	1077
	12	1245	1245	1245	1232	1227
	13	1245	1245	1245	1236	1232
	14	1262	1262	1259	1255	1248
	15	1262	1262	1261	1257	1253
(b)	Number of defects		1	2	4	6
	1	64	62	61	62	61
	2	64	64	64	64	64
	3	343	340	336	336	334
	4	343	340	340	340	337
	5	372	369	366	366	363
	6	551	551	551	547	545
	7	551	551	551	550	550
Mode Number	8	575	571	567	568	564
	9	581	580	580	578	576
	10	581	580	580	579	579
	11	681	679	678	676	669
	12	681	680	679	677	676
	13	812	800	798	794	791
	14	812	812	810	804	795
	15	882	878	877	870	867

Table 4.17: Natural frequencies (GHz) of a cantilever zigzag (a) (10,0), and (b) (15,0) SWNT with double vacancy defect

(a)	Number of defects	0	1	2	4	6
Mode Number	1	43	43	43	38	37
	2	43	43	43	42	42
	3	248	248	245	237	229
	4	248	248	247	241	237
	5	372	373	372	345	333
	6	570	571	570	548	538
	7	632	627	609	598	563
	8	632	631	625	607	607
	9	1112	1079	1033	999	982
	10	1112	1102	1083	1041	1016
	11	1114	1115	1106	1093	1038
	12	1245	1237	1230	1230	1225
	13	1245	1241	1236	1236	1233
	14	1262	1258	1258	1255	1248
	15	1262	1260	1259	1257	1252
(b)	Number of defects	0	1	2	4	6
Mode Number	1	64	64	64	60	59
	2	64	64	64	64	64
	3	343	342	340	325	320
	4	343	343	342	338	330
	5	372	373	372	361	357
	6	551	549	547	547	546
	7	551	550	550	550	549
	8	575	576	576	561	556
	9	581	579	579	578	576
	10	581	580	579	578	577
	11	681	679	677	673	662
	12	681	680	678	674	672
	13	812	806	792	778	767
	14	812	811	805	790	780
	15	882	878	870	862	860

Table 4.18: Natural frequencies (GHz) of a cantilever zigzag (a) (10,0), and (b) (15,0) SWNT with Stone-Wales defect

(a)	Number of defects	0	1	2	4	6
Mode Number	1	43	42	41	40	39
	2	43	42	41	41	40
	3	248	245	245	242	238
	4	248	246	246	244	241
	5	372	367	364	360	354
	6	570	561	553	545	534
	7	632	629	621	608	581
	8	632	631	627	615	596
	9	1112	1100	1069	1029	1004
	10	1112	1105	1087	1051	1035
	11	1114	1110	1100	1085	1070
	12	1245	1191	1173	1168	1163
	13	1245	1233	1225	1225	1207
	14	1262	1255	1253	1233	1211
	15	1262	1257	1257	1252	1243
(b)	Number of defects	0	1	2	4	6
Mode Number	1	64	63	63	61	60
	2	64	64	64	62	62
	3	343	342	341	337	333
	4	343	342	341	338	336
	5	372	371	370	364	360
	6	551	551	551	533	528
	7	551	551	551	545	543
	8	575	572	570	559	551
	9	581	580	577	572	566
	10	581	580	580	577	575
	11	681	678	667	663	640
	12	681	680	677	675	666
	13	812	807	794	790	779
	14	812	808	798	796	784
	15	882	871	860	845	829

Table 4.19: Natural frequencies (GHz) of a cantilever chiral (a) (8,4), and (b) (12,6) SWNT with single vacancy defect

(a)	Number of defects	0	1	2	4	6
Mode Number	1	47	45	44	45	44
	2	47	47	47	47	47
	3	268	265	263	263	260
	4	268	265	265	264	262
	5	370	363	358	358	353
	6	584	577	572	573	568
	7	667	656	654	649	636
	8	667	666	662	656	653
	9	1095	1086	1083	1063	1051
	10	1105	1095	1095	1084	1083
	11	1108	1105	1105	1090	1086
	12	1121	1120	1119	1115	1099
	13	1123	1123	1122	1118	1112
	14	1146	1134	1133	1121	1116
	15	1146	1146	1137	1133	1118
(b)	Number of defects	0	1	2	4	6
Mode Number	1	70	68	67	67	67
	2	70	69	69	69	69
	3	363	358	353	353	348
	4	363	360	360	359	358
	5	374	371	370	370	368
	6	483	489	489	483	482
	7	483	489	489	488	487
	8	518	521	521	520	519
	9	518	522	521	521	520
	10	585	581	578	579	576
	11	636	637	636	635	630
	12	636	638	637	636	635
	13	842	827	821	818	817
	14	842	841	839	836	826
	15	856	855	854	848	845

Table 4.20: Natural frequencies (GHz) of a cantilever chiral (a) (8,4), and (b) (12,6) SWNT with double vacancy defect

(a)	Number of defects	0	1	2	4	6
Mode Number	1	47	43	41	41	41
	2	47	47	47	47	46
	3	268	259	259	256	248
	4	268	264	261	261	258
	5	370	360	352	353	346
	6	584	567	557	559	549
	7	667	651	648	631	597
	8	667	662	651	642	643
	9	1095	1069	1067	1029	1018
	10	1105	1095	1095	1037	1032
	11	1108	1105	1105	1067	1061
	12	1121	1120	1118	1083	1082
	13	1123	1123	1120	1116	1087
	14	1146	1131	1122	1118	1112
	15	1146	1145	1131	1129	1115
(b)	Number of defects	0	1	2	4	6
Mode Number	1	70	66	64	65	63
	2	70	69	69	69	69
	3	363	355	349	349	343
	4	363	359	359	354	345
	5	374	371	370	369	365
	6	483	483	483	480	480
	7	483	483	483	483	482
	8	518	517	517	516	514
	9	518	518	518	517	517
	10	585	575	569	568	562
	11	636	634	632	623	614
	12	636	635	633	632	630
	13	842	823	820	804	792
	14	842	842	836	817	818
	15	856	854	850	840	831

Table 4.21: Natural frequencies (GHz) of a cantilever chiral (a) (8,4), and (b) (12,6) SWNT with Stone-Wales defect

(a)	Number of defects	0	1	2	4	6
Mode Number	1	47	46	45	45	44
	2	47	46	45	45	45
	3	268	266	265	263	256
	4	268	267	266	264	260
	5	370	365	361	359	355
	6	584	575	567	562	552
	7	667	664	657	639	617
	8	667	666	664	647	631
	9	1095	1051	1020	1013	1008
	10	1105	1077	1061	1051	1039
	11	1108	1104	1098	1056	1043
	12	1121	1120	1114	1070	1061
	13	1123	1122	1121	1112	1091
	14	1146	1139	1124	1119	1104
	15	1146	1145	1136	1122	1112
(b)	Number of defects	0	1	2	4	6
Mode Number	1	70	69	68	67	66
	2	70	69	69	68	68
	3	363	361	359	357	351
	4	363	362	360	359	353
	5	374	374	372	366	364
	6	483	489	489	472	468
	7	483	489	489	484	483
	8	518	521	520	517	508
	9	518	522	521	520	516
	10	585	583	581	570	564
	11	636	638	629	622	603
	12	636	639	636	634	627
	13	842	839	816	814	805
	14	842	840	828	824	813
	15	856	854	850	827	823

Table 4.22: Natural frequencies (GHz) of (a) cantilever armchair (10,10), (b) cantilever zigzag (15,0), and (c) cantilever chiral (12,6) with three double vacancy and three Stone-Wales defects.

(a)	Number of defects	0	6
Mode Number	1	76	76
	2	76	76
	3	374	369
	4	384	373
	5	384	374
	6	411	403
	7	411	409
	8	451	439
	9	451	447
	10	587	565
	11	592	583
	12	592	584
	13	837	802
	14	837	818
	15	876	846

(c)	Number of defects	0	6
Mode Number	1	70	64
	2	70	67
	3	363	337
	4	363	352
	5	374	361
	6	483	460
	7	483	476
	8	518	510
	9	518	514
	10	585	559
	11	636	615
	12	636	627
	13	842	802
	14	842	815
	15	856	839

(b)	Number of defects	0	6
Mode Number	1	64	57
	2	64	62
	3	343	318
	4	343	333
	5	372	353
	6	551	530
	7	551	542
	8	575	544
	9	581	574
	10	581	577
	11	681	659
	12	681	669
	13	812	775
	14	812	783
	15	882	853

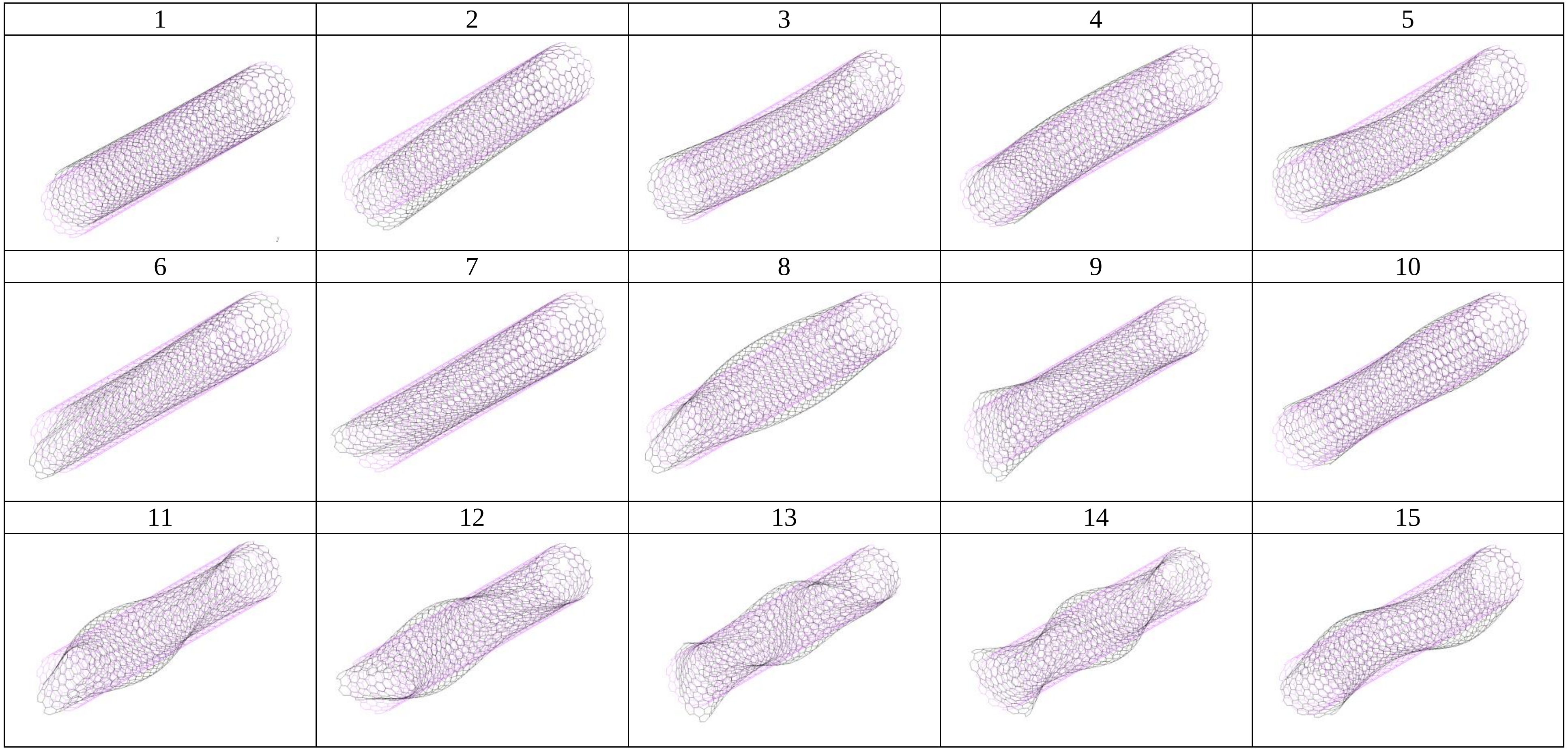

Figure 4.15: Mode shapes of a cantilever armchair (10,10) with three double vacancy and three Stone-Wales defects

The results of the modal analysis of cantilever defective carbon nanotubes indicate that introducing defects has the most negligible effect on the second mode shape of any nanotube. Still, the defects affect the first mode shape more, which can decrease the natural frequency for the first mode shape by up to 1%. Moreover, the effects of defects on SWNTs are more evident as the mode shapes are higher, and it can decrease the natural frequency of SWNT by up to 10%, which is quite a significant margin. It also has to be considered that single vacancy defect has the least impact on the natural frequency of the SWNT, as it is the simplest form of defect that can be introduced to the structure. Furthermore, as the number of double vacancy and Stone-Wales defects increase in the structure, the natural frequency of the SWNT is getting decreased by up to 10%.

In this model, the first two mode shapes, which are the most significant mode shapes of the SWNT, are not affected in the armchair configuration. But in zigzag and chiral, the first two mode shapes are decreased by approximately 1%. Moreover, other mode shapes for all three different chirality got reduced by up to 5%, which goes to show the results for pristine SWNTs are not accurate. If SWNTs are to be implemented in different industries, the analysis for defective SWNTs is required to be conducted more comprehensively.

4.2.2 Bridge Boundary Condition

The SWNTs studied for this section are like the previous section. So, the defective SWNTs studied for this section are:

- Armchair (n=m): (5,5), and (10,10)
- Zigzag (n,0): (10,0), and (15,0)
- Chiral (n≠m): (8,4), and (12,6)

The results of the modal analysis of defective bridge armchair SWNT are depicted in Table 4.23, Table 4.24, and Table 4.25. Similarly, the modal analysis results of defective bridge zigzag SWNT are shown in Table 4.26, Table 4.27, and Table 4.28. Furthermore, the results of the modal analysis of defective bridge chiral SWNT are presented in Table 4.29, Table 4.30, and Table 4.31.Just like in the previous section, a realistic model is being analyzed. This model consists of three double vacancy defects and three Stone-Wales defects introduced to the pristine SWNT. The SWNTs studied are (10,10), (15,0), and (12,6). The results for the modal analysis of this model for all three SWNTs are depicted in Table 4.32. The mode shapes of a bridge armchair (10,10) with three double vacancy defects and three Stone-Wales defects are illustrated in Figure 4.16.

Table 4.23: Natural frequencies (GHz) of a bridge armchair (a) (5,5), and (b) (10,10) SWNT with single vacancy defect

(a)	Number of defects	0	1	2	4	6
Mode Number	1	228	225	225	221	218
	2	228	226	225	223	222
	3	560	551	549	541	533
	4	560	559	554	547	543
	5	734	718	710	682	679
	6	979	963	963	950	924
	7	979	978	968	958	956
	8	1184	1168	1163	1140	1140
	9	1446	1416	1406	1366	1341
	10	1446	1443	1440	1434	1396
	11	1467	1458	1452	1439	1438
	12	1675	1674	1667	1663	1645
	13	1675	1674	1672	1670	1662
	14	1707	1704	1694	1680	1663
	15	1707	1706	1700	1694	1686
(b)	Number of defects	0	1	2	4	6
Mode Number	1	370	364	362	357	356
	2	370	365	365	364	363
	3	444	440	440	439	436
	4	444	441	440	440	440
	5	574	569	568	565	561
	6	574	570	568	567	566
	7	757	743	739	732	731
	8	806	790	790	783	782
	9	806	800	795	793	787
	10	808	801	800	794	791
	11	808	802	801	797	793
	12	1100	1088	1083	1076	1074
	13	1100	1091	1090	1086	1076
	14	1176	1166	1164	1155	1154
	15	1176	1168	1166	1164	1157

Table 4.24: Natural frequencies (GHz) of a bridge armchair (a) (5,5), and (b) (10,10) SWNT with double vacancy defect

(a)	Number of defects	0	1	2	4	6
Mode Number	1	228	220	219	213	202
	2	228	225	224	220	220
	3	560	548	538	516	490
	4	560	557	546	540	538
	5	734	711	701	668	665
	6	979	959	946	925	907
	7	979	977	960	947	913
	8	1184	1141	1134	1079	1085
	9	1446	1405	1391	1353	1289
	10	1446	1437	1433	1413	1327
	11	1467	1457	1447	1433	1418
	12	1675	1674	1671	1667	1656
	13	1675	1674	1673	1671	1665
	14	1707	1705	1697	1687	1677
	15	1707	1706	1702	1697	1691
(b)	Number of defects	0	1	2	4	6
Mode Number	1	370	365	363	357	355
	2	370	366	365	360	357
	3	444	443	443	442	439
	4	444	444	444	443	443
	5	574	572	572	567	559
	6	574	574	572	570	569
	7	757	746	741	722	721
	8	806	794	789	780	776
	9	806	805	796	791	784
	10	808	807	805	797	790
	11	808	808	807	803	800
	12	1100	1095	1087	1074	1060
	13	1100	1097	1093	1081	1074
	14	1176	1164	1153	1139	1128
	15	1176	1176	1176	1174	1171

Table 4.25: Natural frequencies (GHz) of a bridge armchair (a) (5,5), and (b) (10,10) SWNT with Stone-Wales defect

(a)	Number of defects	0	1	2	4	6
Mode Number	1	228	227	226	224	220
	2	228	228	228	227	224
	3	560	557	551	543	521
	4	560	560	556	549	530
	5	734	731	725	718	702
	6	979	972	950	926	897
	7	979	975	956	935	913
	8	1184	1179	1172	1159	1135
	9	1446	1425	1369	1319	1298
	10	1446	1428	1377	1320	1308
	11	1467	1463	1460	1457	1437
	12	1675	1671	1600	1549	1523
	13	1675	1674	1666	1625	1557
	14	1707	1693	1679	1648	1625
	15	1707	1704	1689	1680	1630

(b)	Number of defects	0	1	2	4	6
Mode Number	1	370	368	367	366	363
	2	370	370	370	367	364
	3	444	444	443	442	436
	4	444	444	444	443	442
	5	574	574	570	563	542
	6	574	574	573	571	565
	7	757	755	752	749	740
	8	806	803	787	771	753
	9	806	805	796	793	780
	10	808	807	806	794	781
	11	808	808	808	798	794
	12	1100	1095	1065	1032	1030
	13	1100	1098	1091	1081	1080
	14	1176	1176	1171	1151	1128
	15	1176	1176	1175	1169	1156

Table 4.26: Natural frequencies (GHz) of a bridge zigzag (a) (10,0), and (b) (15,0) SWNT with single vacancy defect

(a)	Number of defects	0	1	2	4	6
Mode Number	1	249	245	245	241	239
	2	249	248	246	244	242
	3	614	605	601	592	588
	4	614	611	609	604	594
	5	749	737	730	708	702
	6	1074	1055	1057	1042	1026
	7	1074	1074	1063	1054	1049
	8	1148	1134	1127	1105	1100
	9	1253	1253	1251	1249	1241
	10	1253	1253	1252	1251	1247
	11	1291	1290	1285	1279	1267
	12	1291	1290	1288	1285	1276
	13	1375	1373	1366	1357	1355
	14	1375	1373	1369	1363	1359
	15	1495	1471	1472	1442	1417
(b)	Number of defects	0	1	2	4	6
Mode Number	1	335	333	331	327	325
	2	335	333	333	330	329
	3	570	570	569	568	566
	4	570	570	570	570	569
	5	664	663	661	659	652
	6	664	663	662	660	659
	7	750	737	730	725	721
	8	762	757	757	737	738
	9	762	761	760	757	749
	10	858	854	853	848	846
	11	858	857	854	850	846
	12	1132	1125	1124	1114	1105
	13	1132	1132	1125	1116	1115
	14	1158	1150	1146	1140	1134
	15	1260	1244	1245	1228	1212

Table 4.27: Natural frequencies (GHz) of a bridge zigzag (a) (10,0), and (b) (15,0) SWNT with double vacancy defect

(a)	Number of defects	0	1	2	4	6
Mode Number	1	249	241	241	234	231
	2	249	246	244	237	234
	3	614	593	586	573	561
	4	614	611	603	591	577
	5	749	725	714	666	655
	6	1074	1039	1042	1017	968
	7	1074	1073	1048	1032	1030
	8	1148	1123	1117	1076	1073
	9	1253	1253	1251	1249	1241
	10	1253	1253	1252	1250	1245
	11	1291	1289	1284	1280	1267
	12	1291	1290	1287	1281	1272
	13	1375	1371	1365	1356	1324
	14	1375	1374	1367	1358	1351
	15	1495	1448	1450	1387	1356
(b)	Number of defects	0	1	2	4	6
Mode Number	1	335	333	331	327	325
	2	335	333	333	330	329
	3	570	570	569	568	566
	4	570	570	570	570	569
	5	664	663	661	659	652
	6	664	663	662	660	659
	7	750	737	730	725	721
	8	762	757	757	737	738
	9	762	761	760	757	749
	10	858	854	853	848	846
	11	858	857	854	850	846
	12	1132	1125	1124	1114	1105
	13	1132	1132	1125	1116	1115
	14	1158	1150	1146	1140	1134
	15	1260	1244	1245	1228	1212

Table 4.28: Natural frequencies (GHz) of a bridge zigzag (a) (10,0), and (b) (15,0) SWNT with Stone-Wales defect

(a)	Number of defects	0	1	2	4	6
Mode Number	1	249	247	246	243	239
	2	249	248	247	246	239
	3	614	611	601	590	563
	4	614	612	602	592	572
	5	749	745	740	729	716
	6	1074	1063	1028	993	973
	7	1074	1065	1043	1017	1003
	8	1148	1139	1128	1108	1083
	9	1253	1252	1232	1217	1196
	10	1253	1253	1249	1237	1212
	11	1291	1286	1267	1249	1232
	12	1291	1290	1281	1261	1240
	13	1375	1360	1340	1317	1315
	14	1375	1372	1358	1345	1340
	15	1495	1476	1458	1401	1355
(b)	Number of defects	0	1	2	4	6
Mode Number	1	335	334	333	331	327
	2	335	335	334	332	328
	3	570	570	568	566	558
	4	570	570	569	569	566
	5	664	661	652	643	615
	6	664	663	660	657	646
	7	750	746	738	737	728
	8	762	759	749	743	732
	9	762	759	756	746	737
	10	858	848	834	809	798
	11	858	855	850	842	838
	12	1132	1104	1089	1061	1054
	13	1132	1126	1119	1105	1104
	14	1158	1152	1145	1134	1117
	15	1260	1245	1234	1193	1190

Table 4.29: Natural frequencies (GHz) of a bridge chiral (a) (8,4), and (b) (12,6) SWNT with single vacancy defect

(a)	Number of defects	0	1	2	4	6
Mode Number	1	267	264	263	260	258
	2	267	265	264	261	259
	3	641	631	627	617	614
	4	641	640	637	633	626
	5	748	737	730	707	700
	6	1101	1083	1084	1068	1051
	7	1101	1101	1091	1087	1083
	8	1119	1119	1117	1116	1110
	9	1119	1119	1118	1117	1113
	10	1163	1163	1157	1138	1134
	11	1164	1163	1159	1154	1144
	12	1177	1165	1161	1158	1151
	13	1261	1259	1255	1247	1243
	14	1263	1262	1256	1251	1248
	15	1423	1419	1415	1404	1396
(b)	Number of defects	0	1	2	4	6
Mode Number	1	352	349	347	342	340
	2	352	350	349	346	345
	3	515	515	515	514	513
	4	515	515	515	515	514
	5	624	623	622	619	615
	6	624	623	623	620	619
	7	757	747	738	730	724
	8	785	777	775	755	754
	9	785	784	783	781	776
	10	834	830	829	824	819
	11	834	833	831	828	826
	12	1115	1106	1105	1097	1093
	13	1115	1114	1111	1107	1098
	14	1179	1171	1167	1155	1151
	15	1287	1268	1267	1249	1243

Table 4.30: Natural frequencies (GHz) of a bridge chiral (a) (8,4), and (b) (12,6) SWNT with double vacancy defect

(a)	Number of defects	0	1	2	4	6
Mode Number	1	267	258	258	249	245
	2	267	264	262	256	254
	3	641	624	619	605	586
	4	641	636	626	615	608
	5	748	732	723	687	679
	6	1101	1071	1070	1045	1025
	7	1101	1100	1075	1058	1050
	8	1119	1118	1117	1093	1085
	9	1119	1119	1118	1117	1113
	10	1163	1146	1137	1118	1115
	11	1164	1163	1158	1155	1148
	12	1177	1163	1162	1159	1154
	13	1261	1260	1252	1243	1239
	14	1263	1261	1258	1254	1249
	15	1423	1418	1411	1388	1368

(b)	Number of defects	0	1	2	4	6
Mode Number	1	352	347	345	339	337
	2	352	349	348	345	341
	3	515	515	514	514	511
	4	515	515	515	514	514
	5	624	622	621	616	608
	6	624	624	622	620	619
	7	757	741	732	725	722
	8	785	775	775	758	756
	9	785	784	780	771	762
	10	834	830	826	819	815
	11	834	833	831	827	820
	12	1115	1107	1102	1085	1077
	13	1115	1112	1108	1100	1086
	14	1179	1159	1155	1142	1133
	15	1287	1267	1269	1257	1230

Table 4.31: Natural frequencies (GHz) of a bridge chiral (a) (8,4), and (b) (12,6) SWNT with Stone-Wales defect

(a)	Number of defects	0	1	2	4	6
Mode Number	1	267	266	265	262	255
	2	267	267	266	264	258
	3	641	638	628	613	592
	4	641	638	630	616	601
	5	748	746	742	732	719
	6	1101	1080	1029	996	990
	7	1101	1089	1064	1037	1033
	8	1119	1118	1114	1088	1070
	9	1119	1119	1117	1113	1078
	10	1163	1155	1144	1115	1100
	11	1164	1161	1155	1133	1109
	12	1177	1170	1160	1142	1115
	13	1261	1239	1227	1210	1206
	14	1263	1255	1244	1232	1228
	15	1423	1383	1379	1326	1254
(b)	Number of defects	0	1	2	4	6
Mode Number	1	352	351	350	348	341
	2	352	352	351	349	343
	3	515	515	513	510	499
	4	515	515	515	514	509
	5	624	623	615	600	583
	6	624	624	622	617	610
	7	757	756	749	745	736
	8	785	783	770	764	756
	9	785	784	777	767	758
	10	834	829	818	790	786
	11	834	833	829	822	821
	12	1115	1100	1085	1063	1027
	13	1115	1112	1107	1100	1090
	14	1179	1175	1167	1156	1136
	15	1287	1276	1258	1222	1218

Table 4.32: Natural frequencies (GHz) of (a) bridge armchair (10,10), (b) bridge zigzag (15,0), and (c) bridge chiral (12,6) with three double vacancy and three Stone-Wales defects.

(a)	Number of defects	0	6
Mode Number	1	370	350
	2	370	361
	3	444	431
	4	444	440
	5	574	549
	6	574	563
	7	757	719
	8	806	768
	9	806	771
	10	808	787
	11	808	797
	12	1100	1042
	13	1100	1067
	14	1176	1121
	15	1176	1153

(c)	Number of defects	0	6
Mode Number	1	352	341
	2	352	344
	3	515	504
	4	515	511
	5	624	596
	6	624	612
	7	757	728
	8	785	748
	9	785	761
	10	834	808
	11	834	813
	12	1115	1055
	13	1115	1084
	14	1179	1147
	15	1287	1209

(b)	Number of defects	0	6
Mode Number	1	335	319
	2	335	326
	3	570	557
	4	570	565
	5	664	632
	6	664	647
	7	750	705
	8	762	728
	9	762	736
	10	858	823
	11	858	838
	12	1132	1061
	13	1132	1093
	14	1158	1114
	15	1260	1188

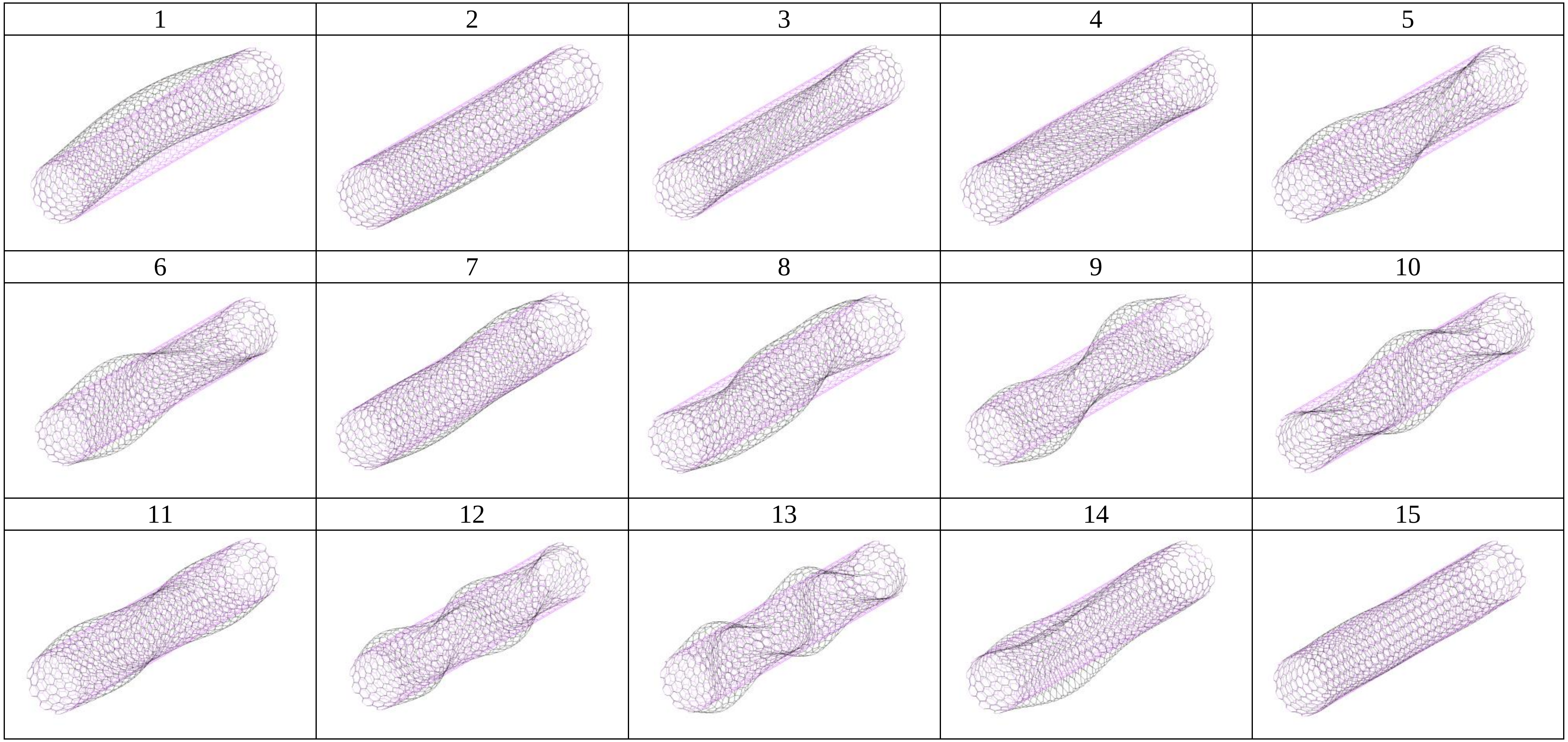

Figure 4.16: Mode shapes of a bridge armchair (10,10) with three double vacancy defects and three Stone-Wales defects.

The results of the modal analysis of defective SWNTs are similar to pristine SWNTs regarding boundary conditions. Applying bridge boundary conditions to defective SWNTs will also increase their natural frequency compared to cantilever boundary condition. And the reason behind that is the nature of the bridge boundary condition, which is the constraint movement compared to the cantilever boundary condition. Nevertheless, unlike the cantilever boundary condition, when any form of defection is introduced to the structure of the SWNT under the bridge boundary condition, its natural frequency gets affected, indicating that SWNTs under this boundary condition are more susceptible to change compared to the cantilever. Moreover, vacancy defects have more effect on the natural frequency of the SWNT compared to Stone-Wales defects. Single vacancy and Stone-Wales defects can decrease the natural frequency of the SWNT by up to 4%. In comparison, the increase in the number of double vacancy defects can reduce the natural frequency of the SWNT by up to 10%, which shows that the natural frequency of the SWNT can get quite affected if the number of defects increases during the synthesis process.

Unlike the cantilever boundary condition, in the bridge boundary condition, all three different configurations of SWNT get affected by these types of defects introduced to the structure. The first two natural frequencies of different chirality of SWNTs decrease up to approximately 6%. Other natural frequencies for different modes and chirality also decrease up to about 7%, showing the effect of defects on the structure of SWNT when its movement is constrained due to the bridge boundary condition.

CHAPTER 5

CONCLUSION AND FUTURE WORK

5.1 Conclusions

The exceptional mechanical properties of carbon nanotubes, since their discovery, have been the point of attention for the field of materials science. Nevertheless, due to the difficulty of synthesizing CNTs and problems associated with the mass production of these materials, it has not been implemented in various sectors yet. Still, research indicates that the significant potential of CNTs could lead to an additional improvement in the world of materials. The purpose of this study is to conduct modal analysis of SWNTs. This analysis provides us with valuable insights into the vibrational behavior of SWNTs. Moreover, it provides us with the natural frequencies and mode shapes of SWNTs, which are crucial for designing devices and structures using SWNTs. Additionally, a comprehensive understanding of the dynamic characteristics of the SWNTs leads to the development of novel nanoscale technologies.

A thorough computational analysis was conducted on SWNTs. This computational analysis was done by utilizing finite element modeling. In this analysis, the fundamental frequencies of pristine and defective SWNTs with several lengths and diameters have been determined. For pristine SWNTs, four different nanotubes with different diameters for each armchair, zigzag, and chiral SWNTs are chosen, and their natural frequency is obtained in various lengths with cantilever and bridge boundary conditions. The results indicated that the natural frequencies of the SWNTs are consistently decreasing with the increase in the length of the nanotube for both boundary conditions. And it also shows that since the natural frequency of the short nanotubes is exceptionally high, they are likely to be unrealistic samples and most likely cannot be synthesized. Meanwhile, the impact of diameter of the nanotube can be neglected by the length when it comes to the natural frequency of the SWNT.

In the other part of the analysis, the defective SWNTs are studied. In this part of the analysis, the effect of vacancy defects and Stone-Wales defects on the natural frequencies of two SWNTs with different diameters for each armchair, zigzag, and chiral SWNTs for cantilever and bridge boundary conditions is investigated. By applying different numbers of vacancy defects and Stone-Wales defects (1, 2, 4, 6) on these SWNTs, their fundamental frequencies are compared with their pristine model. The analysis indicates that for all types of SWNTs, the double vacancy defect has the most degradation effect on the natural frequency of the SWNT. This is because as the number of double vacancy defects increases, the covalent bonds that connect the two carbon atoms decrease, which can significantly affect the properties of the SWNTs. Also, for the single vacancy defects, since it is the simplest form of defect, it does not affect the SWNTs under cantilever boundary conditions by a high margin. It is also observed that Stone-Wales defects can have the same impact on the SWNTs when they are in the cantilever boundary condition, but this type of defect is not as impactful when it comes to the bridge boundary condition, and it does not impact the natural frequency as much as both single and double vacancy.

5.2 Recommendations for Future Work

Although this study is an extensive analysis of SWNTs under vibrational load, there is still much to be done regarding the CNTs in this context. Firstly, modal analysis can be conducted for different boundary conditions on pristine and defective MWNTs. Secondly, due to the remarkable properties of SWNTs, they have been considered one of the essential materials in the world of composites. Therefore, modal analysis can be done on nanomaterials or polymers which are reinforced by SWNT or MWNT.

Moreover, the majority of research papers done on the vibrational properties of single-walled carbon nanotubes (SWNTs) have focused on cantilever and bridge boundary conditions. Given that modal analysis is applicable to free-free boundary conditions, it can be an interesting topic to investigate for future studies.

REFERENCES

[1] Iijima, S. (1991). Helical microtubules of graphitic carbon. *nature*, *354*(6348), 56-58.

[2] Rathinavel, S., Priyadharshini, K., & Panda, D. (2021). A review on carbon nanotube: An overview of synthesis, properties, functionalization, characterization, and the application. *Materials Science and Engineering: B*, *268*, 115095.

[3] Chatterjee, A., & Deopura, B. L. (2002). Carbon nanotubes and nanofibre: an overview. *Fibers and Polymers*, *3*, 134-139.

[4] Breuer, O., & Sundararaj, U. (2004). Big returns from small fibers: a review of polymer/carbon nanotube composites. *Polymer composites*, *25*(6), 630-645.

[5] Dresselhaus, M. S., Dresselhaus, G., & Saito, R. (1995). Physics of carbon nanotubes. Carbon, 33(7), 883-891.

[6] Yengejeh, S. I., Kazemi, S. A., & Öchsner, A. (2015). *A primer on the geometry of carbon nanotubes and their modifications*. Berlin/Heidelberg, Germany: Springer.

[7] Cole, M. W., Crespi, V. H., Dresselhaus, M. S., Dresselhaus, G., Fischer, J. E., Gutierrez, H. R., Kojima, K., Mahan, G. D., Rao, A. M., Sofo, J. O., Tachibana, M., Wako, K., & Xiong, Q. (2010). Structural, electronic, optical and vibrational properties of nanoscale carbons and Nanowires: A colloquial review. Journal of Physics: Condensed Matter, 22(33), 334201. https://doi.org/10.1088/0953-8984/22/33/334201

[8] Patel, D. K., Kim, H. B., Dutta, S. D., Ganguly, K., & Lim, K. T. (2020). Carbon nanotubes-based nanomaterials and their agricultural and biotechnological applications. *Materials*, *13*(7), 1679.

[9] OCSiAl. (2021, May 6). Single-walled carbon nanotubes: Structure, properties, applications. Single-walled Carbon Nanotubes: Structure, Properties, Applications. https://tuball.com/pages/single-walled-carbon-nanotubes?gclid=CjwKCAjw2bmLBhBREiwAZ6ugo4ZATWdOvvE2MHAM3A-NXAnHVftjStuQBE5m6CBXYaERhnaYphMxphoCZuUQAvD_BwE

[10] Kalamkarov, A. L., Georgiades, A. V., Rokkam, S. K., Veedu, V. P., & Ghasemi-Nejhad, M. N. (2006). Analytical and numerical techniques to predict carbon nanotubes properties. *International journal of Solids and Structures*, *43*(22-23), 6832-6854.

[11] Salvetat, J. P., Bonard, J. M., Thomson, N. H., Kulik, A. J., Forro, L., Benoit, W., & Zuppiroli, L. (1999). Mechanical properties of carbon nanotubes. *Applied Physics A*, *69*, 255-260.

[12] Ong, C. C., Jose, R., & Saheed, M. S. M. (2021). Atomic defects of graphene-carbon nanotubes impact on surface wettability. *Applied Surface Science*, *567*, 150803.

[13] Tan, C. W., Tan, K. H., Ong, Y. T., Mohamed, A. R., Zein, S. H. S., & Tan, S. H. (2012). Energy and environmental applications of carbon nanotubes. Environmental Chemistry Letters, 10, 265-273.

[14] Mei, X., Fan, B., Sun, K., & Ouyang, J. (2009, August). High-performance dye-sensitized solar cells with nanomaterials as counter electrode. In *Nanoscale photonic and cell technologies for photovoltaics II* (Vol. 7411, pp. 50-58). SPIE.

[15] Ramasamy, E., Lee, W. J., Lee, D. Y., & Song, J. S. (2008). Spray coated multi-wall carbon nanotube counter electrode for tri-iodide (I3-) reduction in dye-sensitized solar cells. *Electrochemistry Communications*, *10*(7), 1087-1089.

[16] Goldoni, A., Larciprete, R., Petaccia, L., & Lizzit, S. (2003). Single-wall carbon nanotube interaction with gases: sample contaminants and environmental monitoring. *Journal of the American Chemical Society*, *125*(37), 11329-11333.

[17] Goldoni, A., Petaccia, L., Gregoratti, L., Kaulich, B., Barinov, A., Lizzit, S., ... & Larciprete, R. (2004). Spectroscopic characterization of contaminants and interaction with gases in single-walled carbon nanotubes. *Carbon*, *42*(10), 2099-2112.

[18] Upadhyayula, V. K., Deng, S., Mitchell, M. C., Smith, G. B., Nair, V. K., & Ghoshroy, S. (2008). Adsorption kinetics of Escherichia coli and Staphylococcus aureus on single-walled carbon nanotube aggregates. *Water Science and Technology*, *58*(1), 179-184.

[19] Upadhyayula, V. K., Ghoshroy, S., Nair, V. S., Smith, G. B., Mitchell, M. C., & Deng, S. (2008). Single-walled carbon nanotubes as fluorescence biosensors for pathogen recognition in water systems. *Journal of Nanotechnology*, *2008*.

[20] Khodakovskaya, M., Dervishi, E., Mahmood, M., Xu, Y., Li, Z., Watanabe, F., & Biris, A. S. (2009). Carbon nanotubes are able to penetrate plant seed coat and dramatically affect seed germination and plant growth. ACS nano, 3(10), 3221-3227.

[21] Mondal, A., Basu, R., Das, S., & Nandy, P. (2011). Beneficial role of carbon nanotubes on mustard plant growth: an agricultural prospect. *Journal of Nanoparticle Research*, *13*, 4519-4528.

[22] Ratnikova, T. A., Podila, R., Rao, A. M., & Taylor, A. G. (2015). Tomato seed coat permeability to selected carbon nanomaterials and enhancement of germination and seedling growth. *The Scientific World Journal*, *2015*.

[23] Chang, X., Song, Z., Xu, Y., & Gao, M. (2020). Effects of carbon nanotubes on growth of wheat seedlings and Cd uptake. *Chemosphere*, *240*, 124931.

[24] Askeland, D. R. (1990). The science and emerging of materials.

[25] Thess, A., Lee, R., Nikolaev, P., Dai, H., Petit, P., Robert, J., ... & Smalley, R. E. (1996). Crystalline ropes of metallic carbon nanotubes. *science*, *273*(5274), 483-487.

[26] Li, W. Z., Xie, S. S., Qian, L. X., Chang, B. H., Zou, B. S., Zhou, W. Y., ... & Wang, G. (1996). Large-scale synthesis of aligned carbon nanotubes. *Science*, *274*(5293), 1701-1703.

[27] Xie, S., Li, W., Pan, Z., Chang, B., & Sun, L. (2000). Carbon nanotube arrays. *Materials Science and Engineering: A*, *286*(1), 11-15.

[28] Bhushan, B., Luo, D., Schricker, S. R., Sigmund, W., & Zauscher, S. (Eds.). (2014). *Handbook of nanomaterials properties*. Springer Science & Business Media.

[29] Lee, C. J., Lyu, S. C., Kim, H. W., Park, C. Y., & Yang, C. W. (2002). Large-scale production of aligned carbon nanotubes by the vapor phase growth method. *Chemical Physics Letters*, *359*(1-2), 109-114.

[30] Gore, J. P., & Sane, A. (2011). Flame synthesis of carbon nanotubes. *Carbon Nanotubes-Synthesis, Characterization, Applications*, *1*, 16801.

[31] Nozaki, T., Ohnishi, K., Okazaki, K., & Kortshagen, U. (2007). Fabrication of vertically aligned single-walled carbon nanotubes in atmospheric pressure non-thermal plasma CVD. *Carbon*, *45*(2), 364-374.

[32] Doh, J., & Lee, J. (2016). Prediction of the mechanical behavior of double walled-CNTs using a molecular mechanics-based finite element method: Effects of chirality. *Computers & Structures*, *169*, 91-100.

[33] Lengvarský, P., & Bocko, J. (2015). Prediction of Youngs modulus of graphene sheets by the finite element method. *American Journal of Mechanical Engineering*, *3*(6), 225-229.

[34] Belytschko, T., Xiao, S. P., Schatz, G. C., & Ruoff, R. S. (2002). Atomistic simulations of nanotube fracture. *Physical Review B*, *65*(23), 235430.

[35] Meo, M., & Rossi, M. (2006). Tensile failure prediction of single wall carbon nanotube. *Engineering Fracture Mechanics*, *73*(17), 2589-2599.

[36] Rossi, M., & Meo, M. (2009). On the estimation of mechanical properties of single-walled carbon nanotubes by using a molecular-mechanics based FE approach. *Composites Science and Technology*, *69*(9), 1394-1398.

[37] Meo, M., & Rossi, M. (2007). A molecular-mechanics based finite element model for strength prediction of single wall carbon nanotubes. *Materials Science and Engineering: A*, *454*, 170-177.

[38] Li, C., & Chou, T. W. (2003). A structural mechanics approach for the analysis of carbon nanotubes. *International journal of solids and structures*, *40*(10), 2487-2499.

[39] Lu, X., & Hu, Z. (2012). Mechanical property evaluation of single-walled carbon nanotubes by finite element modeling. *Composites Part B: Engineering*, *43*(4), 1902-1913.

[40] Tserpes, K. I., & Papanikos, P. (2005). Finite element modeling of single-walled carbon nanotubes. *Composites Part B: Engineering*, *36*(5), 468-477.

[41] Fan, C. W., Liu, Y. Y., & Hwu, C. (2009). Finite element simulation for estimating the mechanical properties of multi-walled carbon nanotubes. Applied Physics A, 95, 819-831.

[42] Scarpa, F., & Adhikari, S. (2008). A mechanical equivalence for Poisson's ratio and thickness of C–C bonds in single wall carbon nanotubes. *Journal of Physics D: Applied Physics*, *41*(8), 085306.

[43] Zuberi, M. J. S., & Esat, V. (2016). Evaluating the effects of size and chirality on the mechanical properties of single-walled carbon nanotubes through equivalent-continuum modelling. *Proceedings of the Institution of Mechanical Engineers, Part L: Journal of Materials: Design and Applications*, *230*(5), 913-926.

[44] Lee, J. H., & Lee, B. S. (2012). Modal analysis of carbon nanotubes and nanocones using FEM. *Computational Materials Science*, *51*(1), 30-42.

[45] Shariati, A. A., Golkarian, A. R., & Jabbarzadeh, M. (2014). Investigation of Vibrational Behavior of Perfect and Defective Carbon Nanotubes Using Non–Linear Mass–Spring Model. *Journal of Solid Mechanics*, *6*(3), 255-264.

[46] Sakhaee-Pour, A., Ahmadian, M. T., & Vafai, A. (2009). Vibrational analysis of single-walled carbon nanotubes using beam element. *Thin-walled structures*, *47*(6-7), 646-652.

[47] Arghavan, S., & Singh, A. V. (2011). On the vibrations of single-walled carbon nanotubes. *Journal of Sound and Vibration*, *330*(13), 3102-3122.

[48] Miyashiro, D., Taira, H., Hamano, R., Reserva, R. L., & Umemura, K. (2020). Mechanical vibration of single-walled carbon nanotubes at different lengths and carbon nanobelts by modal analysis method. *Composites Part C: Open Access*, *2*, 100028.

[49] Mir, M., Hosseini, A., & Majzoobi, G. H. (2008). A numerical study of vibrational properties of single-walled carbon nanotubes. *Computational Materials Science*, *43*(3), 540-548.

[50] Goel, M., Harsha, S. P., Mishra, M. P., & Mishra, R. K. (2020). Influence of Various Defect Parameters on the Vibration Characteristics of a Single-Walled Carbon Nanotube. *Journal of Failure Analysis and Prevention*, *20*, 1229-1236.

[51] Joshi, A. Y., Sharma, S. C., & Harsha, S. P. (2011). Effect of chirality and atomic vacancies on dynamics of nanoresonators based on SWCNT. *Sensor Review*.

[52] Ghavamian, A., & Öchsner, A. (2013). Numerical modeling of eigenmodes and eigenfrequencies of single-and multi-walled carbon nanotubes under the influence of atomic defects. *Computational Materials Science, 72*, 42-48.

[53] Chowdhury, R., Adhikari, S., Wang, C. Y., & Scarpa, F. (2010). A molecular mechanics approach for the vibration of single-walled carbon nanotubes. *Computational Materials Science*, *48*(4), 730-735.

[54] Yan, Y., Wang, W., Zhang, J., & Zhang, L. (2012). Free vibration of the water-filled single-walled carbon nanotubes. *Procedia Engineering*, *31*, 647-653.

[55] Bocko, J., & Lengvarský, P. (2014). Vibration of single-walled carbon nanotubes by using nonlocal theory. *American Journal of Mechanical Engineering*, *2*(7), 195-198.

[56] Fatahi-Vajari, A., & Imam, A. (2016). Torsional vibration of single-walled carbon nanotubes using doublet mechanics. *Zeitschrift für angewandte Mathematik und Physik*, *67*, 1-22.

[57] Fatahi-Vajari, A., & Imam, A. (2016). Axial vibration of single-walled carbon nanotubes using doublet mechanics. *Indian Journal of Physics*, *90*, 447-455.

[58] Bensattalah, T., Daouadji, T. H., Zidour, M., Tounsi, A., & Bedia, E. A. (2016). Investigation of thermal and chirality effects on vibration of single-walled carbon nanotubes embedded in a polymeric matrix using nonlocal elasticity theories. *Mechanics of Composite Materials*, *52*, 555-568.

[59] Pine, P., Yaish, Y. E., & Adler, J. (2014). Vibrational analysis of thermal oscillations of single-walled carbon nanotubes under axial strain. *Physical Review B*, *89*(11), 115405.

[60] Chang, I. L., & Huang, C. M. (2013). Vibrational behavior of single-walled carbon nanotubes: atomistic simulations. *Japanese Journal of Applied Physics*, *52*(10R), 105101.

[61] Mungra, C., & Webb, J. F. (2015). Free vibration analysis of single-walled carbon nanotubes based on the continuum finite element method. *Global Journal of Technology & Optimization*, *6*(2).

[62] Ansari, R., Rouhi, H., & Rajabiehfard, R. (2012). Free vibration analysis of single-walled carbon nanotubes using semi-analytical finite element. *International Journal for Computational Methods in Engineering Science and Mechanics*, *13*(3), 202-209.

[63] Talla, J., Zhang, D., Kandadai, M., Avadhanula, A., & Curran, S. (2010). A resonance Raman study of carboxyl induced defects in single-walled carbon nanotubes. Physica B: Condensed Matter, 405(21), 4570-4573.

[64] Muc, A., Banaś, A., & Chwał, A. (2013). Free vibrations of carbon nanotubes with defects. Mechanics and Mechanical Engineering, 17(2), 157-166.

[65] Joshi, A. Y., Sharma, S. C., & Harsha, S. P. (2011). The effect of pinhole defect on vibrational characteristics of single walled carbon nanotube. Physica E: Low-Dimensional Systems and Nanostructures, 43(5), 1040-1045.

[66] Goel, M., Harsha, S. P., Mishra, M. P., & Mishra, R. K. (2020). Influence of Various Defect Parameters on the Vibration Characteristics of a Single-Walled Carbon Nanotube. Journal of Failure Analysis and Prevention, 20, 1229-1236.

[67] Goel, Mohit, et al. "Effect of Geometrical Parameters and Hexa-Vacancy Defects on Vibration Characteristics of Bridged Carbon Nanotube." Journal of Failure Analysis and Prevention 20 (2020): 1875-1883.

[68] Ghavamian, A., & Öchsner, A. (2013). Numerical modeling of eigenmodes and eigenfrequencies of single-and multi-walled carbon nanotubes under the influence of atomic defects. Computational Materials Science, 72, 42-48.

[69] Bedi, D., Sharma, S., Tiwari, S. K., & Ajori, S. (2022). Effect of defects and boundary conditions on the vibrational behavior of carbon nanotube and graphene: A molecular dynamics perspective. Diamond and Related Materials, 126, 109052.

[70] Georgantzinos, S. K., Giannopoulos, G. I., & Anifantis, N. K. (2014). The effect of atom vacancy defect on the vibrational behavior of single-walled carbon nanotubes: a structural mechanics approach. Advances in Mechanical Engineering, 6, 291645.

[71] Chen, L. J., Zhao, Q., & Gong, Z. Q. (2011). The effects of different defects on vibration properties of single-walled carbon nanotubes. Advanced Materials Research, 225, 1133-1136.

[72] Hudson, R. B., & Sinha, A. (2018). Vibration of carbon nanotubes with defects: order reduction methods. Proceedings of the Royal Society A: Mathematical, Physical and Engineering Sciences, 474(2211), 20170555.

[73] Parvaneh, V., Shariati, M., & Torabi, H. (2011). Frequency analysis of perfect and defective SWCNTs. Computational materials science, 50(7), 2051-2056.

[74] Shariati, A. A., Golkarian, A. R., & Jabbarzadeh, M. (2014). Investigation of vibrational behavior of perfect and defective carbon nanotubes using non–linear mass–spring model. Journal of Solid Mechanics, 6(3), 255-264